

AWARD NUMBER: W81XWH-21-1-0629

TITLE: Neupilin-2 Inhibitor as a Potent Therapy for Prostate Cancer Bone Metastasis

PRINCIPAL INVESTIGATOR: Benjamin A Teply

CONTRACTING ORGANIZATION: University of Nebraska Medical Center, Omaha, NE

REPORT DATE: August 2022

TYPE OF REPORT: Annual

PREPARED FOR: U.S. Army Medical Research and Development Command
Fort Detrick, Maryland 21702-5012

DISTRIBUTION STATEMENT: Approved for Public Release;
Distribution Unlimited

The views, opinions and/or findings contained in this report are those of the author(s) and should not be construed as an official Department of the Army position, policy, or decision unless so designated by other documentation.

REPORT DOCUMENTATION PAGE

Form Approved
OMB No. 0704-0188

Public reporting burden for this collection of information is estimated to average 1 hour per response, including the time for reviewing instructions, searching existing data sources, gathering and maintaining the data needed, and completing and reviewing this collection of information. Send comments regarding this burden estimate or any other aspect of this collection of information, including suggestions for reducing this burden to Department of Defense, Washington Headquarters Services, Directorate for Information Operations and Reports (0704-0188), 1215 Jefferson Davis Highway, Suite 1204, Arlington, VA 22202-4302. Respondents should be aware that notwithstanding any other provision of law, no person shall be subject to any penalty for failing to comply with a collection of information if it does not display a currently valid OMB control number. **PLEASE DO NOT RETURN YOUR FORM TO THE ABOVE ADDRESS.**

1. REPORT DATE August 2022		2. REPORT TYPE Annual		3. DATES COVERED 01Aug2021-31Jul2022	
4. TITLE AND SUBTITLE Neuropilin-2 Inhibitor as a Potent Therapy for Prostate Cancer Bone Metastasis				5a. CONTRACT NUMBER W81XWH-21-1-0629	
				5b. GRANT NUMBER PC200280P1	
				5c. PROGRAM ELEMENT NUMBER	
6. AUTHOR(S) Kaustubh Datta, Ph.D. and Benjamin Teply, MD E-Mail: ben.teply@unmc.edu				5d. PROJECT NUMBER	
				5e. TASK NUMBER	
				5f. WORK UNIT NUMBER	
7. PERFORMING ORGANIZATION NAME(S) AND ADDRESS(ES) University of Nebraska Medical Center 985870 Nebraska Medical Center Omaha, NE 68198-5870				8. PERFORMING ORGANIZATION REPORT NUMBER	
9. SPONSORING / MONITORING AGENCY NAME(S) AND ADDRESS(ES) U.S. Army Medical Research and Development Command Fort Detrick, Maryland 21702-5012				10. SPONSOR/MONITOR'S ACRONYM(S)	
				11. SPONSOR/MONITOR'S REPORT NUMBER(S)	
12. DISTRIBUTION / AVAILABILITY STATEMENT Approved for Public Release; Distribution Unlimited					
13. SUPPLEMENTARY NOTES					
14. ABSTRACT There is no effective therapy to-date that can effectively cure prostate cancer bone metastasis. Systemic chemotherapy can be used to treat metastatic prostate cancer, however, the tumors often will become resistant. Our studies suggested that a cell-surface protein called neuropilin-2 is highly expressed in metastatic prostate cancer cells especially when they are in bone and is responsible for their ability to resist therapy. Based on our preliminary results, we hypothesized in the current proposal that a neuropilin-2 targeting drug in combination with chemotherapy should be an effective treatment strategy for prostate cancer patients with bone metastasis. Recently, with the help of computer modeling-based screening strategy and supportive wet laboratory-based studies, we have identified a FDA approved drug, which can specifically block neuropilin-2. In this proposal, we will test the potential of this drug in the combination with chemotherapy in preclinical mouse model of prostate cancer bone metastasis. We will also study a blood-based biomarker, which will can indicate high neuropilin-2 expression in metastatic bone tissues. This marker will thus help to stratify metastatic patients, who will be best suited for neuropilin-2 targeting drug therapy. Successful completion of the proposed project will eventually lead to the anti-neuropilin-2 drug as a front-line therapy for the lethal metastatic prostate cancer. Since this anti-NRP2 drug is an FDA approved drug for other disease-specific uses, the detailed information about it regarding its pharmacology, formulation and potential toxicity to human is known. Re-purposing this drug to treat lethal prostate cancer can be done with ease. We expect within 5-8 year time period from now, the drug can complete the necessary clinical trials and can be integrated as a therapy for prostate cancer.					
15. SUBJECT TERMS None listed.					
16. SECURITY CLASSIFICATION OF:			17. LIMITATION OF ABSTRACT Unclassified	18. NUMBER OF PAGES 57	19a. NAME OF RESPONSIBLE PERSON USAMRDC
a. REPORT Unclassified	b. ABSTRACT Unclassified	c. THIS PAGE Unclassified			19b. TELEPHONE NUMBER (include area code)

TABLE OF CONTENTS

	<u>Page</u>
1. Introduction	4
2. Keywords	5
3. Accomplishments	6-12
4. Impact	13
5. Changes/Problems	14
6. Products	15
7. Participants & Other Collaborating Organizations	16-18
8. Special Reporting Requirements	19
9. Appendices	20-57

1. Introduction:

Most men with castration-resistant prostate cancer (CRPC) develop metastasis to bone. One life-prolonging therapy for metastatic CRPC is systemic chemotherapy with the taxane chemotherapy (docetaxel, *Taxotere*®). Unfortunately, most men with metastatic CRPC who receive docetaxel, however, relapse within a matter of months. There is no option for curative treatment available at this stage of the disease, and men with metastatic CRPC unfortunately are highly likely to die from their disease. Additionally, prostate cancer patients with bone metastasis frequently suffer from skeletal-related events (SREs) such as severe bone pain, pathologic fractures, spinal cord and nerve compression syndromes, and hypercalcemia. Therefore, bone metastases remain to be a frequent and fatal complication in CRPC patients, and its management is a clinical challenge, requiring the identification of new molecular target(s) that can be therapeutically exploited to improve patient outcome. Our work has indicated that a cell surface receptor, neuropilin-2 (NRP2), can be a potential molecular target to develop an effective therapy for metastatic CRPC especially when in combination with chemotherapy. Our recent report in a cohort of 400 primary prostate cancer patients showed correlation with NRP2 expression and poor cancer-specific patient survival. The correlation is even more significant for patients with higher grades and clinical stages of prostate cancer. In a different patient cohort with bone metastasis, ~85% of metastatic tissues at bone expressed very high levels of NRP2, whereas close to 60% of advanced CRPC tissue expressed NRP2 and majority of them expressed moderate levels of NRP2. These results therefore indicated a potential role of NRP2 in the metastatic progression of CRPC. We performed extensive mechanistic studies for the last decade, which suggested that the increased expression of NRP2 promotes enhanced rate of endocytic trafficking in the cancer cells, which in turn regulates two major cellular processes important for oncogenic growth, survival, and therapy resistance of PCa cells. One such process is autophagy, which provides survival of PCa cells during therapy-induced stress. Another process that NRP2 regulates is the recycling of signaling receptors such as EGFR, HGF to cell surface and thus favors their oncogenic potential. Because of these mechanistic insights of NRP2's function, we postulated that NRP2 should be targeted in metastatic CRPC. We now observed in a mouse model of bone metastasis that genetic depletion of NRP2 can sensitize prostate tumor toward chemotherapy confirming our *in-vitro* findings that NRP2 is a valid therapeutic target. Importantly, we recently identified a small molecule FDA approved drug as a specific inhibitor of NRP2 axis. We thus hypothesized that targeting NRP2 with small molecule drugs in combination with chemotherapy is an effective therapy for metastatic CRPC (mCRPC) with bone metastasis. Two specific aims have been proposed. In aim 1, we plan to evaluate the effectiveness of NRP2-specific drugs to enhance the therapeutic efficacy of chemotherapy in CRPC. In aim 2, we are performing experiments to identify biomarkers for high NRP2 activity in mCRPC patients who may be candidates for NRP2 directed therapy.

2. Keywords

Castration resistant Prostate Cancer

Bone metastasis

Neuropilin-2

Small molecule inhibitors

Biomarkers

Promoter methylation

3. Accomplishments

- Major goals and accomplishments

Major goals of the project as stated in the approved SOW have been listed as “subtasks” under each specific aim. The accomplishment of these goals has been described individually under each subtask.

Specific Aim 1: Evaluate the effectiveness of NRP2-specific drugs to enhance the therapeutic efficacy of chemotherapy in CRPC.

Subtask 1: Identify and validate the site, where clomipramine binds to neuropilin-2.

We have made the following studies to identify specific amino acids of NRP2 where clomipramine binds.

Active binding site prediction on NRP2:

We wanted to understand how many different conformations NRP2 can take as it will be important to map the clomipramine binding pocket. At first, we generated different conformational ensembles of NRP2 by molecular dynamics (MD) based root mean square deviation (RMSD) cluster analysis using Schrödinger Desmond. We obtained three major clusters of NRP2 protein from this analysis

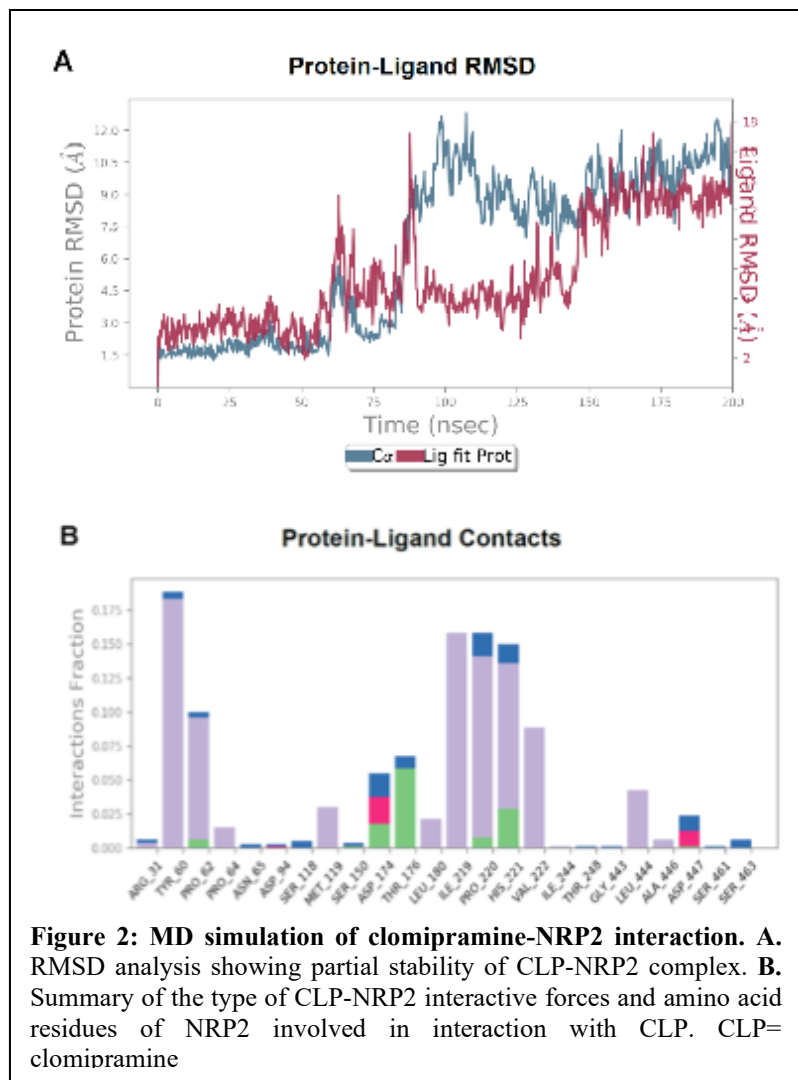
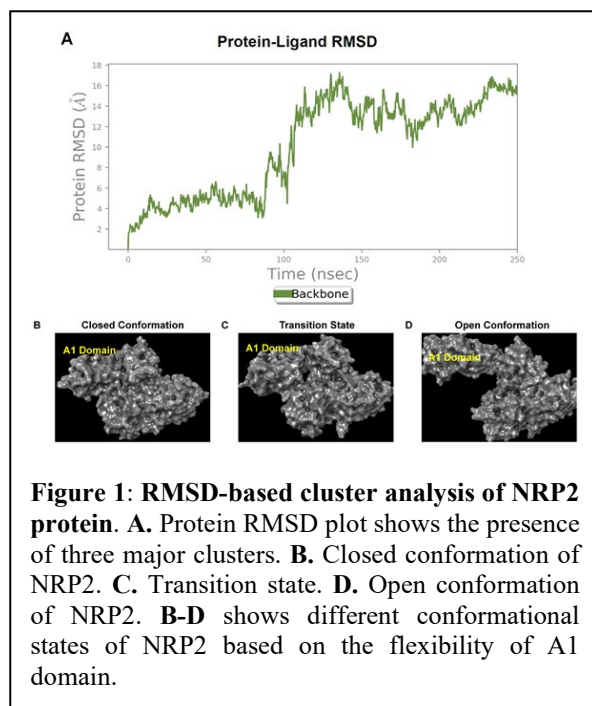
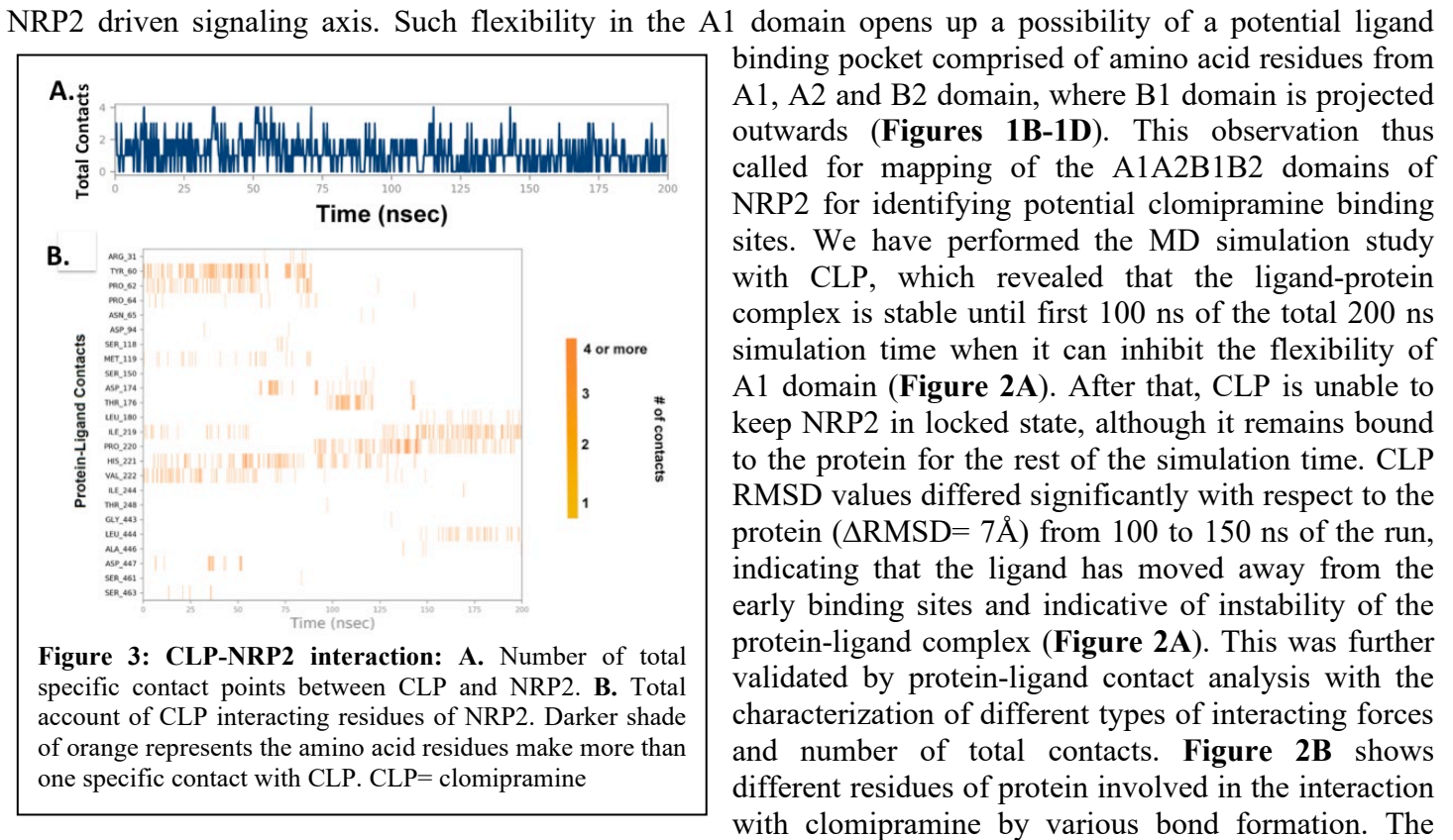


Figure 2: MD simulation of clomipramine-NRP2 interaction. A. RMSD analysis showing partial stability of CLP-NRP2 complex. B. Summary of the type of CLP-NRP2 interactive forces and amino acid residues of NRP2 involved in interaction with CLP. CLP= clomipramine



(Figure 1A). The left Y-axis of the plot shows the RMSD evolution of NRP2. We observed three major conformers of NRP2 based on the RMSD based MD simulation and cluster analysis (Figures 1B-1D). Interestingly, these conformers were generated depending on the flexibility of A1 domain and was termed as closed (Figure 1B), transition (Figure 1C) and open (Figure 1D) states of NRP2. Such structural flexibility in A1 domain is believed to have significant consequence in the functioning of the protein, because NRP2 is known to use its flexible A1 domain to interact with the surrounding biomolecules to initiate

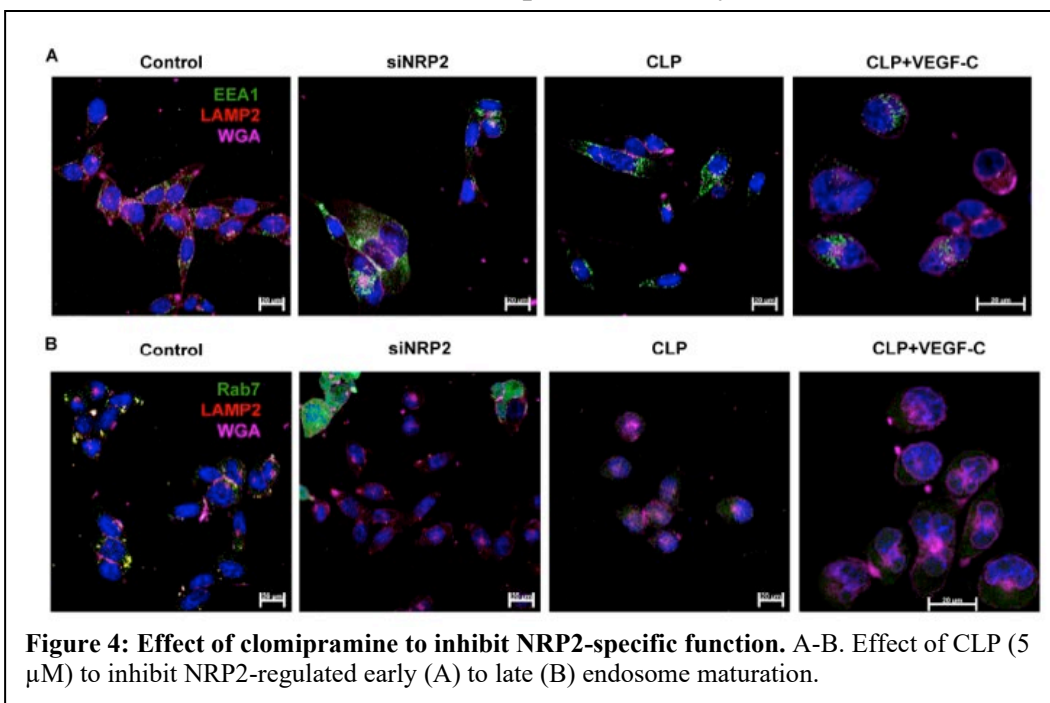


highest interactive force was recorded with Tyr 60, where the specific interaction was maintained for about 19% of the simulation time. The total numbers of specific contact points have been determined (**Figures 3A and 3B**).

To serve as an explanation of the structural basis of NRP2 inhibition by small molecule inhibitors, the above data suggests that the inhibitors function through inhibiting the conformational change in NRP2 by reversing the flexibility of A1 domain.

These in silico observations needs to be validated by biophysical assays and alanine scanning site directed mutagenesis studies, which are currently ongoing.

Subtask 2: To test whether clomipramine delays the maturation of endocytic process in prostate cancer cells.



To prove NRP2-specific inhibition by CLP, we have evaluated the ability of CLP to inhibit NRP2's known specific function of regulating early endosome to late endosome maturation within the cancer cells. NRP2 inhibition would stall the vesicles into the early endosomal compartment. Our data in DKD cells demonstrated that addition of CLP increased the accumulation of early endosome marker (EEA1)

and decreased its co-localization with late endosome marker (LAMP2) compared to control (no treatment), indicating the inhibition of NRP2 regulated early to late endosome maturation (**Figure 4A**). On the other hand, CLP decreased the signal of Rab7, a late endosome marker, and its co-localization with LAMP2, validating the inhibition of NRP2 regulated endosomal maturation (**Figure 4B**). NRP2 genetic depletion was kept as positive control in both the cases. Interestingly, addition of very high concentration of VEGF-C (canonical ligand of NRP2) could not reverse the effect of CLP addition (**Figures 4A-B**), suggesting the action of CLP through binding to a pocket other than the ligand binding site on NRP2.

Subtask 3: To test whether clomipramine inhibits the maturation of autophagosome to autolysosome.

The experiments are currently in progress and the result will be reported in the next annual report.

Subtask 4: To test altered trafficking of Cell surface receptors following clomipramine treatment.

The experiments are currently in progress and the results will be reported in the next annual report.

Subtask 5: Submit documents for IACUC approval.

IACUC protocol for the DoD grant has been approved.

Subtask 6: Submit documents for ACURO approval.

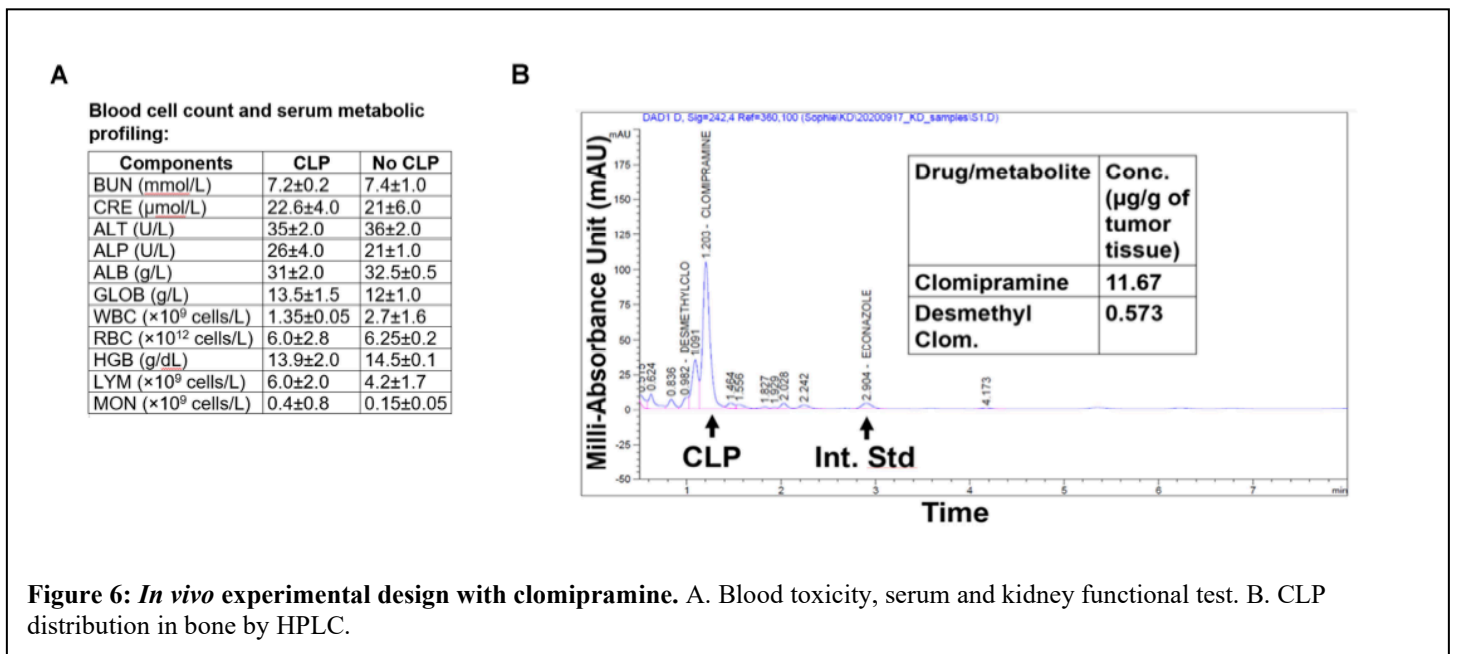
ACURO has been approved.

Subtask 7: Evaluate the effectiveness of targeting neuropilin-2 by clomipramine against therapy-resistant PCa:

Effect of CLP to increase the efficacy of chemotherapy to inhibit PCa will be evaluated in vivo. Bone is one of the major metastatic sites for advanced mCRPC. About 80% of metastatic PCa is accompanied by bone metastasis. Therefore, we will be using intra-tibial bone metastatic tumor model to test the efficacy of CLP. We

$$Animal\ dose\ \left(\frac{mg}{kg}\right) = \frac{Human\ dose\ \left(\frac{mg}{kg}\right) \times Human\ Km}{Animal\ Km}$$

Figure 5: Formula for human to animal dose conversion.



have performed a pilot study using athymic nude mice (n=5), where we provided tumor-bearing mice (neuroendocrine-like prostate cancer cells, intratibial implantation) with CLP via i.p route (20 mg/kg body-wt/mice every alternate days for two weeks). The dose was chosen from the knowledge of maximum tolerated dose (MTD) of CLP in human, i.e., 250 mg/day or 4.2 mg/kg body-wt for an average adult of 60 kg and body surface area of 1.62 m². Human to animal dose conversion was performed using the conversion factor (Km) based calculation prescribed by FDA (<https://www.fda.gov/media/72309/download>). The formula is as in Figure 5.

The chosen dose is below half of the MTD for mice, i.e., 51mg/kg body-wt according to the formula. The mice were also monitored for >20% weight loss and Body Condition Scoring (BCS=3) according to the approved IACUC protocol. The chosen dose did not show any apparent toxicity. To evaluate the toxicity of CLP further, we collected mouse blood to perform blood toxicity profiling. Serum metabolic profiling was done to check liver and kidney functions. No observable toxicity was associated with mice receiving CLP compared to control without CLP (**Figure 6A**). We have performed HPLC analysis to evaluate CLP's distribution in tumor containing bone and observed CLP at a detectable level (**Figure 6B**). Thus, we selected this dosage regimen of 20mg/kg body-wt/mice every alternate days for two weeks for our further investigations in vivo. Of note, about 50% of clomipramine is metabolized in the liver to give the active metabolite, desmethylclomipramine (DCLP). Our HPLC analysis showed that the distribution of DCLP in bone is significantly low compared to that of CLP. Therefore, CLP is expected to be the major active substance to exert any NRP2-targeting antitumor effect in bone.

Milestone(s) Achieved for Aim 1:

Our *in silico* MD simulation study has identified the amino acids of a1, a2, b2 domains at NRP2, which can potentially interact with clomipramine. The MD simulation studies also suggested that by interacting with these amino acids, clomipramine arrest the flexible a1 domain in a folded conformation and thus suggested the mechanism by which clomipramine acts as an inhibitor of NRP2 axis. Biophysical and site-directed mutational studies will be performed to confirm the amino acids of NRP2 that interacts with clomipramine and also the underlying mechanisms by which clomipramine functions as a NRP2 inhibitor.

Our cellular assay suggested that CLP prevents the endosome maturation of prostate cancer cells similar to knocking down NRP2.

We have determined the optimum dose of clomipramine that can be used in the mouse model of prostate cancer to test the efficacy of CLP to enhance the efficacy of chemotherapy. We have detected no obvious toxicity at the optimum dose and detectable level of CLP in mouse tibia.

Specific aim 2: Identify biomarkers for high NRP2 activity in mCRPC patients who may be candidates for NRP2 directed therapy.

Subtask 1: Submit documents for IRB approval.

IRB has been approved for this project.

Subtask 2: Submit documents for HRPO approval.

HRPO has been approved for this project.

Subtask 3: Determine the expression pattern of NRP2 in metastatic tissues of metastatic castration resistant prostate cancer patients:

NRP2 is highly expressed in human NE-like PCa:

We have analyzed NRP2 expression in a tumor microarray (TMA) obtained from the Prostate Cancer Biorepository Network (PCBN). The TMA includes 70 visceral (including liver, lungs, lymph node and kidney) and 51 bone metastatic cores from 45 castration resistant rapid autopsy patients with clinical

history (<https://prostatebiorepository.org/specimens>). 30% of the patients in this PCBN mCRPC cohort had undergone neuroendocrine differentiation during the progression of PCa (**Figure 7A**). Interestingly, 87% of

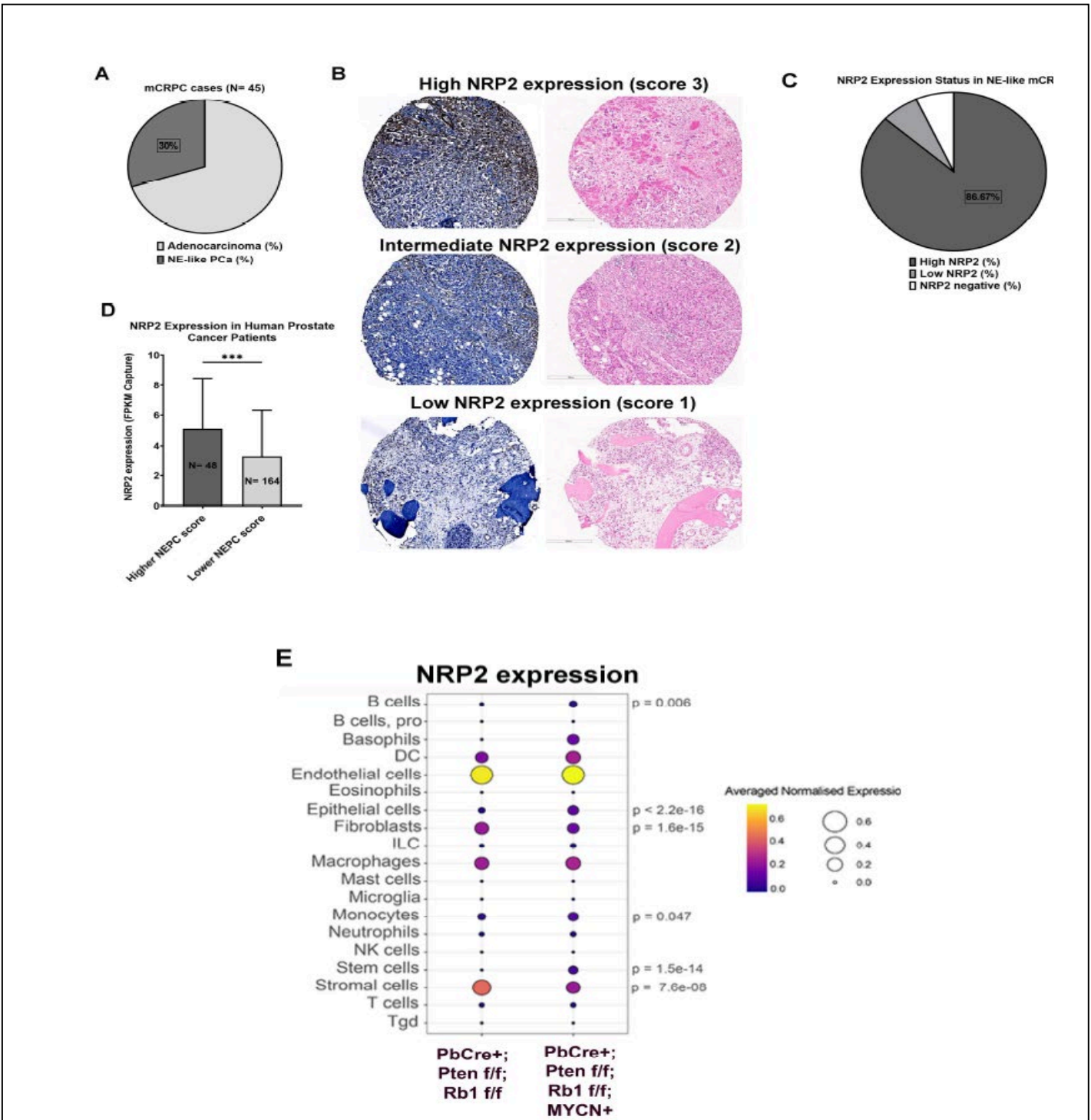


Figure 7: NRP2 is highly expressed in human NE-like PCa and AR negative prostate cancer mouse model.

Analysis of Prostate Cancer Biorepository Network (PCBN) mCRPC patient cohort (N=45). (A) Percentage of mCRPC patients with neuroendocrine differentiation. (B) Representative figures of high, intermediate and low NRP2 expression in patient tissues coming from both visceral and bone metastatic cores. (C) Percentage of patients having high NRP2 expression in NE-like mCRPC patients (IHC score 2 and 3). (D) NRP2 expression in SU2C-PCF patient cohort. (E). Single cell RNA-sequencing analysis of advanced AR negative prostate cancer mouse model (GSE151426) showing NRP2 expression. NEPC score= neuroendocrine prostate cancer score. NE-like PCa= neuroendocrine-like prostate cancer. mCRPC= metastatic castration resistant prostate cancer. SU2C-PCF= Stand Up to Cancer/Prostate Cancer Foundation. Data represented as mean \pm SEM.

the patients with NE-like PCa, having visceral and bone metastatic alike, had very high expression of

NRP2, i.e., NRP2 IHC scores 2 and 3 (**Figures 7B-C**). We further analyzed NRP2 expression in patient cohorts from SU2C-PCF (Stand Up to Cancer/Prostate Cancer Foundation) International Prostate Cancer Dream Team consortium, and a prospective clinical trial (identifier: NCT02432001). Each patient of these cohorts had originally been assigned with a neuroendocrine prostate cancer score (NEPC score). NEPC score was calculated based on the presence of a small-cell population in the samples, expression of canonical NE markers, and androgen receptor (AR) status. While analyzing the NRP2 expression in these cohorts, we found that NRP2 expression was either maintained, or elevated (**Figure 7D**) in NE-like PCa patients. We have analyzed the single-cell RNA-sequencing data of genetically engineered mouse model of advanced AR negative prostate cancer to evaluate if NRP2 upregulation is also observed in PCa animal model. Interestingly, mice with poorly differentiated adenocarcinoma including neuroendocrine trans-differentiation had significantly higher expression of NRP2 (**Figure 7E**). Overall, our analyses of patient and animal samples/databases demonstrated upregulation of NRP2 in poorly differentiated advanced PCa, including NE-like PCa.

Subtask 4: Identify serum markers, which indicates the active NRP2 axis and thus poor prognosis for mCRPC patients: The experiments for this subtask are currently in progress. Enrollment for 60 patients has been completed in Huntsman Cancer Institute at University of Utah. Patient samples have been collected and clinical follow up has begun. Results of the analysis will be reported in the next cycle.

Subtask 5: To determine the independence of NRP2 methylation status as a prognostic biomarker in mCRPC patients undergoing chemotherapy. The experiments for this subtask are currently in progress. After 60 patients that have been enrolled in subtask 4, plasma has been collected serially in all patients 2-3 times each. Cell free DNA is being extracted at present. Germ line DNA has already been purified. Between the two sides in the coming year, NRP2 methylation status will be evaluated. Results will be reported in the next cycle.

Milestone(s) Achieved: High NRP2 expression has been detected in different metastatic sites of prostate cancer. Metastatic neuroendocrine-like prostate cancer cells also express higher level of NRP2.

- Training and professional development provided by the project:

Sanika Bodas (PhD student): Project has provided fellowship to **Ms. Sanika Bodas**, who is doing her PhD under the mentorship of the Principal Investigators of this project, Dr. Kaustubh Datta and Dr. Benjamin A. Teply. The training and research accomplishment that Ms. Bodas received during last year helped her to secure student fellowship from University of Nebraska Medical Center. Ms. Bodas has also attended the following scientific conferences, which has enriched her scientific and professional credentials. She has been selected for OncologyTube interview since her poster was considered as a study of significant clinical relevance.

Presentations and published abstracts in the last year:

1. Sanika Bodas, Ridwan Islam, Sreyashi Bhattacharya, Juhi Mishra, Michael Muders, Samikshan Dutta, Benjamin Teply, Kaustubh Datta. "Understanding the mechanism of Neuropilin-2 upregulation in advanced prostate cancer", AACR 2022, poster presentation at the Annual Conference in April 2022.
2. Sanika Bodas, Ridwan Islam, Sreyashi Bhattacharya, Juhi Mishra, Michael Muders, Samikshan Dutta, Benjamin Teply, Kaustubh Datta. "Understanding the mechanism of Neuropilin-2 upregulation in advanced prostate cancer". Midwest Student Biomedical Research Forum, Oral presentation on March 5, 2022.
3. Pranav Renavikar, Sanika Bodas, Samikshan Datta, Kaustubh Datta, Subodh Lele "Neuropilin-2 expression as a potential marker to predict androgen deprivation therapy outcome in regional node positive prostatic adenocarcinoma" United States and Canadian Academy of Pathology (USCAP) Annual Meeting Abstracts | March 2022

Peer reviewed Publication in the last year:

1. Islam, R., J. Mishra, S. Bodas, S. Bhattacharya, S. K. Batra, S. Dutta and K. Datta (2022). "Role of Neuropilin-2-mediated signaling axis in cancer progression and therapy resistance." *Cancer Metastasis Rev*: May 14;9(1):24. doi: 10.1038/s41413-021-00136-2.
2. Dutta, S., N. S. Polavaram, R. Islam, S. Bhattacharya, S. Bodas, T. Mayr, S. Roy, S. A. Y. Albala, M. I. Toma, A. Darehshouri, A. Borkowetz, S. Conrad, S. Fuessel, M. Wirth, G. B. Baretton, L. C. Hofbauer, P. Ghosh, K. J. Pienta, D. L. Klinkebiel, S. K. Batra, M. H. Muders and K. Datta (2022). "Neuropilin-2 regulates androgen-receptor transcriptional activity in advanced prostate cancer." *Oncogene*. Jul;41(30):3747-3760. doi: 10.1038/s41388-022-02382-y. Epub 2022 Jun 27. PMID: 35754042
3. Islam R, Mishra J, Polavaram NS, Bhattacharya S, Hong Z, Bodas S, Sharma S, Bouska A, Gilbreath T, Said AM, Smith LM, Teply BA, Muders MH, Batra SK, Datta K, Dutta S. (2022) Neuropilin-2 axis in regulating secretory phenotype of neuroendocrine-like prostate cancer cells and its implication in therapy resistance. *Cell Rep*. 2022 Jul 19;40(3):111097. doi: 10.1016/j.celrep.2022.111097.

Dr. Juhi Mishra (Postdoctoral fellow): Dr. Mishra is receiving her post-doctoral training under the mentorship of Dr. Kaustubh Datta. 100% of her FTE is coming from this project. She has recently submitted the "Early Investigator Research Award" (Prostate Cancer Research Program; PC220349) of USAMRAA. The preliminary results presented in this application were developed during her training for last one year while working on the current DoD funded project.

Peer reviewed publication in the last year:

1. Islam, R., J. Mishra, S. Bodas, S. Bhattacharya, S. K. Batra, S. Dutta and K. Datta (2022). "Role of Neuropilin-2-mediated signaling axis in cancer progression and therapy resistance." *Cancer Metastasis Rev*: 1-17.
3. Kobayashi, Y., A. Quispe-Salcedo, S. Bodas, S. Matsumura, E. Li, R. Johnson, M. Choudhury, D. H. Fine, S. Nadimpalli, H. F. Duncan, A. Dudakovic, A. J. van Wijnen and E. Shimizu (2021). "Ezh2 knockout in mesenchymal cells causes enamel hypermineralization." *Biochemical and Biophysical Research Communications* 567: 72-78.

- How were the results disseminated to communities of interest?

Nothing to report

- Plan to do during the next reporting period to accomplish the goals.

We will perform experiments to perform the following subtasks.

For Specific Aim 1:

Subtask 1: We will perform the biophysical analysis to determine whether clomipramine can inhibit the flexibility of the a1 domain of NRP2 as the mechanism for its inhibitory function. We will do site-directed mutagenesis study at the specific amino acid residues of NRP2, which will serve as the binding pocket of clomipramine.

Subtask 3: We will test whether clomipramine inhibits the maturation of autophagosome to autolysosome.

Subtask 4: We will test whether clomipramine can inhibit the recycling of EGFR to the cell surface.

Subtask 7: Efficacy of clomipramine in combination with chemotherapy to prevent prostate tumor growth will be tested in mouse model of prostate cancer bone metastasis.

For Specific Aim 2:

Subtask 4: Patient blood sample collection and other experiments will be performed to identify serum markers, which indicates the active NRP2 axis and thus poor prognosis of mCRPC.

Subtask 5: We will continue our study where we will compare NRP2 methylation profile and AR status in cell free DNA and test whether NRP2 methylation status is an independent prognostic biomarker.

4. Impact

- Impact on the development of the principal discipline (s) of the project

Molecular dynamics simulation study indicated for the first time how an allosteric inhibitor against NRP2 axis can be developed. This finding paves the path for future development of more specific and efficacious inhibitors against NRP2 axis, which could be used as novel drugs to treat therapy resistant prostate cancer patients.

- Impact on other disciplines.

In some specific inflammatory diseases such as sarcoidosis, inflammatory lung disease NRP2 axis in immune cells has been proved to be an effective target. Development of small molecule inhibitors could be useful to treat these diseases.

NRP2 axis is active in other aggressive cancers such as pancreatic cancer, glioblastoma. The small molecule inhibitors against NRP2 axis would be useful for treating these patients.

- Impact on technology transfer.

Nothing to report.

- Impact of society beyond science and technology.

Nothing to report.

5. Changes/Problems

- Changes in approach and reasons for change.

Nothing to report

- Actual or anticipated problems or delays and actions or plans to resolve them.

Nothing to report

- Significant changes in use or care of human subjects, vertebrate animals, biohazards, and/or select agents.

Nothing to report

6. Products

- Journal publications

1. Islam, R., J. Mishra, S. Bodas, S. Bhattacharya, S. K. Batra, S. Dutta and K. Datta (2022). "Role of Neuropilin-2-mediated signaling axis in cancer progression and therapy resistance." *Cancer Metastasis Rev*: May 14;9(1):24. doi: 10.1038/s41413-021-00136-2.

2. Dutta, S., N. S. Polavaram, R. Islam, S. Bhattacharya, S. Bodas, T. Mayr, S. Roy, S. A. Y. Albala, M. I. Toma, A. Darehshouri, A. Borkowetz, S. Conrad, S. Fuessel, M. Wirth, G. B. Baretton, L. C. Hofbauer, P. Ghosh, K. J. Pienta, D. L. Klinkebiel, S. K. Batra, M. H. Muders and K. Datta (2022). "Neuropilin-2 regulates androgen-receptor transcriptional activity in advanced prostate cancer." *Oncogene*. Jul;41(30):3747-3760. doi: 10.1038/s41388-022-02382-y. Epub 2022 Jun 27. PMID: 35754042

3. Islam R, Mishra J, Polavaram NS, Bhattacharya S, Hong Z, Bodas S, Sharma S, Bouska A, Gilbreath T, Said AM, Smith LM, Teply BA, Muders MH, Batra SK, Datta K, Dutta S. (2022) Neuropilin-2 axis in regulating secretory phenotype of neuroendocrine-like prostate cancer cells and its implication in therapy resistance. *Cell Rep*. 2022 Jul 19;40(3):111097. doi: 10.1016/j.celrep.2022.111097.

- Books or other non-periodical, one-time publications

Nothing to report

- Other publications, conference papers, and presentations

1. Sanika Bodas, Ridwan Islam, Sreyashi Bhattacharya, Juhi Mishra, Michael Muders, Samikshan Dutta, Benjamin Teply, Kaustubh Datta. "Understanding the mechanism of Neuropilin-2 upregulation in advanced prostate cancer", AACR 2022, poster presentation at the Annual Conference in April 2022.

2. Sanika Bodas, Ridwan Islam, Sreyashi Bhattacharya, Juhi Mishra, Michael Muders, Samikshan Dutta, Benjamin Teply, Kaustubh Datta. "Understanding the mechanism of Neuropilin-2 upregulation in advanced prostate cancer". Midwest Student Biomedical Research Forum, Oral presentation on March 5, 2022.

3. Pranav Renavikar, Sanika Bodas, Samikshan Datta, Kaustubh Datta, Subodh Lele "Neuropilin-2 expression as a potential marker to predict androgen deprivation therapy outcome in regional node positive prostatic adenocarcinoma" United States and Canadian Academy of Pathology (USCAP) | Annual Meeting Abstracts | March 2022.

7. Participants & Other collaborating organizations.

Individuals who have worked on the project.

Name	Kaustubh Datta
Project Role	PI
Researcher Identifier (e.g. ORCID ID)	0000-0001-5940-6652
Nearest person month worked	1.2 calendar month
Contribution to Project	Dr. Datta is involved in planning, setup, bench experimentation, organization, and supervision of the project. He is responsible for analysis and publication of results.
Funding Support	

Name	Benjamin A. Teply
Project Role	Partnering PI
Researcher Identifier (e.g. ORCID ID)	
Nearest person month worked	0.6 Calendar month
Contribution to Project	Dr. Teply has been involved in the administrative, scientific and collaborative aspects of the project. He is overseeing the prospective sample collection for Aim 2.2 and 2.3 at UNMC, specifically with leading patient recruitment and longitudinal clinical outcome data acquisition. In addition, he is overseeing the research study personnel (research nurse coordinator, PhD student, and data abstractor). He is also responsible for maintaining IRB standards and obligations, and oversees the biomarker analysis.
Funding Support	

Name	Manish Kohli
Project Role	Co-Investigator
Researcher Identifier (e.g. ORCID ID)	
Nearest person month worked	0.36 Calendar months
Contribution to Project	Dr. Kohli has overseen all research (administrative, scientific, and collaborative) aspects pertaining to the bio-repository plasma specimen bank and the prospective collection of samples/clinical outcome data in the mCRPC patients at Huntsman Cancer Institute (HCI) at University of Utah. He is updating the clinical outcomes in the clinical database on longitudinal follow up in concert with database personnel and coordinator and will continue after enrollment as well. He also oversees the prospective sample collection for Aim 2.2 at HCI and interacts with the research study personnel (research nurse; coordinator) and the UNMC team.
Funding Support	NIH, local funding

Name	Ridwan Islam
Project Role	Graduate Student
Researcher Identifier (e.g. ORCID ID)	
Nearest person month worked	3

Contribution to Project	Dr. Islam was responsible for the studies being performed in Aim 1 of the project.
Funding Support	NIH, UNMC graduate fellowship

Name	Samikshan Dutta
Project Role	Co-investigator
Researcher Identifier (e.g. ORCID ID)	
Nearest person month worked	3.6 calendar months
Contribution to Project	Helped graduate students and postdoctoral fellows to perform animal experiments and other cell biology-based experiments.
Funding Support	NIH

Name	Sanika Bodas
Project Role	Graduate Student
Researcher Identifier (e.g. ORCID ID)	
Nearest person month worked	11 calendar months
Contribution to Project	Ms. Bodas has involved in the methylation profile of NRP2 gene in tissues and cell free DNA
Funding Support	

Name	Juhi Mishra
Project Role	Post-Doctoral fellow
Researcher Identifier (e.g. ORCID ID)	
Nearest person month worked	10.8 calendar months
Contribution to Project	performed animal experiments and other biochemical and cell biology-based experiments.
Funding Support	

Name	Dipanwita Das
Project Role	Graduate Student
Researcher Identifier (e.g. ORCID ID)	
Nearest person month worked	1.0 calendar months
Contribution to Project	Performed biochemical and cell biology-based experiments.
Funding Support	

Name	Clair Hanson
Project Role	Laboratory Technician (HCI)
Researcher Identifier (e.g. ORCID ID)	
Nearest person month worked	1.8 calendar months
Contribution to Project	Initial processing of the whole blood large volume (45 ml) blood sample obtained on enrolled patients and extraction of cell free DNA.
Funding Support	

Name	Mathew Larsen
Project Role	Research Study Coordinator (HCI)
Researcher Identifier (e.g. ORCID ID)	
Nearest person month worked	1.2 calendar months
Contribution to Project	Recruitment and follow-up of patients after enrollments. Specifically, this involves recruiting the mCRPC subjects from the clinics for the study aim (who will be scheduled for visits).
Funding Support	

- Has there been a change in the active other support of the PD/PI (s) or senior/key personnel since the last reporting period?

Nothing to Report.

- What other organizations were involved as partners?
 - Organization name:
Huntsman Cancer Institute (HCI) at University of Utah
 - Location of Organization:
Salt Lake City, UT
 - Partner's contribution to the project:
Collaboration

8. **Special Reporting Requirements.**

This is a collaborative award. Independent reports have been submitted by the initiating PI, Dr. Kaustubh Datta and the partnering PI, Dr. Benjamin A. Teply.

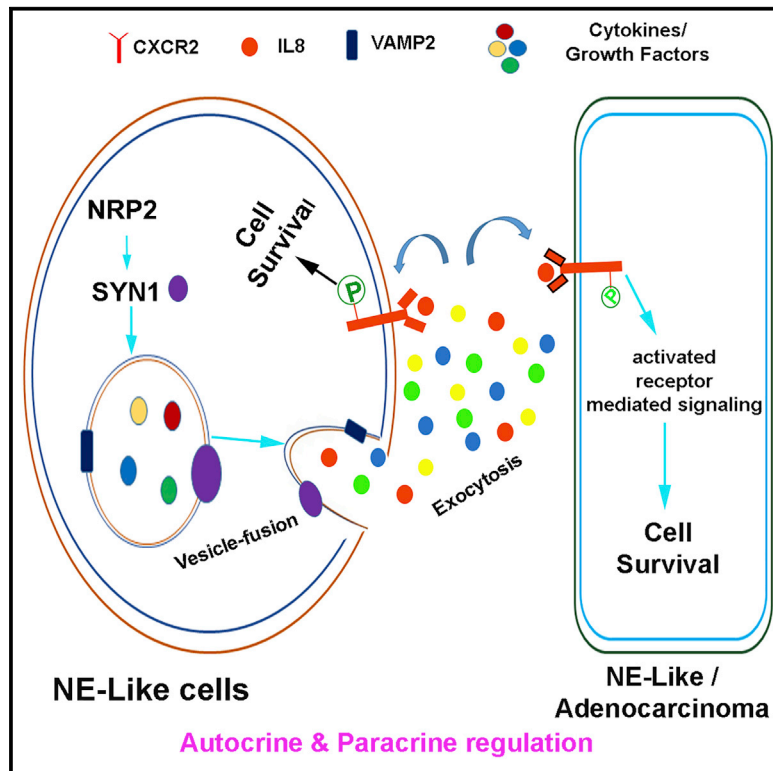
9. Appendices

PDF versions of the following research articles have been provided, whose research were partly supported by the current DoD funding.

1. Islam, R., J. Mishra, S. Bodas, S. Bhattacharya, S. K. Batra, S. Dutta and K. Datta (2022). "Role of Neuropilin-2-mediated signaling axis in cancer progression and therapy resistance." *Cancer Metastasis Rev*: May 14;9(1):24. doi: 10.1038/s41413-021-00136-2.
2. Dutta, S., N. S. Polavaram, R. Islam, S. Bhattacharya, S. Bodas, T. Mayr, S. Roy, S. A. Y. Albala, M. I. Toma, A. Darehshouri, A. Borkowetz, S. Conrad, S. Fuessel, M. Wirth, G. B. Baretton, L. C. Hofbauer, P. Ghosh, K. J. Pienta, D. L. Klinkebiel, S. K. Batra, M. H. Muders and K. Datta (2022). "Neuropilin-2 regulates androgen-receptor transcriptional activity in advanced prostate cancer." *Oncogene*. Jul;41(30):3747-3760. doi: 10.1038/s41388-022-02382-y. Epub 2022 Jun 27. PMID: 35754042

Neuropilin-2 axis in regulating secretory phenotype of neuroendocrine-like prostate cancer cells and its implication in therapy resistance

Graphical abstract



Authors

Ridwan Islam, Juhi Mishra, Navatha Shree Polavaram, ..., Surinder K. Batra, Kaustubh Datta, Samikshan Dutta

Correspondence

kaustubh.datta@unmc.edu (K.D.), samikshan.dutta@unmc.edu (S.D.)

In brief

Islam et al. observe high expression of a cell surface receptor, neuropilin-2 (NRP2), in neuroendocrine-like prostate cancer. NRP2 regulates the secretion of cytokines by facilitating the fusion of secretory vesicles to cell membrane. The secretory products protect not only the neuroendocrine cells but also the adjacent adenocarcinoma from chemotherapies.

Highlights

- NRP2 is highly expressed in NE-like prostate cancer
- NRP2 regulates the fusion of secretory vesicles to plasma membrane
- The secretion of several cytokines, including IL-8, is regulated by NRP2
- NRP2-depletion from NE-like cells sensitizes adjacent adenocarcinoma to chemotherapy



Article

Neuropilin-2 axis in regulating secretory phenotype of neuroendocrine-like prostate cancer cells and its implication in therapy resistance

Ridwan Islam,¹ Juhi Mishra,^{1,4} Navatha Shree Polavaram,^{1,4} Sreyashi Bhattacharya,¹ Zhengdong Hong,¹ Sanika Bodas,¹ Sunandini Sharma,¹ Alyssa Bouska,¹ Tyler Gilbreath,¹ Ahmed M. Said,² Lynette M. Smith,¹ Benjamin A. Teply,¹ Michael H. Muders,³ Surinder K. Batra,¹ Kaustubh Datta,^{1,*} and Samikshan Dutta^{1,5,*}

¹Department of Biochemistry and Molecular Biology, University of Nebraska Medical Center, BCC, Omaha, NE 68198, USA

²Department of Pharmaceutical Organic Chemistry, Faculty of Pharmacy, Helwan University, Ein-Helwan, Helwan, Cairo, Egypt

³Department of Prostate Cancer Research, Center for Pathology, University of Bonn Medical Center, Bonn, Germany

⁴These authors contributed equally

⁵Lead contact

*Correspondence: kaustubh.datta@unmc.edu (K.D.), samikshan.dutta@unmc.edu (S.D.)

<https://doi.org/10.1016/j.celrep.2022.111097>

SUMMARY

Neuroendocrine (NE)-like tumors secrete various signaling molecules to establish paracrine communication within the tumor milieu and to create a therapy-resistant environment. It is important to identify molecular mediators that regulate this secretory phenotype in NE-like cancer. The current study highlights the importance of a cell surface molecule, Neuropilin-2 (NRP2), for the secretory function of NE-like prostate cancer (PCa). Our analysis on different patient cohorts suggests that NRP2 is high in NE-like PCa. We have developed cell line models to investigate NRP2's role in NE-like PCa. Our bioinformatics, mass spectrometry, cytokine array, and other supporting experiments reveal that NRP2 regulates robust secretory phenotype in NE-like PCa and controls the secretion of factors promoting cancer cell survival. Depletion of NRP2 reduces the secretion of these factors and makes resistant cancer cells sensitive to chemotherapy *in vitro* and *in vivo*. Therefore, targeting NRP2 can revert cellular secretion and sensitize PCa cells toward therapy.

INTRODUCTION

Lineage plasticity leading to androgen receptor (AR)-independent prostate cancer (PCa) has gained prominence recently and is being studied as one of the underlying reasons for resistance to second-generation AR inhibitors (ARIs) (Aggarwal et al., 2018; Beltran et al., 2016; Butler and Huang, 2021). Lineage plasticity can be defined as the ability of a cell to change itself into a new phenotype, allowing the cancer cells to survive in a harsh environment such as hypoxia or nutrient deprivation, and is responsible for intratumoral heterogeneity (Beltran et al., 2016; Ku et al., 2017; Mu et al., 2017). Plasticity-driven intratumoral heterogeneity has been attributed as a major reason for acquired resistance to therapy in PCa (Jolly et al., 2018). One of the major histologic subtypes, which appears due to the oncogenic and therapy-induced plasticity of PCa cells, is the transformation from adenocarcinoma to high-grade neuroendocrine (NE)-like tumors (Aggarwal et al., 2018; Beltran et al., 2016; Butler and Huang, 2021; Tritschler et al., 2017). Therefore, the co-existence of adenocarcinoma (AR-high/NE-marker low) and NE-like (AR-low/NE-marker high) tumor cells is often observed in treatment-resistant aggressive PCa (Quintanal-Villalonga et al., 2020; Li et al., 2019). These NE-like PCa cells do not depend on AR-transcriptional activity for their growth and survival (Mu et al., 2017) and are thus resistant to ARIs. About 25% of the

aggressive metastatic castration-resistant PCa (mCRPC) patients develop such treatment-induced NE prostatic adenocarcinoma (t-NEPC) or NE-like PCa (Tritschler et al., 2017; Aparicio et al., 2011). The number of diagnosed t-NEPC cases in PCa patients has been increasing with the advancement of our understanding on the NE-like phenotype (Conteduca et al., 2019). Additionally, patients with NE-like PCa show poor prognosis owing to the heterogeneous feature of the tumors as well as unavailability of effective therapy against this type of cancer (Beltran et al., 2016; Akamatsu et al., 2018). Therefore, lucid understanding on the molecular mechanism of therapy resistance in NE-like PCa and identification of potential molecular targets for developing an effective therapeutic strategy are required.

NE-like cells morphologically display long dendritic processes (Sang et al., 2016) and contain a wide array of dense-core secretory granules (Rindi and Wiedenmann, 2020). The genes that are upregulated during NE-like transdifferentiation include neuronal transcription factors, membrane ion channels, receptors, and secreted biogenic amines, peptides, and cytokines. Neurosecretory peptides like bombesin, gastrin, neuron-specific enolase, parathyroid hormone-related peptide (PTHrP), and cytokines such as interleukin (IL-8) and vascular endothelial growth factor (VEGF) have been reported to act both in an autocrine and paracrine manner to stimulate growth and survival of both the NE-like cancer cells and the surrounding adenocarcinoma



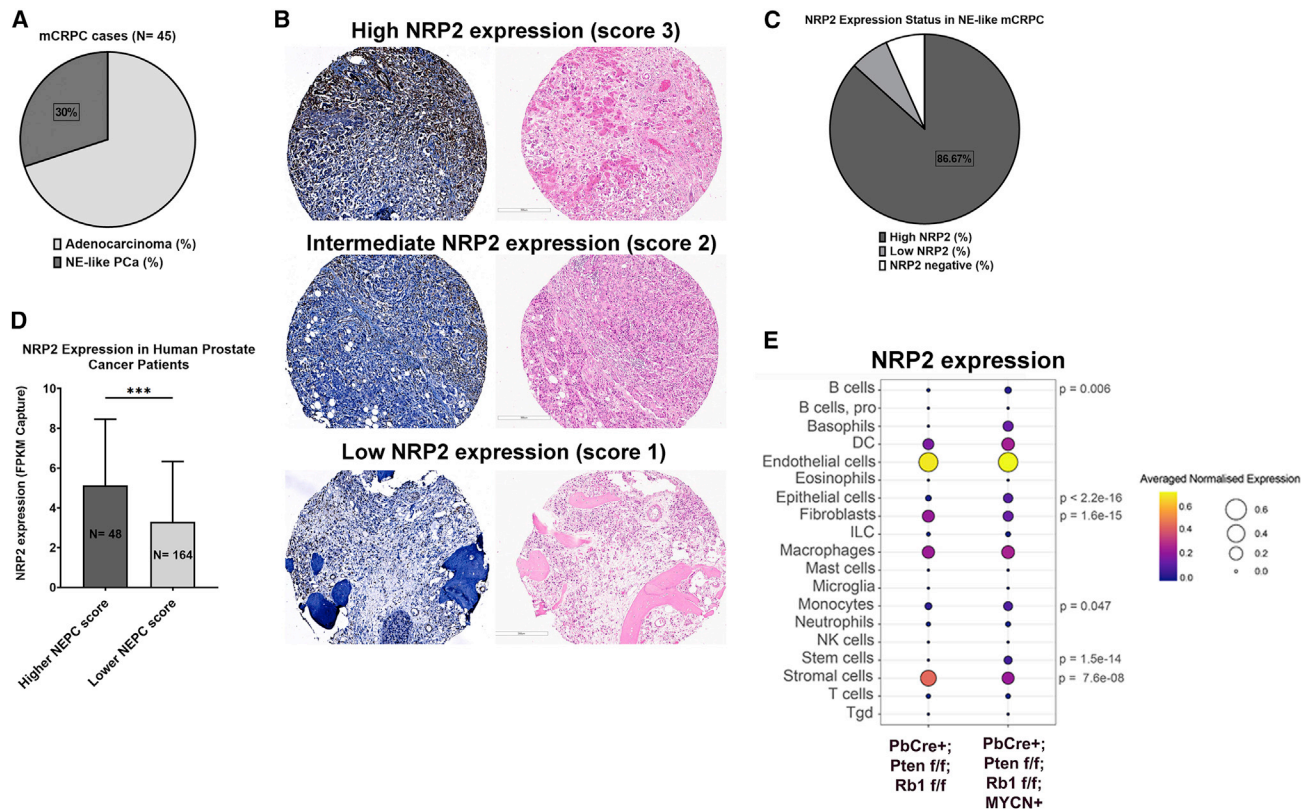


Figure 1. NRP2 is highly expressed in human NE-like PCa and AR-negative PCa mouse model

(A–C) Analysis of Prostate Cancer Biorepository Network (PCBN) mCRPC patient cohort (N = 45).

(A) Percentage of mCRPC patients with NE differentiation.

(B) Representative figures of high, intermediate, and low NRP2 expression in patient tissues coming from both visceral and bone metastatic cores.

(C) Percentage of patients having high NRP2 expression in NE-like mCRPC patients (IHC score 2 and 3).

(D) NRP2 expression in SU2C-PCF patient cohort.

(E) Single-cell RNA sequencing (RNA-seq) analysis of advanced AR-negative PCa mouse model (GSE151426) showing NRP2 expression. NEPC, NE PCa. Data represented as mean \pm SEM.

(Rindi and Wiedenmann, 2020; Cives et al., 2019; Somasundaram and Taraska, 2018; Zhang et al., 2018; Jin et al., 2004). These secretory factors influence the tumor microenvironment by promoting angiogenesis and anti-tumor immune responses and therefore induce cancer progression (Wright et al., 2003; Zhang et al., 2018). Blocking such pathways is important not only to sensitize the NE-like colonies to therapy but also to reprogram the microenvironment toward more favorable prognosis of the disease. However, a lack of comprehensive understanding of the mechanism for the secretory pathways limits its clinical implication. Therefore, it is important to study the molecular mechanisms responsible for the secretory function of NE-like PCa cells and whether the resulting cell-cell communication has an influence on the development of resistance to therapy.

Our results in this paper suggested that neuropilin-2 (NRP2), a transmembrane, non-kinase receptor belonging to the neuropilin (NRP) family (Dutta et al., 2016b; Roy et al., 2018; Stanton et al., 2013), is important for the cellular secretory functions. Previous studies, including several reports published by our group, have suggested that NRP2 promotes metastasis and is associated with poor cancer prognosis (Roy et al., 2018; Stanton et al.,

2013; Borkowetz et al., 2020; Schulz et al., 2019). In this current study, we have identified significant NRP2 expression in NE-like PCa patient tissues. Our *in vitro* experiments and *in vivo* studies suggested that, by regulating secretory function, NRP2 promotes growth and survival of NE-like PCa upon treatment with chemotherapeutic drugs. Our study identifies a novel NE-like PCa-specific mechanism of NRP2 in conferring therapy resistance to cancer cells and raises an opportunity to develop an NRP2 inhibitor for future therapeutic efficacy.

RESULTS

NRP2 is highly expressed in human NE-like PCa

NRP2 expression was analyzed in a tumor microarray (TMA) obtained from the Prostate Cancer Biorepository Network (PCBN) (Labrecque et al., 2019), which includes 70 visceral (including liver, lungs, lymph node, and kidney) and 51 bone metastatic cores from 45 castration-resistant rapid autopsy patients with clinical history. Thirty percent of the patients in this PCBN mCRPC cohort had undergone NE differentiation (NED) during the progression of PCa (Figure 1A). Interestingly, 87% of the patients with NE-like PCa

having visceral and bone metastasis showed high expression of NRP2 with immunohistochemistry (IHC) scores 2 and 3 (Figures 1B and 1C). We further analyzed NRP2 expression in patient cohorts from the Stand Up to Cancer/Prostate Cancer Foundation (SU2C-PCF) (Abida et al., 2019), and a prospective clinical trial (identifier: NCT02432001) (Aggarwal et al., 2018). Each patient of these cohorts had originally been assigned with a NE PCA (NEPC) score (Abida et al., 2019; Aggarwal et al., 2018). NEPC score was calculated based on the presence of a small-cell population in the samples, expression of canonical NE markers, and AR status (Abida et al., 2019; Aggarwal et al., 2018). In these cohorts, we found that NRP2 expression was either maintained (Aggarwal et al., 2018) (Figure S1A), or elevated (Abida et al., 2019) (Figure 1D) in NE-like PCA patients. We further analyzed the single-cell RNA sequencing (RNA-seq) data of genetically engineered mouse model of advanced AR-negative PCA (Brady et al., 2021) to evaluate if NRP2 upregulation is also observed in PCA animal model. Interestingly, mice with poorly differentiated adenocarcinoma including NE transdifferentiation had significantly higher expression of NRP2 (Figure 1E). Overall, our analyses of patient and animal samples/databases demonstrated upregulation of NRP2 in poorly differentiated advanced PCA, including NE-like PCA.

Development and characterization of NE-like PCA cells

To test whether NRP2 can be a potential target against NE-like therapy-resistant PCA, we developed and characterized NE-like PCA cells in our laboratory. Previous studies highlighted that simultaneous loss of function of *RB1* and *TP53* genes often leads to the transdifferentiation of prostate adenocarcinoma into the NE-like phenotype (Ku et al., 2017; Mu et al., 2017). Upon NE-like transdifferentiation, prostate epithelial cells develop long neurite-like branched processes (Sang et al., 2016) with concomitant expression of markers, such as CHGA, Syp, AURKA, SOX2, N-Myc, ASCL1, and NSE (Beltran et al., 2016; Ku et al., 2017). During such transformation, AR-dependent PCA cells become independent of the AR axis for their survival, and eventually resist the second-generation AR-targeted therapies (Mu et al., 2017; Beltran et al., 2011, 2016; Ku et al., 2017). To get the molecular insights of the therapy resistance and identify potential molecular targets against NE-like PCA, we developed two cell line models. First, we used an mCRPC cell line, C4-2, which is an AR-responsive line, and knocked down *RB1* and *TP53* genes using shRNA to develop stable C4-2 *RB1* and *TP53* double-knockdown (DKD) cells. The idea was to mimic the phenotype associated with NE-like transdifferentiation upon *RB1* and *TP53* simultaneous loss of function. Second, we utilized another advanced mCRPC cell line, C4-2B, and cultured it under exposure of 20 μ M enzalutamide for 12 weeks to develop C4-2B enzalutamide-resistant (ER) cells. This mimics the NE-like lineage switch upon prior exposure to second-generation AR-targeted therapies. The two developed cell lines were characterized for NE-like features (Figure 2).

C4-2 *RB1* and *TP53* DKD cells develop NE-like phenotype

We observed that *TP53* and *RB1* genes were efficiently knocked down in C4-2 *RB1* and *TP53* DKD cells (Figures 2A and S1B). The cells developed long neurite-like branched processes (Fig-

ure S1C), suggesting attainment of NE-like morphology (Sang et al., 2016). We have further characterized those neurite structures by staining them with neurite-specific β 3-tubulin (Figure 2B). We performed RNA-seq analyses of the adenocarcinoma cells (C4-2) and the developed NE-like PCA cells (DKD) to characterize the development of NE-like features. Our RNA-seq data revealed that REST-repressed genes, such as *SYP*, *CHGA*, and *INSM1*; transcription factors regulating NE differentiation, such as *SOX2*, *POU3F2*, and *NKX2-1*; and other genes involved in NE-like cancers, such as *NCAM1* and *MYCN* were significantly upregulated in the developed NE-like cells. On the other hand, AR, and other AR-regulated genes, such as *KLK3*, *CHRNA2*, and *NKX3-1*, were significantly downregulated in the NE-like PCA cells compared with adenocarcinoma (Figure 2C). These genetic signatures were previously reported to be present in NE-like PCA and in cancer cells undergoing NE-like transdifferentiation (Labrecque et al., 2019; Mu et al., 2017; Beltran et al., 2016). We validated our RNA-seq data using real-time PCR and western blot to check the expression of canonical NE markers (Figures 2D and S1D). Interestingly, we found either low or no expression of AR and its downstream target in the DKD cells compared with the control (Figures S1E and S1F), suggesting an AR-independent survival mechanism in these cells. We checked whether these cells developed resistance to enzalutamide following *RB1* and *TP53* depletion, as observed in the PCA patients (Labrecque et al., 2019; Ku et al., 2017; Beltran et al., 2016; Tritschler et al., 2017; Nadal et al., 2014). Indeed, the cells developed significant resistance to enzalutamide compared with control (Figure S1G). Together, the above observations suggested the development of NE-like characteristics in DKD cells. We then evaluated the NRP2 expression in the developed NE-like PCA cells. Interestingly, NRP2 was highly upregulated upon *RB1* and *TP53* depletion in the cells (Figure 2E), suggesting the presence of the active NRP2 axis in the NE-like DKD cells. We then evaluated if NRP2 is involved in NE-like transdifferentiation by overexpressing NRP2 in adenocarcinoma cells and observed any changes in NE-marker expression. Significant changes in NE markers were not observed upon NRP2 overexpression in adenocarcinoma cells (Figures S1H and S1I). Therefore, these results suggested that NRP2 is upregulated in PCA cells during NE-like transdifferentiation but it is not an inducer of the cellular process leading to lineage switch.

C4-2B ER cells attain NE-like characteristics

The developed C4-2B ER cells also attained NE-like cell morphology (long neurite-like branched processes) (Figure S1J). We characterized the cells by checking the expression of REST-repressed genes, such as *SYP* and *CHGA*; transcription factors regulating NE differentiation, such as *SOX2*; and other genes implicated in NE-like differentiation, such as *AURKA*, *NSE*, and *MYCN* (Figures 2F and S1K). Our data revealed a downregulation of both *RB1* and *TP53* protein expression upon prolonged exposure to enzalutamide (Figure 2G). NRP2 protein expression was upregulated in C4-2B ER cells (Figure 2H), so we used these cell lines to test whether NRP2 can be a potential molecular target in NE-like therapy-resistant PCA.

In addition, we used *de novo* NEPC cell line, NCI-H660, for further validation of our results. NRP2 expression was also found to be significantly high in NCI-H660 cells (Figure S1L).

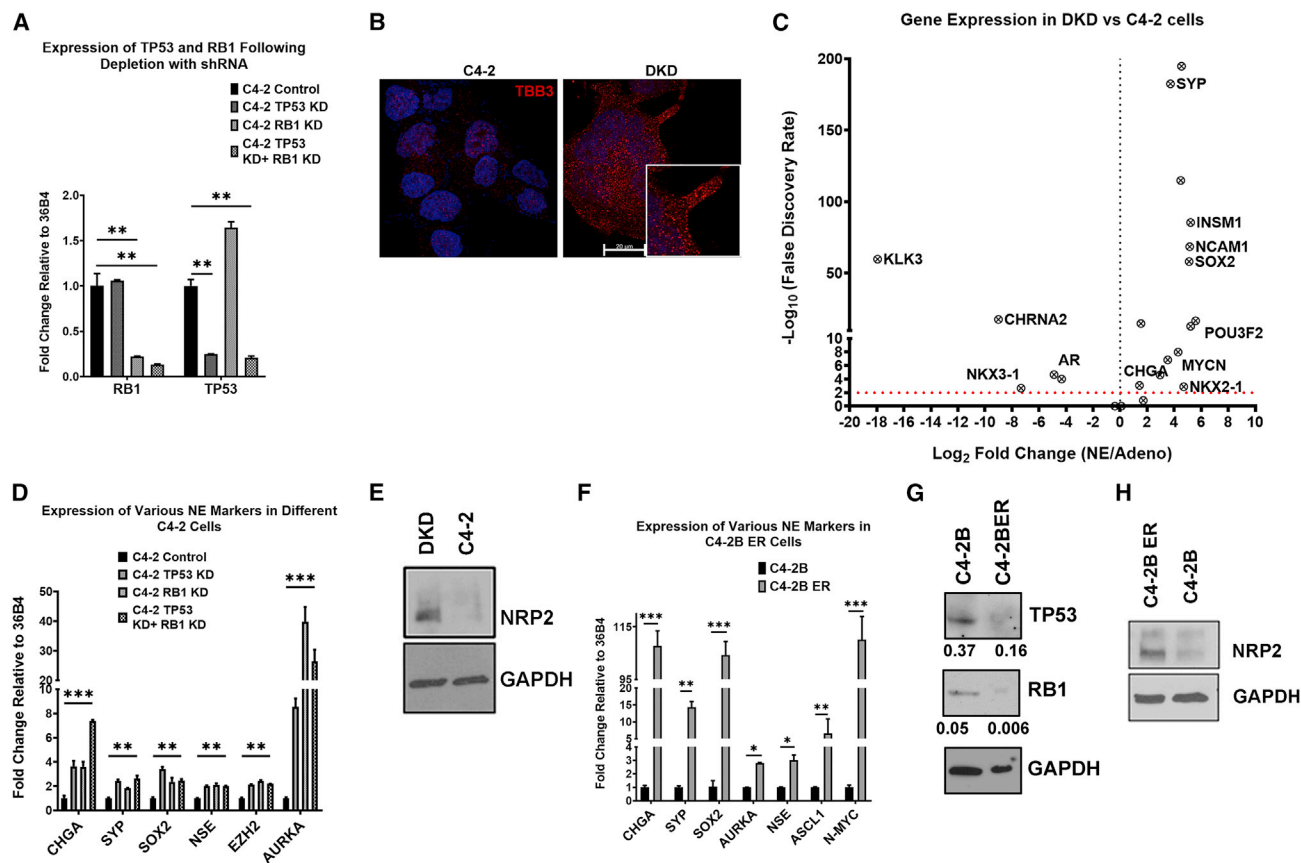


Figure 2. Characterization of NE-like PCa cells

(A–E) Characterization of C4-2 TP53 + RB1 double-knockdown (DKD) cell.

(A) *TP53* and *RB1* expression by real-time PCR.

(B) The appearance of long neurite-like branched processes in DKD cells shown by B3-tubulin staining (red).

(C) RNA-seq analysis of DKD and its syngeneic adenocarcinoma cells, C4-2.

(D) Real-time PCR of canonical NE markers.

(E) NRP2 expression in DKD cells compared with C4-2.

(F–H) Characterization of C4-2B enzalutamide-resistant (ER) cells. (F) Real-time PCR of canonical NE markers. (G) TP53 and RB1 protein expression in C4-2B ER cells compared with its syngeneic adenocarcinoma cells, C4-2B. The densitometric calculations are provided below each panel. (H) NRP2 expression in C4-2B ER cells compared with C4-2B. Data represented as mean \pm SEM ($n = 3$).

NRP2 depletion increases the efficacy of the front-line chemotherapeutic agents

Our study showed that DKD is significantly resistant to docetaxel compared with C4-2 control (Figure S2A). We further observed that NRP2 depletion significantly increased the efficacy of this cytotoxic drug as confirmed by the cell death assays (Figure 3). Initially, we checked the half maximal inhibitory concentration (IC_{50}) of docetaxel alone in DKD cells (Figure S2B) and chose a dose (10 nM) close to IC_{20} for our subsequent experiments, where 80% of cells were still viable. We used two different NRP2-specific small interfering RNAs (siRNAs) for our cell death experiments. Both the siRNAs showed significant NRP2 depletion in DKD cells and could enhance cell death at a similar level following docetaxel treatment, suggesting the on-target effect of NRP2 depletion (Figures 3A–3C). Further, overexpression of NRP2 in NRP2-knockdown DKD cells reverted its chemo-resistant phenotype, confirming the effect of NRP2 in promoting do-

cetaxel resistance of NE-like PCa cells (Figures 3D–3F). Moreover, NRP2 depletion significantly increased the ability of docetaxel to hinder the colony formation of NE-like PCa cells (Figures 3G–3I). In addition, we performed the colony formation assays with DKD (NE-like cells) under the influence of VEGF-C, the ligand of NRP2. Our results demonstrated that the addition of recombinant VEGF-C significantly increased both the number and size of the colonies (Figures S2C and S2D). NRP2 ablation in the presence of exogenous VEGF-C could reduce the number and especially the size of the colonies (Figures S2C–S2E). Our results thus indicated that NRP2 ligands such as VEGF-C secreted by the surrounding cells in the microenvironment can promote the tumorigenic potential of cancer cells, and targeting NRP2 could decrease their tumorigenicity.

We also performed MTT assay and found that NRP2 depletion increased the efficacy of docetaxel (Figures S2F and S2G), recapitulating the results obtained from the above-mentioned cell

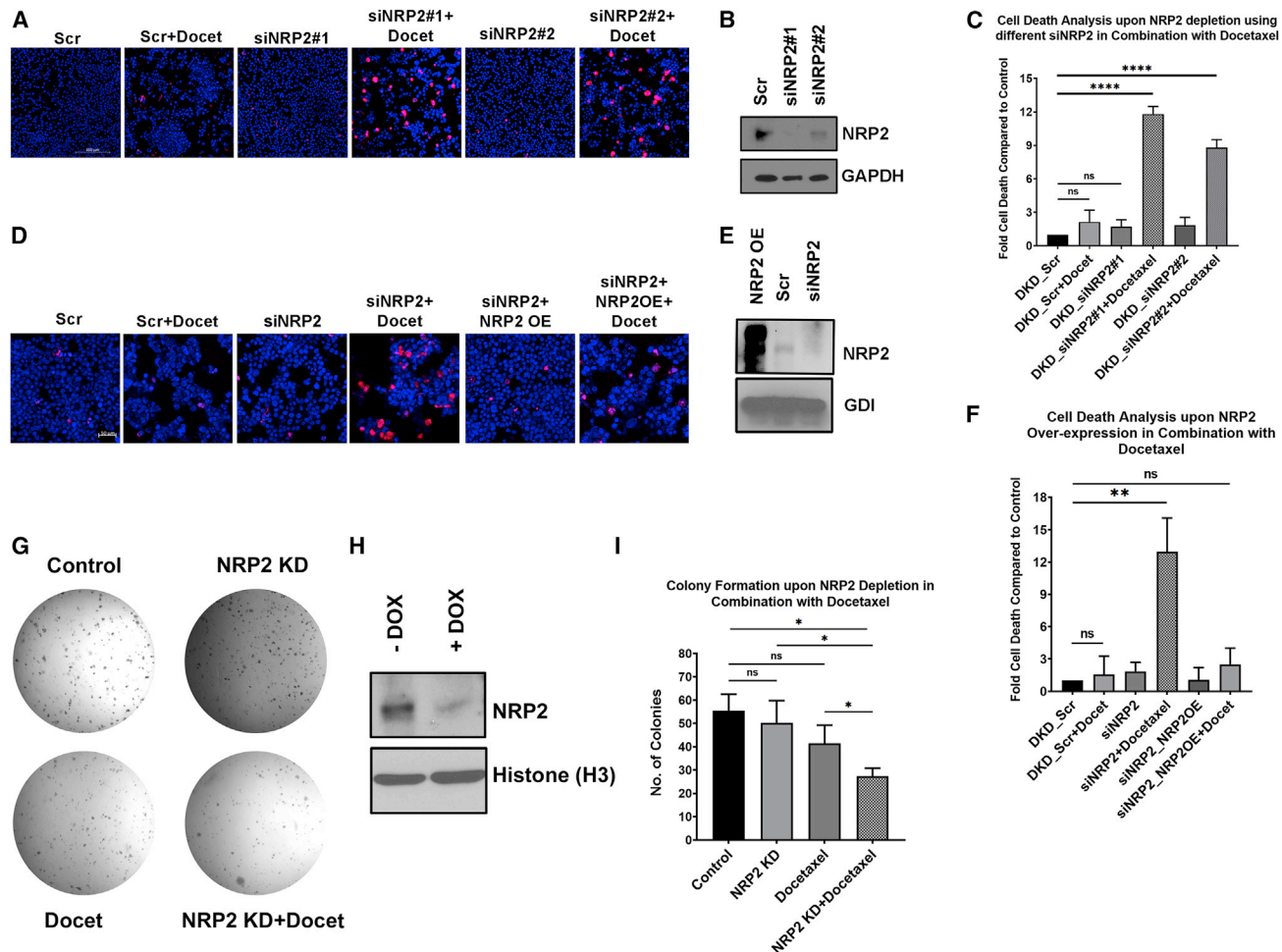


Figure 3. NRP2 depletion increases the efficacy of the front-line chemotherapeutic agents

(A) Effect of NRP2 knockdown on the efficacy of docetaxel by propidium iodide (PI; red)-based cell death analysis.
 (B) Western blot showing the efficiency of different siRNAs to knock down NRP2.
 (C) Quantitation of (A).
 (D) Reversal of the chemo-sensitive phenotype of NRP2 knocked down NE-like (DKD) cells upon NRP2 overexpression by PI (red)-based cell death analysis.
 (E) Western blot showing NRP2 overexpression.
 (F) Quantitation of (D).
 (G–I) DKD cells having stable shNRP2 expression upon Dox induction were used.
 (G) Colony formation assay showing the effect of NRP2 depletion on the efficacy of docetaxel to inhibit the clonogenic potential of the cells.
 (H) Western blot of Dox-inducible NRP2 knockdown.
 (I) Quantitation of (G). OE, overexpression; DOX, doxycycline. Data represented as mean \pm SEM (n = 3).

death analyses. Similarly, NE-like C4-2B ER PCa cells were also highly resistant to docetaxel (Figures S2H and S2I), and NRP2 depletion significantly increased docetaxel efficacy in C4-2B ER cells (Figures S2J and S2K). These results demonstrate that, despite docetaxel therapy having been found to be less effective against the NE-like PCa (Akamatsu et al., 2018), its efficacy can be significantly improved if combined with NRP2 depletion.

We next tested whether targeting NRP2 can increase the efficacy of platinum chemotherapy-etoposide combination in NE-like PCa. Since NE-like PCa is resistant to docetaxel, platinum chemotherapy in combination with etoposide is an option to manage patients with NE-like phenotype (Akamatsu et al., 2018; Tritschler et al., 2017). Therefore, cisplatin and etoposide

were tested for their efficacies in DKD cells, with and without NRP2 knockdown (NRP2 KD). MTT assay revealed that the efficacy of cisplatin-etoposide combination was significantly increased when NRP2 was depleted in the cancer cells; i.e., lower dose of the platinum-etoposide doublet therapy is required to obtain potent cytotoxic effect (Figure S2L).

NRP2 depletion increases the efficacy of chemotherapy *in vivo*

NRP2 depletion increased the efficacy of platinum chemotherapy-etoposide doublet

A subcutaneous PCa mouse model was used to evaluate the efficacy of cisplatin-etoposide doublet therapy upon NRP2

depletion. For this, we have developed NE-like DKD cells that stably express shNRP2 (DKD-shNRP2) under the control of doxycycline (Dox) (Figure S3A). DKD-shNRP2 cells (1×10^6 cells) were implanted into the right flank of athymic nude mice. Once the tumors became palpable, animals were randomly divided into four groups ($n = 5$). The first group acts as a control. The second group received Dox (2 mg/mL) in water (2% sucrose) to deplete NRP2 in the cancer cells. In the third group, cisplatin (5 mg/kg body weight) and etoposide (8 mg/kg body weight) were administered (intraperitoneally [i.p.]) on day 1 and day 2, respectively, on a weekly basis for 3 weeks. The fourth group received both Dox in water and cisplatin-etoposide doublet. Tumors were regularly monitored, and tumor size was measured over the period until sacrifice. We observed that the growth of NE-like tumors in mice was slower initially. However, once formed, the tumors became very aggressive and grew persistently. A similar trait was reported previously for NE tumors, including NE-like PCa (Guo et al., 2019; Benten et al., 2018). Depletion of NRP2 along with the doublet therapy significantly reduced the tumor volume compared with control, only doublet therapy, and only NRP2 depletion, respectively (Figures 4A and S3B). In addition, tumor growth curve was constructed by plotting the tumor volumes of the four groups over the duration of treatment (Figure 4B). We observed that NRP2 depletion or the chemotherapeutic treatment alone can reduce the tumor growth; however, growth stall was profound in the NRP2-depleted group simultaneously receiving chemotherapy. NRP2 knockdown (Figures S3C and S3F), cancer cell proliferation, and cell death upon NRP2 depletion in combination with doublet therapy were evaluated by IHC. Ki67 staining was reduced in groups receiving chemotherapy and NRP2 knockdown alone; however, significant reduction of proliferation was observed in the group receiving simultaneous NRP2 knockdown and doublet therapy treatment compared with control (Figures S3D and S3G). On the other hand, NRP2 depletion significantly increased the efficacy of the cisplatin-etoposide doublet to induce cell death as demonstrated by the cleaved caspase-3 staining (Figures S3E and S3H).

NRP2 knockdown increased the efficacy of docetaxel

As bone is one of the major metastatic sites of advanced PCa, including NE-like PCa (Aggarwal et al., 2018; Conteduca et al., 2019), we decided to test the effect of NRP2 depletion in tumor growth in bone. Therefore, we injected DKD-shNRP2 cells into the bones of athymic nude male mice by intra-tibial injection. While C4-2 cells do not grow in the bone, interestingly, the DKD cells showed tumor formation in mouse bone, as confirmed by histological analyses (Figure 4). To test the role of NRP2 depletion on tumor growth, mice were randomly divided into four treatment groups with 10 mice in each group. The first group acts as a control. The second group received Dox (2 mg/mL) in water (2% sucrose) to deplete NRP2 in the cancer cells. In the third group, docetaxel (5 mg/kg body weight, once every 7 days for 3 weeks) was injected by the i.p. route. The fourth group received both docetaxel injection and Dox in water. Dox-induced knockdown of NRP2, cancer cell proliferation, and cell death upon NRP2 depletion in combination with docetaxel were evaluated. NRP2 was efficiently knocked down upon Dox addition as revealed by IHC analysis and real-time

PCR (Figures S3I–S3K). NRP2 depletion significantly increased the efficacy of docetaxel to inhibit NE-like PCa cell proliferation, and to exert profound cytotoxic action *in vivo*. NRP2 knockdown in combination with docetaxel significantly reduced the proliferation of NE-like PCa cells compared with control, only docetaxel treatment, and only NRP2 depletion, respectively (Figures 4C and 4F). In addition, the mouse bones having NRP2 knockdown in combination with docetaxel treatment were associated with more necrotic areas than the other three groups (Figures 4D and 4G). Moreover, cleaved caspase-3 staining revealed that NRP2 knockdown significantly increased the docetaxel-induced cell death compared with the control group as well as the groups under only docetaxel treatment and only NRP2 depletion (Figures 4E and 4H). Overall, our *in vivo* data demonstrated that the anti-tumorigenic actions of cisplatin-etoposide doublet as well as docetaxel are significantly increased upon NRP2 depletion in the NE-like therapy-resistant PCa, recapitulating our *in vitro* results.

NRP2 confers chemo-resistance to the surrounding cancer cells in paracrine manner

Transformed cancer cells in NE-like PCa share neural cells and secretory phenotype (Rindi and Wiedenmann, 2020). Thus, NE-like cells gain the ability to secrete biogenic amines, neuropeptides, peptide hormones, growth factors, and cytokines to establish cell-cell communication within the tumor microenvironment (TME) (Wiedenmann et al., 1998). Attainment of such a secretory phenotype to establish a crosstalk within the TME gives the NE-like cancer cells a survival advantage under stress (Laskaratos et al., 2021; Cives et al., 2019). Therefore, we tested whether the secretory pathways and molecular mediators to establish cellular communications are also enriched in NE-like PCa. Interestingly, functions related to secretion and players mediating cellular crosstalk were significantly enriched in patient cohorts with NE-like differentiation (SU2C-PCF) (Abida et al., 2019) as well as in NE-like DKD cells, as revealed by the pathway analyses of the respective RNA-seq data (Figures 5A and 5B). Previously, we have reported NRP2's function in vesicular trafficking and endosomal recycling processes (Roy et al., 2018; Dutta et al., 2016a), indicating its role in mediating secretory functions in the cancer cells. Hence, we evaluated whether NRP2 upregulation in the NE-like PCa cells has any role in the secretory phenotype of the cells, and thus in their enhanced survival. We performed co-culture experiments, where adenocarcinoma as well as NE-like PCa cells were co-cultured with another set of NRP2 +/- NE-like PCa cells, to understand if the NE-like PCa cells transmit NRP2-mediated pro-survival signals to the surrounding adenocarcinoma and NE-like cells. Both NE-like (Figures 5C and 5F) adenocarcinoma (Figures 5D and 5G) cells co-cultured with NE-like PCa cells having NRP2 showed higher cell viability compared with cells co-cultured with NE-like PCa cells having NRP2 knocked down, under the treatment with docetaxel. We also depleted NRP2 in an NEPC cell line, NCI-H660, collected the NRP2 +/- conditioned media (CM), and cultured adenocarcinoma cells under both the CM. While NRP2-positive CM could protect the adenocarcinoma cells from therapeutic pressure, cells cultured under NRP2-depleted CM were sensitive to chemotherapy (Figures S4A and S4B). pAKT (Ser 473)

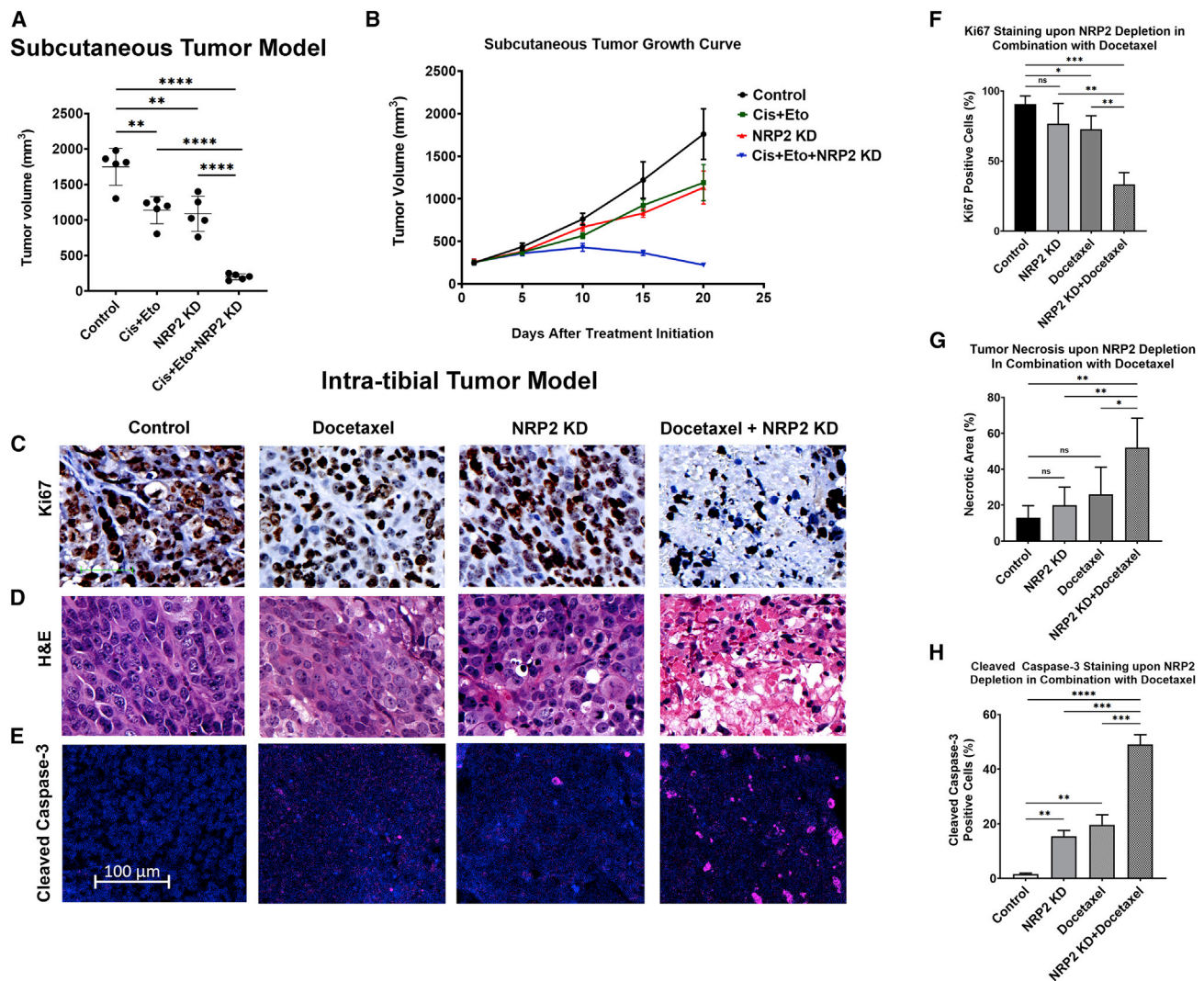


Figure 4. NRP2 depletion increases the efficacy of chemotherapy *in vivo*

(A and B) Effect of NRP2 depletion with or without cisplatin-etoposide (cis + eto) treatment in subcutaneous tumor model.

(A) Calculation of tumor volume in different treatment groups.

(B) Tumor growth curve over the period of treatment.

(C–H) Immunohistochemistry (IHC), immunofluorescence (IF), and H&E staining to evaluate cell proliferation, necrosis, and apoptosis upon NRP2 depletion with or without docetaxel treatment in intra-tibial tumor model.

(C) IHC of ki67.

(D) H&E staining.

(E) IF analysis of cleaved caspase-3 (purple).

(F) Quantitation of (C).

(G) Quantitation of (D).

(H). Quantitation of (E). Data represented as mean ± SEM.

levels were found to be significantly downregulated both in NE-like (Figures 5I and S4C) and adenocarcinoma (Figures 5J and S4D) cells co-cultured with NRP2-deficient NE-like PCa cells, suggesting the presence of NRP2-mediated pro-survival signal in the cancer cells present in the tumor milieu. Interestingly, the difference in the survival of adenocarcinoma cells upon docetaxel treatment was not observed when they were co-cultured with another set of adenocarcinoma cells under NRP2 +/- conditions (Figures 5E and 5H). We then overexpressed NRP2 in

adenocarcinoma cells, collected the CM, and cultured another set of adenocarcinoma cells to check response to therapy. Interestingly, NRP2 overexpression in adenocarcinoma cells could not provide resistance to another set of adenocarcinoma cells against therapy (Figures S4E–S4G). Overall, the results suggested a function of NRP2 in NE-like PCa cells to regulate secretory phenotype and establish cell-cell communication in a paracrine manner to regulate survival of the surrounding cancer cells under chemotherapeutic stress.

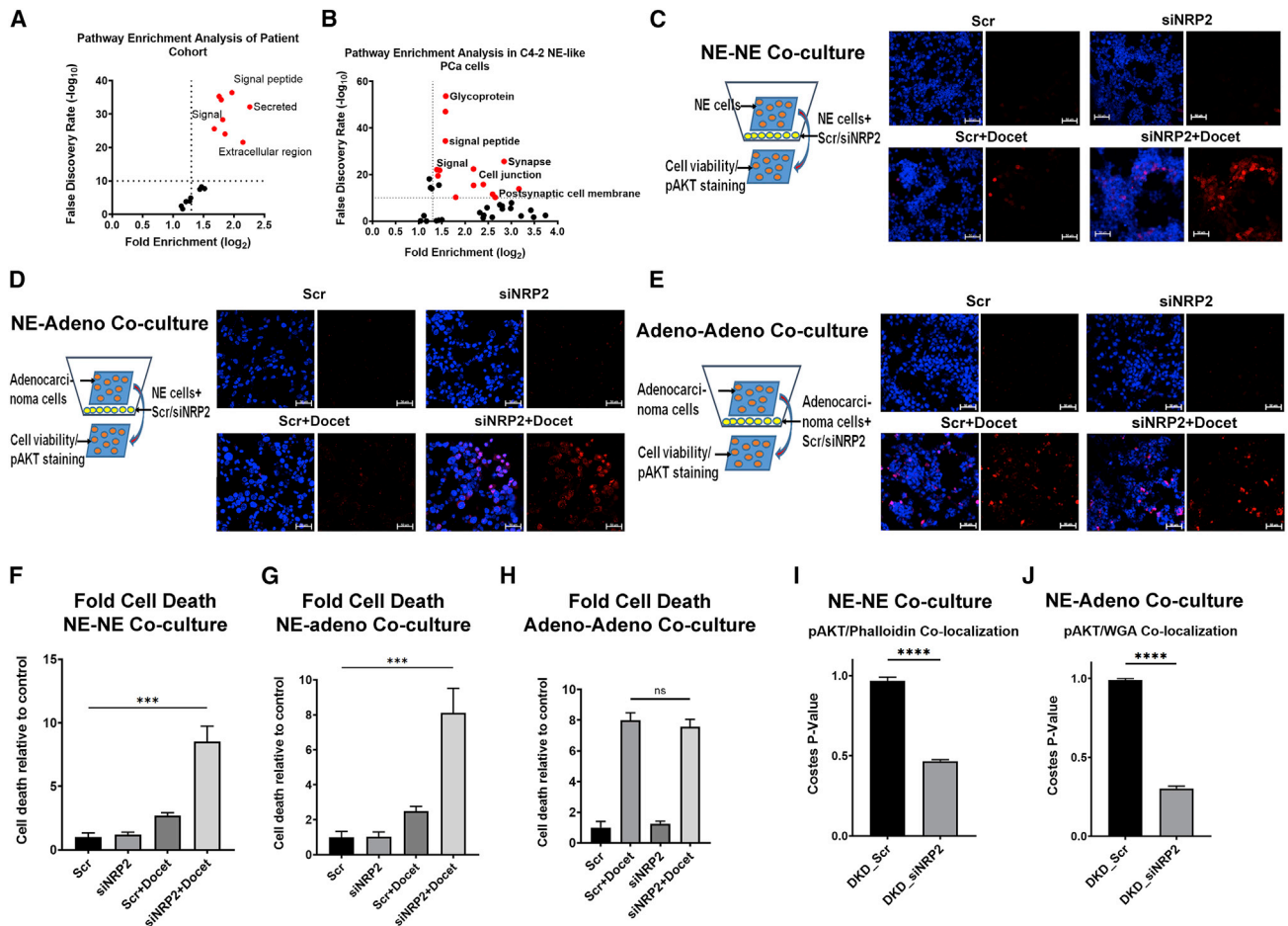


Figure 5. NRP2 confers chemo-resistance to the surrounding cancer cells in a paracrine manner

(A) Pathway analysis from the RNA-seq data of SU2C-PCF patient cohort. Graph showing enriched pathways in the NE-like PCa patients compared with adenocarcinoma.

(B) Pathway analysis from the RNA-seq data of DKD and C4-2 cells. Graph showing enriched pathways in the NE-like PCa cells (DKD) compared with adenocarcinoma cells (C4-2).

(C–H) PI (red)-based cell viability analysis of different co-culture assays as indicated.

(C) Cell viability of NE-like PCa (DKD) cells co-cultured with NRP2 +/- NE-like PCa (DKD) cells.

(D) Cell viability of adenocarcinoma (C4-2) cells co-cultured with NRP2 +/- NE-like PCa (DKD) cells.

(E) Cell viability of adenocarcinoma (C4-2) cells co-cultured with NRP2 +/- adenocarcinoma (C4-2B).

(F–H) Graphs showing fold change in cell death relative to control.

(F) Quantitation of (C).

(G) Quantitation of (D).

(H) Quantitation of (F).

(I) Quantitation of co-localization pAKT (Ser 473) staining with plasma membrane when NE-like PCa (DKD) cells were co-cultured with NRP2 +/- NE-like PCa (DKD) cells.

(J) Quantitation of co-localization pAKT (Ser 473) staining with plasma membrane when adenocarcinoma (C4-2) cells were co-cultured with NRP2 +/- NE-like PCa (DKD) cells. Data represented as mean \pm SEM (n = 3).

NRP2 regulates exocytosis in the NE-like PCa cells by controlling the vesicular fusion pathway

As we observed NRP2 downregulation affect the paracrine communication among the cells, we evaluated whether inhibition of NRP2 has any effect on vesicular fusion signature and therefore on the regulation of secretory phenotype in the NE-like cells. For that, we conducted vesicle-associated membrane protein 2 (VAMP2) staining. Soluble N-ethylmaleimide-sensitive factor attachment proteins receptor (SNARE)-mediated exocytosis is

important for the release of secretory molecules by NE cells (So-masundaram and Taraska, 2018). VAMP2 or synaptobrevin is a vesicle-associated SNARE, which, in association with other plasma membrane-associated SNAREs, promotes fusion of secretory vesicles to the plasma membrane. The vesicles then release their content into the extracellular milieu (Rindi and Wiedenmann, 2020). To understand the mechanism of how NRP2 confers chemo-resistance to the surrounding cancer cells in paracrine manner, we investigated the localization of VAMP2-

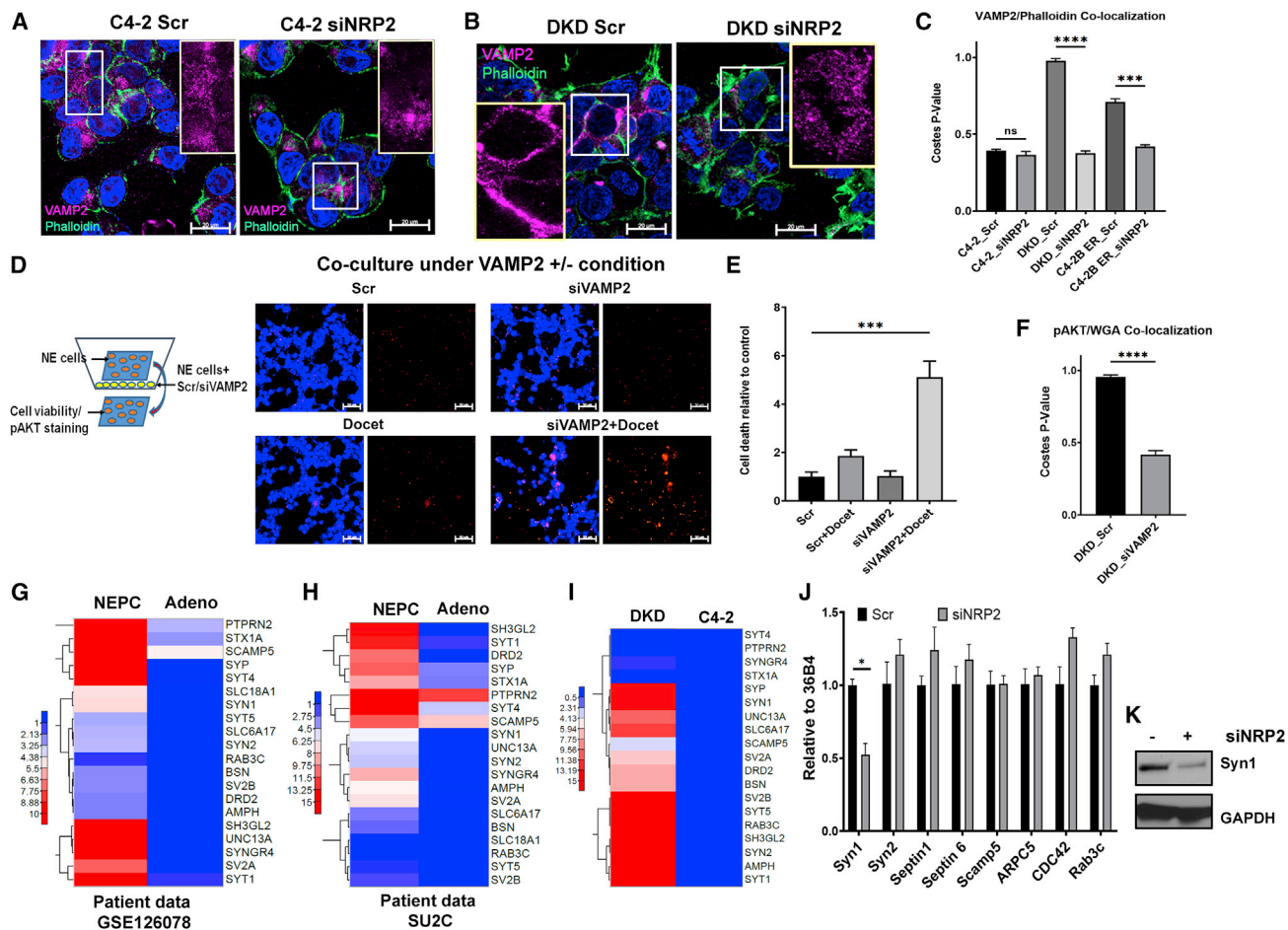


Figure 6. NRP2 regulates exocytosis in the NE-like PCa cells by controlling the vesicular fusion pathway

- (A) VAMP2-positive vesicle localization (pink) in C4-2 cells under +/- NRP2 condition.
 (B) VAMP2-positive vesicle localization (pink) in DKD cells under +/- NRP2 condition.
 (C) Quantitation of (A) and (B).
 (D) Cell viability of DKD cells co-cultured with VAMP2 +/- DKD cells (PI, red).
 (E) Quantitation of (D).
 (F) Quantitation of pAKT (Ser 473) (green) co-localization with plasma membrane in DKD cells co-cultured with VAMP2 +/- DKD cells.
 (G) Differential gene expression in NE-like PCa patients compared with adenocarcinoma (GSE126078).
 (H) Differential gene expression in NE-like PCa patients compared with adenocarcinoma (SU2C/PCF).
 (I) Differential gene expression in DKD cells compared with C4-2.
 (J) Real-time PCR of a set of genes identified in gene set enrichment analysis (GSEA).
 (K) Western blot of Syn1 upon NRP2 knockdown. Data represented as mean \pm SEM (n = 3).

positive exocytic vesicles in the NE-like PCa cells and compared with adenocarcinoma cells. While VAMP2-positive vesicles were found to be diffused and mainly located in the perinuclear region in C4-2 (Figure 6A), they were predominantly localized around the plasma membrane in both DKD and C4-2B ER cells (Figures 6B and S4H). The result suggests an active exocytosis process in NE-like PCa cells in comparison with adenocarcinoma. Interestingly, NRP2 depletion did not significantly change VAMP2 localization in C4-2 (Figure 6A). However, it significantly reduced VAMP2's membrane localization both in DKD and C4-2B ER cells (Figures 6B, 6C, and S4H). We also checked the VAMP2 protein levels in the NE-like PCa cells compared with adenocarcinoma cells. The expression level of VAMP2 was un-

changed in NE-like PCa cells compared with adenocarcinoma (Figures S4I). Our result thus indicates the involvement of NRP2 in the translocation of VAMP2-positive vesicles to the cytoplasmic membrane and thus their fusion to the cell membrane in the NE-like PCa cells. We also performed a co-culture experiment like is the one described in the previous section, where NE-like cells were co-cultured with VAMP2 +/- NE-like PCa cells. We observed higher cell death when cells were co-cultured with VAMP2-deficient NE-like cells in combination with docetaxel treatment (Figures 6D and 6E). Similarly, a decrease in pAKT (Ser 473) level was observed in cancer cells co-cultured with VAMP2-knockdown NE-like cells (Figures 6F and S4J). We also overexpressed NRP2 in adenocarcinoma cells

to evaluate VAMP2-positive vesicle localization. Interestingly, NRP2 overexpression could not significantly change the localization of exocytic vesicles from the perinuclear region to the plasma membrane in adenocarcinoma cells (Figures S4K and S4L). Together, our observations indicate NRP2's ability to regulate the vesicular fusion pathway in NE-like PCa cells and that its inhibition decreases exocytosis in NE-like PCa cells.

We then questioned how NRP2 gains the ability to regulate exocytosis mainly in NE-like PCa cells. To understand the underlying molecular mechanism by which NRP2 regulates such secretory functions, we investigated the patient database to determine which molecular events are preferentially altered in NE-like cancer. We analyzed a treatment-refractory mCRPC patient cohort having PCa patients with NE-like phenotype (GSE126078) (Labrecque et al., 2019). Through gene set enrichment analysis (GSEA), we identified an array of genes that are upregulated in NE-like PCa compared with adenocarcinoma (Figure 6G). They regulate pathways involved in vesicular secretion, exocytosis, and neurotransmitter release (Figure S5). Similar gene profiles were also identified to be upregulated in NE-like PCa when we analyzed the SU2C-PCF patient cohort (Abida et al., 2019) (Figure 6H). Interestingly, the majority of the genes found in the analysis of patient cohorts were also upregulated in DKD cells compared with C4-2 when we re-evaluated our RNA-seq data described previously in Figures 2A, 5B, and 6I. We speculated whether the expression of these genes is regulated by NRP2. Our RT-PCR result (Figure 6J) indicated that synapsin-1 (*Syn1*) among the identified candidate genes was downregulated following NRP2 knockdown. This result was further confirmed in protein level by western blot in DKD cells following the depletion of NRP2 (Figure 6K). The above observations thus suggested the upregulation of molecular mediators such as *Syn1* in NE-like PCa, which enhances its secretory phenotype. *Syn1* tethers the reserve pool of secretory vesicles to the cytoskeleton and thus plays an important role in promoting their migration to the active zone of the cell membrane where secretion occurs (Orlando et al., 2014; Bloom et al., 2003; Chenouard et al., 2020). Thus, NRP2, by regulating *Syn1* expression in NE-like PCa cells, controls the vesicular fusion and exocytosis that is important to establish paracrine communication among the cancer cells in the tumor milieu and to confer therapy resistance.

Characterization of NRP2-regulated secretome in NE-like PCa cells

We performed mass spectrometric analysis of the spent media of NE-like PCa cells with and without NRP2 depletion to identify the biomolecules (secretome) whose secretions are dependent on NRP2. The secretome we obtained in NE-like DKD cells under control conditions matches 63% with the published secretome for NE tumor (Wang et al., 2019), showing similarity of the secretory proteins across the NE-like cancer cells. Interestingly, the analysis of RNA-seq results of NE-like cells (DKD) and its syngeneic adenocarcinoma cells (C4-2) showed that the expression of many of these secretory products is significantly enhanced in NE-like cells (Figure S6A), suggesting specific functions of these proteins in NE-like PCa. Pathway analysis of these secretory proteins in the control-spent media suggested that they regulate functions such as

cellular metabolic process, amide biosynthesis, protein translation, vesicle-mediated transport, exocytosis, mitotic cell cycle process, axon guidance, and extracellular exosomes (Figure 7A). Enrichment of these pathways in the secretome is typical for NE tumor cells and is important to maintain their secretory and functional characteristics (Wang et al., 2019). Many of the proteins in the secretome, such as TGFB1, IGF2BP2, CNTN1, NCAM1, EPHA7, NRAS, and ABCE1, which have roles in cancer progression, aggressiveness, and therapy resistance (Li et al., 2020; Shiota et al., 2021; Xu et al., 2019; Liang et al., 2020; Guan et al., 2020; Huang et al., 2010; Kara et al., 2015; Wang et al., 2019), were downregulated in the secretome upon NRP2 knockdown (Figure 7B). To confirm that NRP2 depletion affected the secretion but not the synthesis of these secretory products, we analyzed our RNA-seq result of DKD cells following the knocking down of NRP2. Gene expressions of most of the secretory products were not significantly affected following NRP2 depletion, confirming our finding that NRP2 regulates the secretion of these proteins in NE-like PCa cells (Figure 7C). We also observed the upregulation of several cytokines in NE-like cancer cells compared with adenocarcinoma cells in our RNA-seq data, which have roles in tumor progression (Figure S6B). However, those cytokines were not detected in our mass spectrometric analysis. Therefore, we performed a separate cytokine array to understand whether NRP2 also regulates their secretion. Our results suggested that some cytokines, such as IL-8, PTX3, PLAUR, and VEGF, were significantly less in the spent media of NRP2-knockdown NE-like PCa cells compared with control (Figure 7D). Our RNA-seq data once again confirmed that the expression of majority of these cytokines was not significantly changed upon NRP2 depletion (Figure S6C). These cytokines are known to regulate cancer cell growth, proliferation, invasion, migration, and metastasis to impart aggressiveness to the tumor cells (Bakouny and Choueiri, 2020; Gilder et al., 2018). Notably, IL-8 was shown to be highly upregulated in NE tumor cells to promote androgen-independent growth of PCa (Huang et al., 2005). IL-8 was also present in the previously published secretome of NE tumor (Wang et al., 2019). Considering the importance of IL-8 in androgen-independent advanced PCa, we performed experiments to address whether IL-8 can be one of the NRP2-regulated secretory molecules that protect PCa cells from chemotherapy. We observed the expression of the IL-8 receptors, especially CXCR2, in the RNA-seq analysis of adenocarcinoma and NE-like PCa cells, and their ligand-induced activation in both of them (Figure S6D). In addition, we also cultured the adenocarcinoma cells under NRP2 +/- CM of NE-like PCa cells to evaluate IL-8 receptor activation (phosphorylation of CXCR2 as readout) in adenocarcinoma cells. As expected, the CM of NRP2-depleted NE-like PCa cells was less capable of activating IL-8 receptors than the control (Figure S6E). Moreover, exogenous addition of IL-8 in NRP2-depleted NE-like cells could partially protect the PCa cells from chemotherapy-induced cell death (Figures S6F and S6G). Together, these results thus suggested that IL-8 is one of the key NRP2-regulated secretory factors of NE-like PCa cells, which enables the NE-like cells to promote resistance to chemotherapy in the neighboring cancer cells. To further evaluate NRP2's role in the regulation of secretory phenotype in PCa cells, we collected the CM of the NRP2-expressing adenocarcinoma cells (C4-2B), performed mass spectrometric

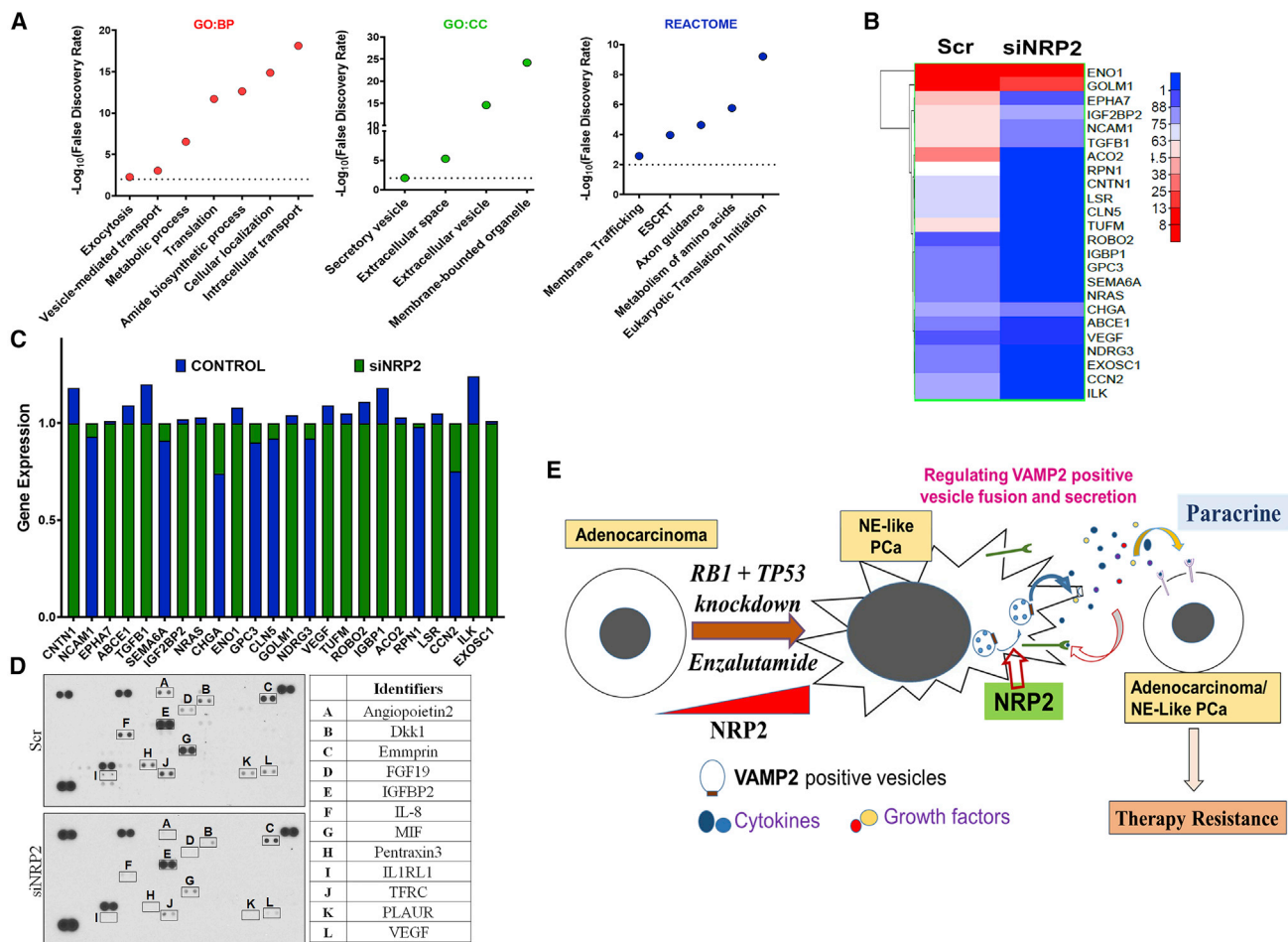


Figure 7. Characterization of NRP2-regulated secretome in NE-like PCa cells

- (A) Pathway analysis of secretome enriched in the spent media of NE-like PCa cells (DKD).
 (B) Effect of NRP2 knockdown on the secretome in DKD cells shown by mass spectrometric analysis.
 (C) Gene expression of different proteins in the secretome in DKD cells with and without NRP2 depletion.
 (D) Cytokine array using the spent media of DKD cells with and without NRP2 depletion.
 (E) Schematic diagram showing NRP2's role in regulating secretory phenotype in NE-like PCa cells.

analysis, and compared with that performed for NE-like PCa cells. Our results indicate a decrease of secretory factors in adenocarcinoma CM compared with that of NE-like PCa cells (Figure S7A). Since some of the cytokines, including IL-8, was not detected in our mass spectrometry studies, we tested the presence of cytokines in the CM of NRP2-expressing and NRP2-knockdown adenocarcinoma (C4-2B) cells by cytokine array analysis. Surprisingly, we observed that the level of some of the cytokines, including IL-8, were partially decreased in the CM of NRP2-knockdown adenocarcinoma cells, while cytokines such as VEGF were unchanged in either of these conditions (Figure S7B). Our results thus suggest that NRP2 in addition to NE-like cells can control the secretion of some of the cytokines in aggressive adenocarcinoma such as C4-2B. To answer how NRP2 can control the secretory function in C4-2B, which is also an adenocarcinoma, although more aggressive than C4-2, we evaluated the localization pattern of VAMP2-positive secretory vesicles in C4-2B. Our results indicated that VAMP2-positive vesicles can be seen at some specific

protruding regions of the cell membrane of C4-2B (Figure S7C). Such a distribution pattern of VAMP2-positive vesicles was not seen in C4-2 (Figure 6). Interestingly, NRP2 depletion in C4-2B affected the localization of VAMP2-positive vesicles (Figure S7C). Our results thus showed that adenocarcinoma at its advanced stages can also gain some degree of secretory ability. The question then can be raised why we could not detect any difference in chemotherapy-induced death of C4-2 when they were co-cultured with NRP2-expressing and NRP2-depleted C4-2B (Figure 5). One explanation could be that C4-2B secretes a lower level of several growth factors/cytokines as it expresses those factors at significantly low level compared with DKD (Figure S7A). Interestingly, our data indicated that IL-8 expression is comparable between C4-2B and DKD (Figure S7D). We therefore compared IL-8 level in the CM of NE-like PCa cells with both C4-2B and C4-2 and observed that IL-8 is present at significantly higher level in the CM of DKD and NCI-H660 compared with C4-2B and C4-2 (Figure S7E). Our results thus suggested that advanced

adenocarcinoma can gain some secretory ability, but it is not comparable with the robust NRP2-regulated secretory function of NE-like cells.

Overall, our results demonstrated that NRP2 is highly upregulated in NE-like PCa, which is required for secretory function of the NE-like cells to protect themselves from chemotherapy through autocrine and paracrine mechanism. Our results further indicated that NRP2 is not the sole regulator of the secretory function; rather, it works along with other molecular modulators. NRP2 overexpression in adenocarcinoma cells therefore is not sufficient to induce any secretory function. The likely reason is the absence of other necessary molecular mediators for secretion. The proposed mechanism is illustrated in [Figure 7E](#).

DISCUSSION

The transdifferentiation of prostate adenocarcinoma to attain NE-like characteristics has recently received more attention as an important mechanism for the development of an aggressive therapy-resistant PCa phenotype (Ku et al., 2017; Beltran et al., 2016; Tritschler et al., 2017; Abida et al., 2019; Labrecque et al., 2019; Patel et al., 2019). Recent investigation on an SU2C-PCF patient cohort (Abida et al., 2019) has revealed the presence of some altered genes commonly upregulated in patients with NE-like phenotype. Interestingly, these genes regulate some important neuronal functions (Abida et al., 2019), as well being implicated in the poor prognosis in cancer progression, and thus they become lucrative candidates for further study. One such molecule is NRP2 (Roy et al., 2018; Stanton et al., 2013; Borkowetz et al., 2020; Schulz et al., 2019).

Currently, platinum-based chemotherapies are used to treat small-cell NE tumors and have shown sensitivity in the range of 10%–50% (Aparicio et al., 2013; Flechon et al., 2011). For non-small-cell variants of NEPC, both taxane-based and platinum chemotherapies are used (Aparicio et al., 2013). Regardless of some initial chemosensitivity, the overall outcome to those therapies for treating NE-like PCa is poor, which thus warrants novel treatment options. In this context, we tested whether targeting the NRP2 axis, especially in combination with chemotherapies, can enhance the treatment response against NE-like PCa. Our *in vitro* and *in vivo* studies suggested that depletion of NRP2 significantly sensitized NE-like PCa cells toward the combined treatment of cisplatin and etoposide. Our results thus highlighted the potential benefit of targeting NRP2 axis to sustain the chemosensitivity of platinum-based chemotherapeutic regimens, which, therefore, is expected to yield a better overall outcome for NE-like PCa patients with small-cell morphology.

Moreover, NRP2 depletion significantly increases the efficacy of docetaxel in the NE-like PCa cells, the first-line chemotherapy they typically are resistant to (Tritschler et al., 2017; Akamatsu et al., 2018). Once again, we tested both *in vitro* and *in vivo* models to test the efficacy of docetaxel in NE-like PCa upon NRP2 axis inhibition. Bone is one of the major metastatic sites for mCRPC, including t-NEPC (Labrecque et al., 2019; Liu et al., 2020). Although previous reports indicated that t-NEPC has a preference to metastasize in visceral sites, the recent SPARTAN trial concluded that there were no significant differences between the frequency of visceral and bone metastases

of t-NEPC patients (Smith et al., 2018). Our results suggest that NRP2 is expressed at high level in tumors metastasized to bone in mCRPC, including NE-like PCa patients. Therefore, in our *in vivo* study, we used an intra-tibial model to show that docetaxel treatment following NRP2 significantly reduced NE-like PCa cell proliferation and induced cell death of NE-like PCa cells. Our findings thus create an opportunity of developing a better patient management strategy by targeting NRP2 in combination with docetaxel.

Like *de novo* NE cells, it is believed that PCa cells with NE differentiation also regulate their own functions and the functions of the surrounding cells (such as adenocarcinoma) through autocrine, paracrine, endocrine, and neurocrine mechanisms. The secretory ability of NE-like cells is therefore critical for these functions (Butler and Huang, 2021). We observed that NRP2 has role in regulating the secretory function of NE-like PCa cells, which thus regulates paracrine communication among the cancer cells in the tumor microenvironment. Our mass spectrometric analysis identified several proteins enriched in the secretome of NE-like PCa cells, such as growth factors (such as TGFB1 and IGF2BP2), cytokines (such as IL-8, PTX3, PLAUR, and VEGF), and ATP-binding cassette protein (ABCE1), which were decreased when NRP2 was knocked down. TGFB1 functions as a tumor promoter in metastatic PCa and leads to poor prognosis in patients with androgen deprivation therapy (Shiota et al., 2021). Earlier, IL-8 was reported to be associated with aggressive nature of NE-like PCa (Huang et al., 2005). A mitogenic and angiogenic cytokine, IL-8, is detected in high amounts in the serum of advanced PCa patients and promotes NE differentiation of prostate tumors (Inoue et al., 2000; Koch et al., 1992). In this context, our data further validated that IL-8 is an important factor secreted by NE-like tumor that provides therapy resistance in the tumor microenvironment. Moreover, our results showed that NRP2 is one of the important molecular regulators of IL-8 secretion and thereby influences the development of treatment-resistant PCa. As there are still limited opportunities for treatment of NE-like cancers in clinical setups, our result in this connection brings a new strategy by targeting NRP2 to sensitize such highly aggressive NE-like cancers to chemotherapies. Although we focused our study on IL-8, we are not ruling out the importance of other factors in association with the progression and development of therapy resistance in NE-like cancer. Reports have suggested that TGFB1 can lead to docetaxel resistance by transcriptionally upregulating an apoptosis suppressor, Bcl-2, and promotes PCa cells' switch from androgen dependence to androgen independence (Li et al., 2020; Lin et al., 2007). On the other hand, IGF2BP2 promotes tumor growth and progression by activating the phosphoinositide 3-kinase/protein kinase B (PI3K/Akt) signaling pathway (Xu et al., 2019). Finally, ABCE1 stimulates tumor cell proliferation, inhibits apoptosis, and imparts therapy resistance in different cancers, including small-cell lung carcinoma, quite similar to NE-like PCa (Huang et al., 2010; Kara et al., 2015). Likewise, the other cytokines differentially expressed under NRP2 +/- conditions are also implicated in tumor progression and cancer cell survival (Rathore et al., 2019; Gilder et al., 2018; Zhan et al., 2013). Thus, NRP2 in NE-like PCa promotes the survival of both NE-like and adenocarcinoma cells, which often coexist

in the advanced PCa tissues resistant to ARIs or first-line chemotherapies.

As a mechanism, our results suggested that NRP2 regulates the secretory phenotype in the NE-like PCa cells through Syn1. Syn1 ensures the availability of vesicles at the active zone of the synapse by tethering vesicles to actin filament and other cytoskeletons (Orlando et al., 2014). NRP2 depletion leads to the downregulation of syn1, which results in impaired localization of the exocytic vesicles around the plasma membrane. Thus, NRP2 controls the secretory phenotype in the NE-like PCa cells and impedes paracrine communication mediated by the NE-like PCa cells by regulating Syn1. Therefore, this study identifies a novel mechanism of NRP2 in NE-like PCa cells, which aid in conferring therapy resistance to cancer cells and raises an opportunity to develop an NRP2 inhibitor for enhanced therapeutic efficacy against aggressive and therapy-resistant NE-like PCa. Of note, our results also suggested that NRP2 can control a similar secretory phenotype in NRP2-expressing advanced adenocarcinoma cells. However, the robust NRP2-regulated protective effect conferred by the paracrine signaling of the NE-like PCa cells is a combined effect of high NRP2 expression and accompanying molecular mediators of secretory pathways developed in the PCa cells upon NE transdifferentiation. We concluded that NRP2 is one of the important regulators in controlling the secretion of NE-like and aggressive adenocarcinoma, although these cells acquire the secretory ability upon lineage switch through a molecular mechanism independent of NRP2.

Overall, our results demonstrate that NRP2 regulates the secretory function of the NE-like PCa cells, which helps them to communicate with the surrounding heterogeneous cancer cells typically present in the NE-like PCa setting. Thus, NRP2 enhances the ability of the cancer cells present in the tumor milieu to resist therapeutic stress, whereas depletion of NRP2 enhances the efficacy of chemotherapies of NE-like PCa.

Limitations of the study

Treatment-refractory NE-like PCa represents a spectrum of disorder that carries various genetic and epigenetic modifications. Currently, there is no model including GEM or PDX that can represent these wide spectra of NE-like PCa. Using different *in vitro* and *in vivo* model systems, here we tried to mimic the diverse nature of NE-like cancer to address the common endocrine functions maintained by these cells. Since most of these NE-like cancers lack functional RB1 alone or in association with TP53 in their genomes, we have focused on NE-like tumors that possess this specific genotype. However, we agree that there are other NE-like PCa with specific genotypes, which were not represented by the model system.

STAR★METHODS

Detailed methods are provided in the online version of this paper and include the following:

- KEY RESOURCES TABLE
- RESOURCE AVAILABILITY
 - Lead contact
 - Materials availability

- Data and code availability
- REAGENTS
- EXPERIMENTAL MODELS AND SUBJECT DETAILS
 - Retrospective study of human mCRPC and NE-like PCa
 - Patient cohorts and animal model for bioinformatics data analysis
 - Generation of C4-2 TP53, RB1 and TP53 + RB1 (DKD) knockdown cells
 - Generation of C4-2B ER cells
- METHOD DETAILS
 - Cell culture and transfection
 - Western blot
 - Real-time quantitative PCR
 - Colony formation assay
 - Cell viability assay
 - MTT assay
 - *In-vivo* prostate cancer subcutaneous mouse model
 - *In-vivo* prostate cancer bone metastatic mouse model
 - Immunohistochemistry (IHC) and immunofluorescence (IF)
 - Co-culture experiment
 - Immunocytochemistry
 - Confocal microscopy
 - Co-localization calculation
 - RNA sequencing
 - Mass spectrometry analysis
 - Cytokine assay
 - Bioinformatics
- QUANTIFICATION AND STATISTICAL ANALYSIS

SUPPLEMENTAL INFORMATION

Supplemental information can be found online at <https://doi.org/10.1016/j.celrep.2022.111097>.

ACKNOWLEDGMENTS

The authors are grateful to the members of the Advanced Microscopy and Histology core of UNMC. The authors are also thankful for the sincere support received from Prostate Cancer Biorepository Network. Funding. Grant support was received by S.D. (1R21CA241234-01, NE-LB506, Lageschulte Fund) and K.D. (R01CA182435, R01CA239343, DOD W81XWH2110628).

AUTHOR CONTRIBUTIONS

R.I. contributed to designing the project and performed most of the work. N.S.P. developed the cell lines, J.M. contributed to Figures 5 through 7 and performed cytokine assay. Z.H., S. Bhattacharya, S. Bodas, and T.G. assisted some of the work. S.S. and A.B. did the bio-informatic analysis. A.M.S. did the mass spectrometry analysis. L.M.S. supervised the statistical analysis. B.A.T. and S.K.B. supervised the study. M.H.M. evaluated IHC images. S.D. and K.D. designed and wrote the project.

DECLARATION OF INTERESTS

The authors declare no competing interests.

Received: October 12, 2021
Revised: April 6, 2022
Accepted: June 23, 2022
Published: July 19, 2022

REFERENCES

- Abida, W., Cyrta, J., Heller, G., Prandi, D., Armenia, J., Coleman, I., Cieslik, M., Benelli, M., Robinson, D., Van Allen, E.M., et al. (2019). Genomic correlates of clinical outcome in advanced prostate cancer. *Proc. Natl. Acad. Sci. USA* *116*, 11428–11436.
- Aggarwal, R., Huang, J., Alumkal, J.J., Zhang, L., Feng, F.Y., Thomas, G.V., Weinstein, A.S., Friedl, V., Zhang, C., Witte, O.N., et al. (2018). Clinical and genomic characterization of treatment-emergent small-cell neuroendocrine prostate cancer: a multi-institutional prospective study. *J. Clin. Oncol.* *36*, 2492–2503.
- Akamatsu, S., Inoue, T., Ogawa, O., and Gleave, M.E. (2018). Clinical and molecular features of treatment-related neuroendocrine prostate cancer. *Int. J. Urol.* *25*, 345–351.
- Aparicio, A., Logothetis, C.J., and Maity, S.N. (2011). Understanding the lethal variant of prostate cancer: power of examining extremes. *Cancer Discov.* *1*, 466–468.
- Aparicio, A.M., Harzstark, A.L., Corn, P.G., Wen, S., Araujo, J.C., Tu, S.M., Paggiaro, L.C., Kim, J., Millikan, R.E., Ryan, C., et al. (2013). Platinum-based chemotherapy for variant castrate-resistant prostate cancer. *Clin. Cancer Res.* *19*, 3621–3630.
- Aran, D., Looney, A.P., Liu, L., Wu, E., Fong, V., Hsu, A., Chak, S., Naikawadi, R.P., Wolters, P.J., Abate, A.R., et al. (2019). Reference-based analysis of lung single-cell sequencing reveals a transitional profibrotic macrophage. *Nat. Immunol.* *20*, 163–172.
- Babicki, S., Arndt, D., Marcu, A., Liang, Y., Grant, J.R., Maciejewski, A., and Wishart, D.S. (2016). Heatmapper: web-enabled heat mapping for all. *Nucleic Acids Res.* *44*, W147–W153.
- Bakouny, Z., and Choueiri, T.K. (2020). IL-8 and cancer prognosis on immunotherapy. *Nat. Med.* *26*, 650–651.
- Beltran, H., Rickman, D.S., Park, K., Chae, S.S., Sboner, A., Macdonald, T.Y., Wang, Y., Sheikh, K.L., Terry, S., Tagawa, S.T., et al. (2011). Molecular characterization of neuroendocrine prostate cancer and identification of new drug targets. *Cancer Discov.* *1*, 487–495.
- Beltran, H., Prandi, D., Mosquera, J.M., Benelli, M., Puca, L., Cyrta, J., Marotz, C., Giannopoulou, E., Chakravarthi, B.V., Varambally, S., et al. (2016). Divergent clonal evolution of castration-resistant neuroendocrine prostate cancer. *Nat. Med.* *22*, 298–305.
- Benten, D., Behrang, Y., Unrau, L., Weissmann, V., Wolters-Eisfeld, G., Burdak-Rothkamm, S., Stahl, F.R., Anlauf, M., Grabowski, P., Mobs, M., et al. (2018). Establishment of the first well-differentiated human pancreatic neuroendocrine tumor model. *Mol. Cancer Res.* *16*, 496–507.
- Bloom, O., Evergren, E., Tomilini, N., Kjaerulf, O., Low, P., Brodin, L., Pieribone, V.A., Greengard, P., and Shupliakov, O. (2003). Colocalization of synapsin and actin during synaptic vesicle recycling. *J. Cell Biol.* *161*, 737–747.
- Borkowetz, A., Froehner, M., Rauner, M., Conrad, S., Erdmann, K., Mayr, T., Datta, K., Hofbauer, L.C., Baretton, G.B., Wirth, M., et al. (2020). Neuropilin-2 is an independent prognostic factor for shorter cancer-specific survival in patients with acinar adenocarcinoma of the prostate. *Int. J. Cancer* *146*, 2619–2627.
- Brady, N.J., Bagadion, A.M., Singh, R., Conteduca, V., Van Emmenis, L., Arceci, E., Pakula, H., Carelli, R., Khani, F., Bakht, M., et al. (2021). Temporal evolution of cellular heterogeneity during the progression to advanced AR-negative prostate cancer. *Nat. Commun.* *12*, 3372.
- Butler, W., and Huang, J. (2021). Neuroendocrine cells of the prostate: Histology, biological functions, and molecular mechanisms. *Precis. Clin. Med.* *4*, 25–34.
- Chenouard, N., Xuan, F., and Tsien, R.W. (2020). Synaptic vesicle traffic is supported by transient actin filaments and regulated by PKA and NO. *Nat. Commun.* *11*, 5318.
- Cives, M., Pelle, E., Quaresmini, D., Rizzo, F.M., Tucci, M., and Silvestris, F. (2019). The tumor microenvironment in neuroendocrine tumors: Biology and therapeutic implications. *Neuroendocrinology* *109*, 83–99.
- Conteduca, V., Oromendia, C., Eng, K.W., Bareja, R., Sigouros, M., Molina, A., Faltas, B.M., Sboner, A., Mosquera, J.M., Elemento, O., et al. (2019). Clinical features of neuroendocrine prostate cancer. *Eur. J. Cancer* *121*, 7–18.
- Dutta, S., Roy, S., Polavaram, N.S., Baretton, G.B., Muders, M.H., Batra, S., and Datta, K. (2016a). NRP2 transcriptionally regulates its downstream effector WDFY1. *Sci. Rep.* *6*, 23588.
- Dutta, S., Roy, S., Polavaram, N.S., Stanton, M.J., Zhang, H., Bhola, T., Honscheid, P., Donohue, T.M., Jr., Band, H., Batra, S.K., et al. (2016b). Neuropilin-2 regulates endosome maturation and EGFR trafficking to support cancer cell pathobiology. *Cancer Res.* *76*, 418–428.
- Flechon, A., Pouessel, D., Ferlay, C., Perol, D., Beuzebec, P., Gravis, G., Joly, F., Oudard, S., Deplanque, G., Zanetta, S., et al. (2011). Phase II study of carboplatin and etoposide in patients with anaplastic progressive metastatic castration-resistant prostate cancer (mCRPC) with or without neuroendocrine differentiation: results of the French Genito-Urinary Tumor Group (GETUG) P01 trial. *Ann. Oncol.* *22*, 2476–2481.
- Gilder, A.S., Natali, L., Van Dyk, D.M., Zalfa, C., Banki, M.A., Pizzo, D.P., Wang, H., Klemke, R.L., Mantuano, E., and Gonias, S.L. (2018). The urokinase receptor induces a mesenchymal gene expression signature in glioblastoma cells and promotes tumor cell survival in neurospheres. *Sci. Rep.* *8*, 2982.
- Guan, G., Niu, X., Qiao, X., Wang, X., Liu, J., and Zhong, M. (2020). Upregulation of neural cell adhesion molecule 1 (NCAM1) by hsa-miR-141-3p suppresses ameloblastoma cell migration. *Med. Sci. Monit.* *26*, e923491.
- Guo, H., Ci, X., Ahmed, M., Hua, J.T., Soares, F., Lin, D., Puca, L., Vosoughi, A., Xue, H., Li, E., et al. (2019). ONECUT2 is a driver of neuroendocrine prostate cancer. *Nat. Commun.* *10*, 278.
- Heng, T.S., Painter, M.W., and Immunological genome project, C. (2008). The Immunological Genome Project: networks of gene expression in immune cells. *Nat. Immunol.* *9*, 1091–1094.
- Huang, J., Yao, J.L., Zhang, L., Bourne, P.A., Quinn, A.M., di Sant’Agnese, P.A., and Reeder, J.E. (2005). Differential expression of interleukin-8 and its receptors in the neuroendocrine and non-neuroendocrine compartments of prostate cancer. *Am. J. Pathol.* *166*, 1807–1815.
- Huang Da, W., Sherman, B.T., and Lempicki, R.A. (2009a). Bioinformatics enrichment tools: paths toward the comprehensive functional analysis of large gene lists. *Nucleic Acids Res.* *37*, 1–13.
- Huang Da, W., Sherman, B.T., and Lempicki, R.A. (2009b). Systematic and integrative analysis of large gene lists using DAVID bioinformatics resources. *Nat. Protoc.* *4*, 44–57.
- Huang, B., Gao, Y., Tian, D., and Zheng, M. (2010). A small interfering ABCE1-targeting RNA inhibits the proliferation and invasiveness of small cell lung cancer. *Int. J. Mol. Med.* *25*, 687–693.
- Inoue, K., Slaton, J.W., Eve, B.Y., Kim, S.J., Perrotte, P., Balbay, M.D., Yano, S., Bar-Eli, M., Radinsky, R., Pettaway, C.A., and Dinney, C.P. (2000). Interleukin 8 expression regulates tumorigenicity and metastases in androgen-independent prostate cancer. *Clin. Cancer Res.* *6*, 2104–2119.
- Jin, R.J., Wang, Y., Masumori, N., Ishii, K., Tsukamoto, T., Shappell, S.B., Hayward, S.W., Kasper, S., and Matusik, R.J. (2004). NE-10 neuroendocrine cancer promotes the LNCaP xenograft growth in castrated mice. *Cancer Res.* *64*, 5489–5495.
- Jolly, M.K., Kulkarni, P., Weninger, K., Orban, J., and Levine, H. (2018). Phenotypic plasticity, bet-hedging, and androgen dependence in prostate cancer: role of non-genetic heterogeneity. *Front. Oncol.* *8*, 50.
- Kara, G., Tuncer, S., Turk, M., and Denkbaz, E.B. (2015). Downregulation of ABCE1 via siRNA affects the sensitivity of A549 cells against chemotherapeutic agents. *Med. Oncol.* *32*, 103.
- Kersemans, V., Cornelissen, B., Allen, P.D., Beech, J.S., and Smart, S.C. (2013). Subcutaneous tumor volume measurement in the awake, manually restrained mouse using MRI. *J. Magn. Reson. Imaging* *37*, 1499–1504.
- Koch, A.E., Polverini, P.J., Kunkel, S.L., Harlow, L.A., Dipietro, L.A., Elnor, V.M., Elnor, S.G., and Strieter, R.M. (1992). Interleukin-8 as a macrophage-derived mediator of angiogenesis. *Science* *258*, 1798–1801.

- Ku, S.Y., Rosario, S., Wang, Y., Mu, P., Seshadri, M., Goodrich, Z.W., Goodrich, M.M., Labbe, D.P., Gomez, E.C., Wang, J., et al. (2017). Rb1 and Trp53 cooperate to suppress prostate cancer lineage plasticity, metastasis, and anti-androgen resistance. *Science* 355, 78–83.
- Labrecque, M.P., Coleman, I.M., Brown, L.G., True, L.D., Kollath, L., Lakely, B., Nguyen, H.M., Yang, Y.C., da Costa, R.M.G., Kaipainen, A., et al. (2019). Molecular profiling stratifies diverse phenotypes of treatment-refractory metastatic castration-resistant prostate cancer. *J. Clin. Invest.* 129, 4492–4505.
- Laskaratos, F.M., Levi, A., Schwach, G., Pfragner, R., Hall, A., Xia, D., von Stempel, C., Bretherton, J., Thanapirom, K., Alexander, S., et al. (2021). Transcriptomic profiling of in vitro tumor-stromal cell paracrine crosstalk identifies involvement of the integrin signaling pathway in the pathogenesis of mesenteric fibrosis in human small intestinal neuroendocrine neoplasms. *Front. Oncol.* 11, 629665.
- Li, Y., He, Y., Butler, W., Xu, L., Chang, Y., Lei, K., Zhang, H., Zhou, Y., Gao, A.C., Zhang, Q., et al. (2019). Targeting cellular heterogeneity with CXCR2 blockade for the treatment of therapy-resistant prostate cancer. *Sci. Transl. Med.* 11.
- Li, Y., Zhang, B., Xiang, L., Xia, S., Kucuk, O., Deng, X., Boise, L.H., and Dong, J.T. (2020). TGF- β causes docetaxel resistance in prostate cancer via the induction of Bcl-2 by acetylated KLF5 and protein stabilization. *Theranostics* 10, 7656–7670.
- Liang, Y., Ma, C., Li, F., Nie, G., and Zhang, H. (2020). The role of contactin 1 in cancers: what we know so far. *Front. Oncol.* 10, 574208.
- Lin, Y., Fukuchi, J., Hiiipakka, R.A., Kokontis, J.M., and Xiang, J. (2007). Up-regulation of Bcl-2 is required for the progression of prostate cancer cells from an androgen-dependent to an androgen-independent growth stage. *Cell Res.* 17, 531–536.
- Liu, D., Kuai, Y., Zhu, R., Zhou, C., Tao, Y., Han, W., and Chen, Q. (2020). Prognosis of prostate cancer and bone metastasis pattern of patients: a SEER-based study and a local hospital based study from China. *Sci. Rep.* 10, 9104.
- Mu, P., Zhang, Z., Benelli, M., Karthaus, W.R., Hoover, E., Chen, C.C., Wongvipat, J., Ku, S.Y., Gao, D., Cao, Z., et al. (2017). SOX2 promotes lineage plasticity and antiandrogen resistance in TP53- and RB1-deficient prostate cancer. *Science* 355, 84–88.
- Nadal, R., Schweizer, M., Kryvenko, O.N., Epstein, J.I., and Eisenberger, M.A. (2014). Small cell carcinoma of the prostate. *Nat. Rev. Urol.* 11, 213–219.
- Orlando, M., Lignani, G., Maragliano, L., Fassio, A., Onofri, F., Baldelli, P., Giovedi, S., and Benfenati, F. (2014). Functional role of ATP binding to synapsin I in synaptic vesicle trafficking and release dynamics. *J. Neurosci.* 34, 14752–14768.
- Patel, G.K., Chugh, N., and Tripathi, M. (2019). Neuroendocrine differentiation of prostate cancer—an intriguing example of tumor evolution at play. *Cancers* 11, 1405.
- Quintanal-Villalonga, A., Chan, J.M., Yu, H.A., Pe'er, D., Sawyers, C.L., Sen, T., and Rudin, C.M. (2020). Lineage plasticity in cancer: a shared pathway of therapeutic resistance. *Nat. Rev. Clin. Oncol.* 17, 360–371.
- Rathore, M., Girard, C., Ohanna, M., Tichet, M., Ben Jouira, R., Garcia, E., Larbret, F., Gesson, M., Audebert, S., Lacour, J.P., et al. (2019). Cancer cell-derived long pentraxin 3 (PTX3) promotes melanoma migration through a toll-like receptor 4 (TLR4)/NF- κ B signaling pathway. *Oncogene* 38, 5873–5889.
- Raudvere, U., Kolberg, L., Kuzmin, I., Arak, T., Adler, P., Peterson, H., and Vilo, J. (2019). g:Profiler: a web server for functional enrichment analysis and conversions of gene lists (2019 update). *Nucleic Acids Res.* 47, W191–W198.
- Rindi, G., and Wiedenmann, B. (2020). Neuroendocrine neoplasia of the gastrointestinal tract revisited: towards precision medicine. *Nat. Rev. Endocrinol.* 16, 590–607.
- Roy, S., BAG, A.K., Dutta, S., Polavaram, N.S., Islam, R., Schellenburg, S., Banwait, J., Guda, C., Ran, S., Hollingsworth, M.A., et al. (2018). Macrophage-Derived neuropilin-2 exhibits novel tumor-promoting functions. *Cancer Res.* 78, 5600–5617.
- Sang, M., Hulsurkar, M., Zhang, X., Song, H., Zheng, D., Zhang, Y., Li, M., Xu, J., Zhang, S., Iltmann, M., and Li, W. (2016). GRK3 is a direct target of CREB activation and regulates neuroendocrine differentiation of prostate cancer cells. *Oncotarget* 7, 45171–45185.
- Schulz, A., Gorodetska, I., Behrendt, R., Fuessel, S., Erdmann, K., Foerster, S., Datta, K., Mayr, T., Dubrovskaya, A., and Muders, M.H. (2019). Linking NRP2 with EMT and chemoradioresistance in bladder cancer. *Front. Oncol.* 9, 1461.
- Shiota, M., Fujimoto, N., Matsumoto, T., Tsukahara, S., Nagakawa, S., Ueda, S., Ushijima, M., Kashiwagi, E., Takeuchi, A., Inokuchi, J., et al. (2021). Differential impact of TGF β 1 variation by metastatic status in androgen-deprivation therapy for prostate cancer. *Front. Oncol.* 11, 697955.
- Smith, M.R., Saad, F., Chowdhury, S., Oudard, S., Hadaschik, B.A., Graff, J.N., Olmos, D., Mainwaring, P.N., Lee, J.Y., Uemura, H., et al. (2018). Apalutamide treatment and metastasis-free survival in prostate cancer. *N. Engl. J. Med.* 378, 1408–1418.
- Somasundaram, A., and Taraska, J.W. (2018). Local protein dynamics during microvesicle exocytosis in neuroendocrine cells. *Mol. Biol. Cell* 29, 1891–1903.
- Stanton, M.J., Dutta, S., Zhang, H., Polavaram, N.S., Leontovich, A.A., Honscheid, P., Sinicrope, F.A., Tindall, D.J., Muders, M.H., and Datta, K. (2013). Autophagy control by the VEGF-C/NRP-2 axis in cancer and its implication for treatment resistance. *Cancer Res.* 73, 160–171.
- Subramanian, A., Tamayo, P., Mootha, V.K., Mukherjee, S., Ebert, B.L., Gillette, M.A., Paulovich, A., Pomeroy, S.L., Golub, T.R., Lander, E.S., and Mesirov, J.P. (2005). Gene set enrichment analysis: a knowledge-based approach for interpreting genome-wide expression profiles. *Proc. Natl. Acad. Sci. USA* 102, 15545–15550.
- Tritschler, S., Erdelkamp, R., Stief, C., and Hentrich, M. (2017). [Neuroendocrine prostate cancer]. *Urologe A* 56, 1475–1484.
- Wang, X.D., Hu, R., Ding, Q., Savage, T.K., Huffman, K.E., Williams, N., Cobb, M.H., Minna, J.D., Johnson, J.E., and Yu, Y. (2019). Subtype-specific secretomic characterization of pulmonary neuroendocrine tumor cells. *Nat. Commun.* 10, 3201.
- Wiedenmann, B., John, M., Ahnert-Hilger, G., and Riecken, E.O. (1998). Molecular and cell biological aspects of neuroendocrine tumors of the gastroenteropancreatic system. *J. Mol. Med. (Berl)* 76, 637–647.
- Wright, M.E., Tsai, M.J., and Aebbersold, R. (2003). Androgen receptor represses the neuroendocrine transdifferentiation process in prostate cancer cells. *Mol. Endocrinol.* 17, 1726–1737.
- Xu, X., Yu, Y., Zong, K., Lv, P., and Gu, Y. (2019). Up-regulation of IGF2BP2 by multiple mechanisms in pancreatic cancer promotes cancer proliferation by activating the PI3K/Akt signaling pathway. *J. Exp. Clin. Cancer Res.* 38, 497.
- Zhan, P., Ji, Y.N., and Yu, L.K. (2013). VEGF is associated with the poor survival of patients with prostate cancer: a meta-analysis. *Transl. Androl. Urol.* 2, 99–105.
- Zhang, Y., Zheng, D., Zhou, T., Song, H., Hulsurkar, M., Su, N., Liu, Y., Wang, Z., Shao, L., Iltmann, M., et al. (2018). Androgen deprivation promotes neuroendocrine differentiation and angiogenesis through CREB-EZH2-TSP1 pathway in prostate cancers. *Nat. Commun.* 9, 4080.
- Zheng, G.X.Y., Terry, J.M., Belgrader, P., Ryvkin, P., Bent, Z.W., Wilson, R., Ziraldo, S.B., Wheeler, T.D., McDermott, G.P., Zhu, J., et al. (2017). Massively parallel digital transcriptional profiling of single cells. *Nat. Commun.* 8, 14049.

STAR★METHODS

KEY RESOURCES TABLE

REAGENT or RESOURCE	SOURCE	IDENTIFIER
Antibodies		
NRP2 (Western Blotting)	R&D Systems	AF2215
NRP2 (IHC)	Atlas Antibodies,	HPA039980
AR	Cell Signaling	5153
TP53	Cell Signaling	2524
RB1	Cell Signaling	9309
SYP	Cell Signaling	36406
SOX2	Cell Signaling	23064
Synapsin-1	Cell Signaling	5297
IL-8	R&D Systems	MAB208
NKX3.1	Cell Signaling	83700
GAPDH	Cell Signaling	5174
Histone H3	Cell Signaling	5192
Rho-GDI	Cell Signaling	2564
HSC70	B-6	7298
Donkey anti-goat IgG-HRP	Promega	V805A
goat anti-rabbit IgG-HRP	Invitrogen	65-6120
goat anti-mouse IgG-HRP	Invitrogen	62-6520
Ki67	Cell Signaling	9027
Biotin conjugated goat anti-rabbit IgG	Invitrogen	31820
Cleaved Caspase-3	Cell Signaling	9579
p-AKT (S473)	Cell Signaling	3787
VAMP2	Cell Signaling	13508
P-CXCR2	Thermo Fisher Scientific	PA5-104850
B3-tubulin	Cell Signaling	5568
Alexa Fluor 647 donkey anti-rabbit	Thermo Fisher	A31573
Alexa Fluor 488 goat anti-rabbit	Thermo Fisher	A11008
Fluorescein Phalloidin	Thermo Fisher	F432
WGA Alexa Fluor 647 Conjugate	Thermo Fisher	W32466
SUMO1	Cell Signaling	4930
Other		
TP53 shRNA	Open BioSystems Inc Corporation	V3LHS_333919 V3LHS_333920 V3LHS_404717
RB1 shRNA	Open BioSystems Inc Corporation	V2LHS_130606 V2LHS_340824 V2LHS_340827
NRP2 siRNA	Dharmacon RNA Technologies	L-017721-00-0010 J-017721-06-0005 J-017721-07-0005 J-017721-08-0005 J-017721-09-0005
VAMP2 siRNA	Dharmacon RNA Technologies	L-012498-00-0005
Non targeted control	Dharmacon RNA Technologies	LU-017721-00-005
Bacterial and virus strains		
Top10	Thermo Fisher Scientific	C404003

(Continued on next page)

Continued		
REAGENT or RESOURCE	SOURCE	IDENTIFIER
Experimental models: Cell lines		
C4-2	ATCC and gift from Prof. Allen Gao	CRL-3314
C4-2B	ATCC and gift from Prof. Allen Gao	CRL-3315
HEK293T	ATCC	CRL-3216
NCI-H660	ATCC	CRL-5813
Critical commercial assays		
cDNA kit	Roche	04379012001
Proteome profiler array (Human XL cytokine Array kit)	R&D Systems	ARY022B
Vybrant Apoptosis Assay Kit	Molecular Probes (Invitrogen)	V13243
MTT assay	Cayman Chemical	10009365
Other reagents		
Reagent A: Avidin	Thermo Scientific	1852280
Reagent B: Biotinylated HRP	Thermo Scientific	1852310
ImmPACT DAB	Vector Laboratories	SK-4105
Recombinant human IL-8	R&D Systems	208-IL
Recombinant VEGFC	R&D Systems	9199-VC-025
Halt phosphatase inhibitor	ThermoFisher Scientific	1862495
TRIzol Reagent	ThermoFisher Scientific	15596018
PowerSYBR Green master mix	ThermoFisher Scientific	4367659
Enzalutamide	Sellekchem	S1250
Docetaxel	Mylan	NDC 67457-531-02
Doxycycline hyclate	Sigma-Aldrich	D9891-5G
Ketamine hydrochloride	Zoetis	NADA #043-304
Xylazine	Patterson Veterinary	NDC 14043-700-50
Cisplatin	Teva Generics	NDC 0703-5747-11
Etoposide	Abcam	ab120227
Gibco RPMI 1640	ThermoFisher Scientific	11875-093
FBS	Sigma-Aldrich	F2442
BSA	Sigma-Aldrich	A7906-500G
DPBS	Corning	21-031-CV
Trypsin	ThermoFisher Scientific	25200-056
TransIT-X2 Transfection Reagent	Dharmacon RNA Technologies	T-2005-02
precast 4–20% Mini-PROTEAN® TGX™ Gel	BioRad	4561094
PVDF membrane	BioRad	1620184
SuperSignal™ West Femto Maximum Sensitivity Substrate	ThermoFisher Scientific	34095
SuperSignal™ Pico Maximum Sensitivity Substrate	ThermoFisher Scientific	
Dako antigen retrieval solution (pH6)	Agilent Technologies	S1700

RESOURCE AVAILABILITY

Lead contact

Requests for further information and/or resources should be directed to and will be fulfilled by the lead contact, Samikshan Dutta (samikshan.dutta@unmc.edu).

Materials availability

All materials generated in this study are available from the any of the lead authors.

Data and code availability

RNA-seq data deposited at GSE202299. Mass spectrometry data are submitted in Mendeley Data (Mass Spectrometry_Sup_Prostate Cancer; Dutta, samikshan (2022), "Mass Spectrometry_Sup_Prostate Cancer", Mendeley Data, V2, <https://doi.org/10.17632/sx2fhffmt7.2>). Any additional information required to reanalyze the data reported in this work paper is available from the [Lead contacts](#) upon request.

This paper does not report original code.

REAGENTS

Cell culture media- RPMI 1640 (Thermo Fisher Scientific, Gibco, NY, 11875093), DPBS, 0.25% (w/v) Trypsin, (100X), and Penicillin-Streptomycin (5,000 U/mL) were acquired from ThermoFisher Scientific. Fetal bovine serum and goat serum were procured from GIBCO. For Western blot, primary antibodies against NRP2 (R&D Systems, AF2215), AR (Cell Signaling, 5153), TP53 (Cell Signaling, 2524), RB1 (Cell Signaling, 9309), SYP (Cell Signaling, 36406), SOX2 (Cell Signaling, 23064), Synapsin-1 (Cell Signaling, 5297), IL-8 (R&D Systems, MAB208), NKX3.1 (Cell Signaling, 83700), GAPDH (Cell Signaling, 5174), Histone H3 (Cell Signaling, 5192), Rho-GDI (Cell Signaling, 2564) and HSC70 (B-6, sc-7298) were used. Donkey anti-goat IgG-HRP (Promega, V805A), goat anti-rabbit IgG-HRP (Invitrogen, 65-6120) and goat anti-mouse IgG-HRP (Invitrogen, 62-6520) were used as secondary antibodies. For immunohistochemistry, primary antibodies against NRP2 (Atlas Antibodies, HPA039980) and Ki67 (Cell Signaling, 9027) were used. Biotin conjugated goat anti-rabbit IgG (Invitrogen, 31820) was used as secondary antibody followed by Reagent A: Avidin (Thermo Scientific, 1852280) and Reagent B: Biotinylated HRP (Thermo Scientific, 1852310). ImmPACT DAB (Vector Laboratories, SK-4105) was used for protein visualization. For immunofluorescence and immunocytochemistry, primary antibody against Cleaved Caspase-3 (Cell Signaling, 9579), p-AKT (S473) (Cell Signaling, 3787), VAMP2 (Cell Signaling, 13508), P-CXCR2 (Thermo Fisher Scientific, PA5-104850), B3-tubulin (Cell Signaling, 5568), and secondary Alexa Fluor 647 donkey anti-rabbit (Thermo Fisher A31573), and Alexa Fluor 488 goat anti-rabbit (Thermo Fisher A11008) antibodies were used. siRNA against human NRP2 and non-targeting control (ON-TARGET plus, smart pool) was bought from Dharmacon (Dharmacon RNA Technologies, L-017721-00-0010, LU-017721-00-005). siRNA against human VAMP2 was bought from Dharmacon (Dharmacon RNA Technologies, L-012498-00-0005). Recombinant human IL-8 was procured from R&D Systems (Cat# 208-IL). Reagents such as HEPES, KCl, DTT, NP-40, Glycerol, MgCl₂, EDTA, PMSF, cyclosporine A, protease inhibitors such as aprotinin, and leupeptin were purchased from Sigma-Aldrich. Halt phosphatase inhibitor (1862495), Trizol and Powerup SYBR Green master mix were bought from ThermoFisher Scientific. cDNA kit was obtained from Roche, and primers from IDT. Proteome profiler array (Human XL cytokine Array kit; ARY022B) was procured from R&D Systems.

EXPERIMENTAL MODELS AND SUBJECT DETAILS

Retrospective study of human mCRPC and NE-like PCa

Commercially available mCRPC tumor microarray was procured from the Prostate Cancer Biorepository Network (PCBN; TMA number 92 A, B, C and D). The tissue microarray contained tumor cores obtained from different visceral and bone metastatic sites of forty-five mCRPC patients with known clinical diagnosis. Out of forty-five patients, fifteen (one-third) were clinically diagnosed with NE-like PCa. Expression of NRP2 in the TMA was evaluated by immunohistochemistry (described below), and the staining was validated by pathologist, Dr. Michael Muders, who also scored the TMA for NRP2. For gene expression data analysis, GSE32269, Stand Up to Cancer/Prostate Cancer Foundation) International Prostate Cancer Dream Team consortium, prospective clinical trial (identifier: NCT02432001) patient cohorts containing primary, mCRPC and NE-like PCa patient data were utilized.

Patient cohorts and animal model for bioinformatics data analysis

Publicly available RNA-seq data of the following human patient cohorts were analyzed: SU2C-PCF (Stand Up to Cancer/Prostate Cancer Foundation) International Prostate Cancer Dream Team consortium ([Abida et al., 2019](#)), a prospective clinical trial ([Aggarwal et al., 2018](#)) (identifier: NCT02432001), treatment refractory mCRPC patient cohort having PCa patients with NE-like phenotype (GSE126078) ([Labrecque et al., 2019](#)), and advanced AR negative prostate cancer mouse model (GSE151426).

Generation of C4-2 TP53, RB1 and TP53 + RB1 (DKD) knockdown cells

A panel of GIPZ TP53 and RB1 shRNA containing plasmids tagged with GFP (TP53- V3LHS_333919, 333920, 404717; RB1- V2LHS_130606, 340824, 340827) were purchased from ThermoFisher scientific. Development of C4-2 cells containing TP53/ RB1 and TP53 with RB1 shRNA was conducted as per manufacturer's protocol. Briefly, the lentivirus from each clone was generated by using HEK293T cells transfected with the shRNA containing plasmids. The generated lentivirus was transduced into C4-2 (kind gift from Prof. Allen Gao) followed by puromycin (Sigma-Aldrich) selection of the cells positive for each clone. The GFP-cells were then sorted by FACS. Following this, the clones were expanded and evaluated for the efficiency of knockdown of TP53 and RB1 at RNA level. Based on the efficacy of knockdown of TP53 and RB1, the clones with highest knockdown were selected for all experiments.

Generation of C4-2B ER cells

C4-2B cells (kind gift from Prof. Allen Gao) were cultured under prolonged exposure of 20 μ M enzalutamide for 12 weeks (31 passages) to develop C4-2B enzalutamide resistant cells.

METHOD DETAILS

Cell culture and transfection

The developed NE-like cells were cultured in RPMI 1640 with 10% FBS in the presence of antibiotics penicillin-streptomycin. Upon confluency, these cells were washed with DPBS and brief rinse with 0.25% (w/v) Trypsin-EDTA to detach the cells from the plate. The cells were collected in equal volumes of complete medium to neutralize the effect of trypsin. The cells were pelleted by centrifugation at 1000 g for 5 min. The cells are then suspended in fresh complete media and plated in a T-75 flask and cultured in a tissue culture incubator maintained at 37°C and 5% CO₂. Cells were transfected using TransIT-X2 Transfection Reagent (Madison, WI, Mirus, MIR6000) (Dharmacon RNA Technologies, T-2005-02).

Western blot

Cells were lysed with ice-cold RIPA buffer (Boston Bioproduct, BP-115; pH 7.4) and combination of protease inhibitors, 20 μ g/mL Leupeptin, 10 μ g/mL Aprotinin, 1mM PMSF and Halt protease.

For separation of nuclear and post-nuclear fraction in osteoclasts, 250 μ L of buffer A (10 mM HEPES pH 7.8, 10 mM KCl, 2 mM MgCl₂, 0.1 mM EDTA, 10 μ g/mL Leupeptin, 10 μ g/mL Aprotinin, 3 mM DTT, 1mM PMSF and Halt phosphatase inhibitor was added to each sample. Cells were scrapped, lysed properly with 26G and centrifuged at 13,500 RPM for five mins. The supernatant was separated from the pellet and used for protein analysis. Total protein was estimated using Bradford reagent and the samples were prepared by the addition of SDS sample buffer containing β -mercaptoethanol and boiled at 95°C for five minutes. The prepared samples were run on a precast 4–20% Mini-PROTEAN® TGX™ Gel (BioRad) and transferred on to a PVDF membrane (Life Technologies). The membrane was blocked in 5% non-fat dry milk in 1X TBST (1X Tris-Buffered Saline, 0.1% Tween 20) for at least 30 min and primary antibody diluted in 1X PBS was added and incubated overnight at 4°C with continuous shaking at low speed. On the next day, membrane was washed with 1X TBST for four times for 5min and incubated in appropriate dilution of secondary antibody conjugated with HRP for 1hr in 1X TBST, or in 5% non-fat dry milk in 1X TBST for anti-goat secondary antibody, with continuous shaking at low speed at room temperature. Following this, the membranes were washed in 1X TBST every 10 min for at least 10–12 times, and the protein bands were detected using a combination dilution of SuperSignal™ West Femto Maximum Sensitivity Substrate and SuperSignal™ Pico Maximum Sensitivity Substrate captured on an X-ray film.

Real-time quantitative PCR

Total RNA was isolated by adding 1mL of TRIzol Reagent (ThermoFisher Scientific, CA) per 1 million cells as per manufacturer's protocol and allowed to stand for 5 min at room temperature. Phase separation by chloroform followed by RNA precipitation with ethanol was done. The supernatant obtained by centrifugation was decanted, and the pellet was air-dried briefly resuspended in UltraPure DNase and RNase free water (Life Technologies, 10977-015). The concentration and quality of the RNA were analyzed using Nano-drop Spectrophotometer. cDNA was synthesized with Transcriptor First strand cDNA synthesis kit (Roche Diagnostics Corporation) as per the instructions provided by the manufacturers. 1 μ g RNA was used to generate cDNA. For real-time PCR, cDNA (50ng) was used, and each reaction was performed in duplicates in 25 μ L volume in a 96-well PCR plates using SYBR green detection system (Applied Biosystems Group) in an ABI 7500 Fast and Real-Time PCR (2 min at 50°C, 10 min at 95°C and 40 cycles of 15 s at 94°C and 1 min at 60°C) with 200–300 nM concentration of primers. The list of the primers used in this study is listed in table the following table.

Gene	Forward	Reverse
36B4	ATGCAGCAGATCCGCATGT	TCATGGTGTCTTGCCCATCA
NRP2	GTGAAGAGCGAAGAGACAACCA	GCAGTTCTCCCCCACTCTG
RB1	CTCTCACCTCCCATGTTGCT	GGTGTTCGAGGTGAACCATT
TP53-common 1	CCTCACCATCATCACACTGG	CACAAACACGCACCTCAAAG
CHGA	TGTCTGGCTCTTCTGCTCT	CAACGATGCATTTTCATCACC
Syp	GATGTGAAGATGGCCACAGA	TCAGCTCCTTGATGTGTTC
SOX2	CAAGATGCACAACCTCGGAGA	GCTTAGCCTCGTCGATGAAC
Ezh2	TGGGAAAGTACACGGGGATA	GCATTCACCAACTCCACAAA
Enolase 2 (NSE2)	TGGATCGGCAACTAAACCAT	TTCTGGACGTTCTTCTTTCACA
AURKA	CCTGAGGAGGAACCTGGCCTC	CAGAGAGTGGTCTCCTCGGA
MYCN	CAAAGGCTAAGAGCTTGAGC	GAAGTGCACAGGGGACCGAT
ASCL1	AGAAGATGAGTAAGGTGGAG	AGTTCAAGTCGTTGGAGTAG

(Continued on next page)

Continued

Synapsin1	TACCCCGTGGTTGTGAAGAT	GTCCTGGAAGTCATGCTGGT
Synapsin2	AACATCAGGTGGAGGACAG	AGGAGACAGGGCAGGAGT
SEPTIN1	TCTGTCAAGAAGGGGTTTG	CATAGAGTTGGTGAGGAAG
SEPTIN6	CAGTATCCTTGGGGCACTGT	GTTGACCCGAATCAGCATCT
SCAMP5	AAATTTTACCGGGGAAGTGG	TGCTGCACATGTGGATTCTT
ARPC5	AGAGCCCGTCTGACAATAGC	CAATGGACCCTACTCCTCCA
CDC42	ACGACCGCTGAGTTATCCAC	GGCACCCACTTTTCTTTTCCAC
Rab3C	GAGCGCCTTGTGGATATCAT	TTCTGCTTTCAGCAGTGTAT

The expression was calculated relative to that of control cells and normalized with 36B4 measured under the same conditions (Applied Biosystems/Roche, Branchburg, NJ), using the $2^{-\Delta\Delta CT}$ method.

Colony formation assay

Cells were mixed in 0.3% Noble agar (in RPMI medium supplemented with 10% FBS) at 37°C and immediately plated at 5000 cells/well on the top of a solidified agar layer of the 6-well plates (0.5% Noble agar in the same growth medium). Media was supplemented every third day along with the respective treatments. After 21 days, colonies were stained with crystal violet solution (0.05% crystal violet-2% ethanol in PBS) for 1 h followed by washing with PBS and then was photographed. The size of the colonies was measured using ImageJ.

Cell viability assay

Vybrant Apoptosis Assay Kit 7 was purchased from Molecular Probes (Invitrogen) and was used according to the manufacturer's protocol. Briefly, the cells were seeded at a density of 75,000 cells per well of a two-well chamber slide (LabTek Rochester, NY). NRP2 were depleted using siRNA and 24 h later the cells were treated with docetaxel (Mylan, NDC 67457-531-02). After 24 h of docetaxel treatment, adherent cells were washed with $1 \times$ PBS and incubated with $1 \mu\text{L}$ of Hoechst 33342 and propidium iodide (PI) at room temperature for 15 min. The cells were viewed under a confocal microscope.

MTT assay

MTT assay was performed according to manufacturer's protocol (Cayman Chemical, 10009365). In brief, cells were seeded in a 96-well plate at a density of 5000 cells/well in $100 \mu\text{L}$ of culture medium. Cells were cultured in a CO_2 incubator at 37°C for 48 h. $10 \mu\text{L}$ of MTT reagent was added to each well using a repeating pipettor, and mixed gently for one minute on an orbital shaker. The cells were then incubated for three to four hours at 37°C in a CO_2 incubator. After incubation, the formazan crystals were produced in the cells, which appeared as dark crystals in the bottom of the wells. $100 \mu\text{L}$ of crystal dissolving solution was added to each well, and was incubated for 4 h in a 37°C CO_2 incubator. A purple solution was produced. Absorbance was measured at 570 nm using a microplate reader.

In-vivo prostate cancer subcutaneous mouse model

All animal studies were conducted in accordance with the University of Nebraska medical center IACUC guidelines. To evaluate the effect of NRP2 depletion on the efficacy of chemotherapy, we have developed stable shNRP2 expressing clones of C4-2 TP53 + RB1 double knockdown cells (DKD-shNRP2), where shRNA can be inducibly expressed upon administration of doxycycline (Dox). DKD-shNRP2 cells (1×10^6 cells) were implanted into the right flank of athymic nude mice. Once the tumors became palpable, animals were randomly divided into four groups ($n = 5$). Briefly, the first group acts as a control. The second group received doxycycline in water (2 mg/mL) to deplete NRP2 in the cancer cells. In the third group, cisplatin (5 mg/kg body weight) and etoposide (8 mg/kg body weight) were administered (i.p) on day 1 and day 2, respectively, on a weekly basis for three weeks. And, the fourth group received both doxycycline in water and cisplatin-etoposide doublet. Tumors were regularly monitored and tumor size was measured over the period of time until sacrifice. Tumor volume was calculated by using the formula: $\frac{1}{2} ab^2$ (Kersemans et al., 2013).

In-vivo prostate cancer bone metastatic mouse model

All animal studies were conducted in accordance with the University of Nebraska medical center IACUC guidelines. To evaluate the effect of NRP2 depletion on the efficacy of chemotherapy, we have developed stable shNRP2 expressing clones of C4-2 TP53 + RB1 double knockdown cells (DKD-shNRP2), where shRNA can be inducibly expressed upon administration of doxycycline (Dox). The requirement of NRP2 for PCa growth in bone was tested by implanting DKD-shNRP2 cells in the tibia of immunocompromised mice and then knocking down NRP2 by Dox from cancer cells with or without concomitant docetaxel administration. Briefly, DKD-shNRP2 cells stably expressing GFP-luciferase tagged shNRP2 under the control of doxycycline were injected intratibially in athymic nude male mice in the age group of 8–12 weeks purchased from Jackson labs. $100,000$ cells per $30 \mu\text{L}$ PBS were injected into the left tibia of mice. The right tibia received PBS only. Tumor burden in the bone was monitored by IVIS imaging and after 4 days

of injection, the mice were randomized into four groups with 10 mice in each group. The first group acts as a control and received sucrose in water. The second group received doxycycline in water (2 mg/mL) to deplete NRP2 in the cancer cells. The third group was injected intraperitoneally with docetaxel (5 mg/kg body weight: once every 7 days for three weeks) and sucrose in water. The fourth group received docetaxel injection and doxycycline in water. After 3 weeks, all mice were sacrificed and the tumor cells containing bones were obtained. Bone marrow from three bones from each group were used to sort tumor cells expressing GFP by flow cytometry. These tumor cells were processed to obtain RNA and Real-time PCR was conducted to check the efficiency of NRP2 depletion. The rest of tumor bearing bones were used for evaluating NRP2 knockdown efficiency by IHC. The tumor bearing bones were formalin-fixed for further processing and evaluation of cancer cell proliferation, apoptosis and necrosis.

Immunohistochemistry (IHC) and immunofluorescence (IF)

Patient TMA and slides containing mouse bone sections (4 mm thick) were kept on heat block at 58°C for 1 h. They were then rehydrated in a sequential passage of solutions starting with xylene for 30 min, 100% ethanol for 15 min, 95%, 90%, 80%, 75%, 50%, and 20% ethanol for 5 min each followed by immersion in double distilled water for 10 min. Antigen retrieval was performed by heat induced epitope retrieval at 95°C using Dako antigen retrieval solution (pH6). The antigen unmasking solution was first preheated at a high temperature in the microwave until boiling and then the slides were immersed into it and heated in a 95°C water bath for 30 min. Following this, the slides were gradually allowed to cool to room temperature and washed with double distilled water. For IHC only, slides were next immersed in 3% hydrogen peroxide (H₂O₂) in methanol for 10 min at room temperature. Slides were then blocked with 1% BSA+0.2% saponin in TBST at 4°C for 1 h and incubated overnight with primary antibody in the blocking buffer at 4°C. Biotinylated secondary antibodies (IHC) or fluorophore-conjugated secondary antibody (IF) were added. For IHC staining, slides were next washed with TBST and then incubated with avidin-biotin complex (Reagent A and Reagent B) for 30 min at room temperature, following the manufacturer's instructions. Next, diaminobenzidine solution (ImmPACT DAB) was added as a substrate for peroxidase until the desired staining intensity was developed. Hematoxylin was used to counter staining. Slides were dehydrated by gradual passage of slides from double distilled water to xylene in a reverse order mentioned earlier for rehydration of slides and mounted with Permount and covered with glass cover slips. The whole slides were next digitally scanned at Tissue Science Facility, UNMC. For IF, following incubation with secondary antibody cells were washed and mounted with Vectashield mounting media containing DAPI (Vector Laboratories, H1200) and photomicrographs were captured using confocal microscope. Images were processed using Ventana image viewer and ImageScope Viewer (for IHC) and Zen software (for IF). Quantification was performed based on number of ki67 positive/cleaved caspase-3 positive tumor cells compared to total number of tumor cells in each zone using ImageJ Immunohistochemistry (IHC) Image Analysis Toolbox plugin and was validated by pathologist, Dr. Michael Muders. Graphical illustrations were made using GraphPad Prism 8 software.

Co-culture experiment

For NE-NE and NE-Adeno co-culture experiments, DKD cells were cultured in 6-well plate, transfected with Scr or siNRP2 and incubated for 12h. DKD (NE-NE co-culture) or C4-2 (NE-Adeno co-culture) cells were cultured separately on the coverslips without any transfection. The coverslips with either DKD or C4-2 cells were then placed into the 6-well chambers of transfected DKD cells. For Adeno-Adeno co-culture experiment, C4-2B cells were cultured in 6-well plate, transfected with Scr or siNRP2 and incubated for 12h. Coverslips with separately cultured C4-2 cells was then added into the 6-well chambers with transfected C4-2B cells. 48hr post transfection immunocytochemistry was performed for p-AKT and observed under confocal microscopy. For cell death assessment, after 12h of coverslip transfer, cells were treated with Docetaxel for 24h, PI staining was performed and observed under confocal microscopy. Co-culture experiment with VAMP2 +/- condition was performed in the similar way described above.

Immunocytochemistry

The cells were grown on the coverslips and after treatment, were washed with PBS and fixed in 4% paraformaldehyde solution. Cells were blocked with 3% BSA+0.2% saponin in TBST at 4°C for 1 h, followed by overnight incubation in primary antibody at 4°C. Next, fluorophore-conjugated secondary antibody was added for 60min and cells were co-immunostained with WGA or Phalloidin for 15 min. Coverslips were washed, mounted onto the glass slides using VECTASHIELD mounting medium with DAPI and photomicrographs were captured using confocal microscope.

Confocal microscopy

All the confocal images were captured in Zeiss LSM 800 Confocal Laser Scanning Microscope equipped with 4 lasers located in the UNMC confocal core facility, and images were analyzed using Zeiss Zen 2010 software. All confocal data was quantified using ImageJ software and graphical illustrations were prepared using GraphPad Prism 8 software.

Co-localization calculation

Co-localization of pAKT and VAMP2 with plasma membrane, either stained with phalloidin or wheat germ agglutinin (WGA), was quantified using Fiji ImageJ software with Coloc2 plugin. Costes p-values were calculated for each experiment.

RNA sequencing

RNA-seq was carried out for C4-2, DKD, C4-2B, C4-2B-ER, DKD-Scr and DKD-SiNRP2 in triplicate samples. RNA was isolated from the cells using the RNeasy Mini Kit (Qiagen, Germantown, MD) and RNA integrity quality was confirmed using the Agilent Bioanalyzer. A paired end read (2x 50 bp) sequencing run of RNA libraries were carried out with Illumina NextSeq 500. Sequences were aligned to human reference genome hg38. Data analysis was performed with the help of the Bioinformatics Core at UNMC. RNA abundance was estimated with feature Counts from the Sub-read package version 1.6.3. Downstream analyses were performed with the DESEQ2 R package version 1.18.1. A Principal component analysis (PCA) was performed using <https://biit.cs.ut.ee/clustvis/>. Differentially expressed genes (DEGs) were identified by pairwise comparisons with the DESEQ2 package (v.1.12.3). Genes were retained as differentially expressed when the fold-change (FC) was >2 or < -2.

Mass spectrometry analysis

Mass Spectrometry was carried out on C4-2B, DKD Scr and DKD SiNRP2 cells. Cells were grown in 6-well plate in two different condition - control and knockdown of NRP2. Cells were transfected and grown in serum free RPMI media for 48hrs. After 48hrs, cell supernatant/conditioned media (CM) was collected (~2mL), cell debris were removed by centrifuging CM @3000g for 30-min. RPMI media only was used for background correction. Proteins were purified by acetone precipitation to remove vitamins, cholines and other small molecules contaminants. Mass Spectrometry analysis was carried out through LC-MS/MS using Thermo Q-Exactive-HF mass spectrometer and a nano RSLC Ultimate 3000 from Dionex. Spectra was processed using Mascot (Matrix Science, London, UK; version 2.6.1) and were subjected to a cutoff of 1% false discovery rate. Spectra was processed by MODIRO ver.1.1 (Protagen, Germany) software (from Proteomics & Metabolomics Facility of the Nebraska Center for Biotechnology at University of Nebraska, Lincoln).

Cytokine assay

Presence of cytokines in the CM of DKD and C4-2B Scr vs. siNRP2 cells was detected using human XL cytokine array kit following manufacturer's protocol. CM from the transfected cells was collected, centrifuged@3000g for 15-min, and stored at -80°C until further use. Assay membranes containing 105 different capture antibodies was blocked for 60min followed by overnight incubation in CM at 4°C. On the following day, the membranes were washed thrice (10min each), incubated with detection antibody cocktail for 60min, washed thrice (10min each) and incubated in streptavidin-HRP solution for 30min. The membranes were then washed thrice (10min each) and developed with chemiluminescent detection reagent using an X-ray film developer and cytokines spots were identified using transparency overlay template.

Bioinformatics

Gene Set Enrichment Analysis (GSEA) and pathway analysis using RNA-seq data of the above patient cohorts and the developed NE-like cells were performed using GSEA Software and Molecular Signature Database (MSigDB) (Subramanian et al., 2005), and DAVID bioinformatics resources 6.8 (Huang Da et al., 2009b) and (Huang Da et al., 2009a). Pathway analysis of the enriched proteomes after mass spectrometric analysis was done using g:Profiler (Raudvere et al., 2019). The RNA-seq data was downloaded from NCBI GEO using SRAtoolKit (url: <https://trace.ncbi.nlm.nih.gov/Traces/sra/sra.cgi?view=software>). The reads were aligned to mm10 with STAR (v.2.5.3a) and gene counts quantified with HTSeq (v.0.9.1). The raw counts were processed and normalized in DESeq2. Heatmap of normalized gene expression were generated using Heatmapper (Babicki et al., 2016). For the single cell RNA-seq analysis, the molecule_info.h5 files were downloaded from NCBI GEO (GSE151426). The matrix.h5 files were generated from molecule_info.h5 file using cellranger aggr software (10x Genomics) (Zheng et al., 2017). The matrix.h5 files for each sample were read into R using Seurat package (V4). The data was normalized, and doublet cells were removed. Cell type annotation was performed using SingleR (Aran et al., 2019) with mouse reference from Immunological Genome Project (ImmGen) (Heng et al., 2008). Mean difference between the groups were estimated using Student's t-test.

QUANTIFICATION AND STATISTICAL ANALYSIS

All the graphical illustrations and statistical tests were performed using GraphPad Prism 8 software (GraphPad software, Inc.). All data reported in graphs are expressed as mean ± standard error of mean (SEM), unless otherwise mentioned and were compared using standard two-tailed unpaired t test, unless otherwise mentioned. p values were considered statistically significant when less than 0.05. All experiments were repeated at least 3 times unless specified.

ARTICLE



Neuropilin-2 regulates androgen-receptor transcriptional activity in advanced prostate cancer

Samikshan Dutta¹✉, Navatha Shree Polavaram¹, Ridwan Islam¹, Sreyashi Bhattacharya¹, Sanika Bodas¹, Thomas Mayr^{2,3,4}, Sohini Roy¹, Sophie Alvarez Y. Albalá⁵, Marieta I. Toma^{3,4}, Anza Darehshouri⁶, Angelika Borkowetz⁷, Stefanie Conrad^{8,9}, Susanne Fuessel⁷, Manfred Wirth⁷, Gustavo B. Baretton^{4,10,11}, Lorenz C. Hofbauer^{8,9,10}, Paramita Ghosh¹², Kenneth J. Pienta¹³, David L. Klinkebiel¹³, Surinder K. Batra¹³, Michael H. Muders^{2,3,4} and Kaustubh Datta¹✉

© The Author(s), under exclusive licence to Springer Nature Limited 2022

Aberrant transcriptional activity of androgen receptor (AR) is one of the dominant mechanisms for developing of castration-resistant prostate cancer (CRPC). Analyzing AR-transcriptional complex related to CRPC is therefore important towards understanding the mechanism of therapy resistance. While studying its mechanism, we observed that a transmembrane protein called neuropilin-2 (NRP2) plays a contributory role in forming a novel AR-transcriptional complex containing nuclear pore proteins. Using immunogold electron microscopy, high-resolution confocal microscopy, chromatin immunoprecipitation, proteomics, and other biochemical techniques, we delineated the molecular mechanism of how a specific splice variant of NRP2 becomes sumoylated upon ligand stimulation and translocates to the inner nuclear membrane. This splice variant of NRP2 then stabilizes the complex between AR and nuclear pore proteins to promote CRPC specific gene expression. Both full-length and splice variants of AR have been identified in this specific transcriptional complex. In vitro cell line-based assays indicated that depletion of NRP2 not only destabilizes the AR-nuclear pore protein interaction but also inhibits the transcriptional activities of AR. Using an in vivo bone metastasis model, we showed that the inhibition of NRP2 led to the sensitization of CRPC cells toward established anti-AR therapies such as enzalutamide. Overall, our finding emphasize the importance of combinatorial inhibition of NRP2 and AR as an effective therapeutic strategy against treatment refractory prostate cancer.

Oncogene (2022) 41:3747–3760; <https://doi.org/10.1038/s41388-022-02382-y>

INTRODUCTION

Majority of metastatic castration-resistant prostate cancer (mCRPC) relapses due to the failure of second-generation anti-androgen therapies [1–3]. In mCRPC, androgen-receptor (AR) activity is still the major driving force for the progression of the disease [4, 5]. Therefore, targeting AR-signaling pathways is important to achieve the treatment benefit. Present FDA-approved AR-targeting drugs are raised against its C-terminal regions [6]. During the progression of prostate cancer (PCa), AR amplification, formation of AR-splice variants with C-terminal deletions, generation of AR point mutation at the C-terminal ligand-binding site of AR, or hyper-activity of the various growth factor signaling pathways is responsible for evasion of existing AR-directed therapies [7–9]. Therefore, efforts are under way to target other domains of AR. However, there is an unsuccessful clinical trial to target N-terminal trans-activating domain, thus raising the concerns of direct targeting of AR in advanced PCa [10]. An

alternative approach has been taken to inhibit AR-signaling in CRPC. Interestingly, one of the family members of bromodomain and extra-terminal domain (BET) protein, named BRD4, has been shown to interact with AR [11, 12]. A specific BRD4 inhibitor, JQ1, has been studied in advanced PCa. However, irrespective of its early success, JQ1 failed in PCa clinical trial [13, 14]. Therefore, there is an urgent need to develop a new druggable target for the AR-signaling pathway for treating mCRPC patients.

While studying the molecular signature responsible for CRPC, we observed that increased expression of Neuropilin-2 (NRP2) is associated with poor PCa survival. NRP2 is a transmembrane non-tyrosine kinase protein and is known to serve as co-receptors for other receptors such as plexins in neuronal cells and vascular endothelial growth factor receptors (VEGFRs) in endothelial cells [15, 16]. Broadly, NRP2 has two major membrane-bound isomers, called NRP2A and NRP2B [17]. However, the functional significance of these two isomers has not been adequately studied.

¹Department of Biochemistry and Molecular Biology, University of Nebraska Medical Center, Omaha, NE, USA. ²Rudolf Becker Laboratory for Prostate Cancer Research, Medical Faculty, University of Bonn, Bonn, Germany. ³Institute of Pathology, Medical Faculty, University of Bonn, Bonn, Germany. ⁴Institute of Pathology, Technische Universitaet Dresden, Dresden, Germany. ⁵Department of Agronomy and Horticulture, University of Nebraska-Lincoln, Lincoln, NE, USA. ⁶Department of Cell Biology, UT Southwestern Medical Center, Dallas, TX, USA. ⁷Department of Urology, Technische Universitaet Dresden, Dresden, Germany. ⁸Division of Endocrinology and Metabolic Bone Diseases, Department of Medicine III, Technische Universitaet Dresden, Dresden, Germany. ⁹Center for Healthy Aging, Technische Universitaet Dresden, Dresden, Germany. ¹⁰German Cancer Consortium (DKTK), Partner Site Dresden, German Research Center (DKFZ), Heidelberg, Germany. ¹¹Tumor and Normal Tissue Bank of the University Cancer Center (UCC), University Hospital and Faculty of Medicine, Technische Universitaet Dresden, Dresden, Germany. ¹²Department of Biochemistry and Molecular Medicine, University of California Davis, Davis, CA, USA. ¹³The Brady Urological Institute, Johns Hopkins University School of Medicine, Baltimore, MD, USA. ✉email: samikshan.dutta@unmc.edu; kaustubh.datta@unmc.edu

Received: 23 September 2021 Revised: 3 June 2022 Accepted: 10 June 2022
Published online: 27 June 2022

Table 1. NRP2 expression in various prostate cancer group.

Group	n = no of people
High risk prostate cancer group	325
Intermediate risk prostate cancer	24
Low risk prostate cancer	51
NRP2 positive in overall cases	268
NRP2 positive in High risk group	107

In this current study, we have analyzed NRP2 expression in human PCa tissues and detected that a fraction of NRP2 is localized in the nucleus of aggressive PCa cells. Utilizing immunogold transmission electron-microscopy (ITEM), structural illumination microscopy (SIM), and other biochemical approaches we have observed the ligand dependent localization of NRP2B in the inner nuclear membrane (INM) of PCa cells, indicating its novel nuclear-specific role. Sumoylation at the C-terminal region of NRP2B has been detected as the required molecular event for its retrograde transport to INM. Our study further indicates that NRP2B stabilizes the transcriptional complex between nuclear pore proteins (nucleoporins) and AR at the nucleus and thus promotes the AR-driven gene expression in mCRPC. Interestingly, both full length and AR-splice variants have been observed to be a part of NRP2B-nuclear pore protein complex. Depletion of NRP2 thus can deregulate this specific AR-transcriptional complex and can enhance the therapeutic efficiency of the anti-androgen inhibitors, such as enzalutamide. This has been observed in both in vitro tissue culture systems and intratibial mouse models of PCa. Therefore, the results presented here have highlighted the presence of unique AR-NRP2B transcriptional complex and the benefits of combining NRP2 inhibition and anti-androgen therapies for treating mCRPC patients.

RESULTS

NRP2 is present in the nuclear membrane of PCa cells

Nuclear NRP2 expression is associated with a poor PCa prognosis. NRP2 expression was analyzed within a tissue microarray consists of 396 formalin-fixed paraffin-embedded (FFPE) specimens from patients with prostate acinar adenocarcinoma who were treated at the Department of Urology, University Hospital Dresden, Germany between 1996 and 2005 and underwent radical prostatectomy. Around 80% of these PCa patients had a high risk of disease progression (pT \geq 3, Gleason score \geq 8 or pN1). Earlier, evaluation of the above tissue microarray, we have demonstrated that nearly 33% high-risk group patients [stage \geq pT3 33%, GS \geq 8 34%, pN1 31%] are positive for membranous and cytoplasmic staining of NRP2 (Table 1). In this study, re-analysis of NRP2 staining revealed that almost one third of adenocarcinomas with Gleason grade 5 showed a distinct nuclear staining pattern for NRP2 (Fig. 1A, B). In contrast, only eight percent in adenocarcinomas with Gleason 4 pattern and only about two percent in adenocarcinomas with Gleason 3 pattern exhibited nuclear staining (Fig. 1A, B). Overall, our results suggested an association of nuclear-specific NRP2 staining with high Gleason grading and thus with aggressive PCa.

Nuclear-NRP2 localizes within the nuclear envelope in an isoform-specific manner. To understand the exact location of NRP2 in the nucleus, we immunostained endogenous NRP2 in PCa cell lines such as LNCaP C4-2B and PC3 (Figs. 1C, S1A). Our results with structured illumination microscopy (SIM) indicated the presence of NRP2 at the nucleus. Because the NRP2 antibody used for SIM only recognizes the membrane-bound extracellular region and not the soluble form of NRP2, we assumed that the NRP2 was anchored to the membrane/lipid droplets in the nucleus. Nuclear membrane-

bound NRP2 was further confirmed when we co-immunostained with Lamin A/C (Figs. 1C, S1A). Localization of NRP2 occurs around the nuclear membrane and often runs into the nuclear invaginations or the nucleoplasmic reticulum [18, 19] (observed when we made virtual sections of the cells through the x-axis and rotated 90 degrees around the plane) (Figs. 1C, S1A). The ectopic expression of full-length NRP2 showed the similar nuclear localization as endogenous NRP2 with characteristic nuclear membrane invaginations (Fig. S1B, C), while membrane-bound NRP2 devoid of the C-terminal cytosolic domain (NRP2 Δ C) showed diffuse non-nuclear staining of NRP2 (Fig. S1D–G) often residing within the ER. Our results therefore indicated that C-terminal region of NRP2 is required for its localization at the nuclear membrane.

NRP2 has two major splice variants or isoforms, NRP2A and NRP2B. The isoforms are identical in structure and sequence in large parts of the N-terminal domains (a1, a2, b1, and b2), whereas they are different in the transmembrane and C-terminal cytoplasmic tail regions (Fig. 1D) [17]. Because the C-terminus is important for nuclear localization, we wanted to determine whether both NRP2A and NRP2B could localize to the nuclear membrane. No isoform-specific antibody for NRP2 is commercially available; therefore, we ectopically expressed either NRP2A or NRP2B in cancer cells and analyzed their sub-cellular locations by immunogold transmission electron-microscopy (ITEM). We observed the nuclear membrane localization of both NRP2A and 2B as gold-labeled puncta in a PCa cell line C4-2B and human embryonic kidney cell line HEK293T (Figs. 1E, F, S2A–E). The electron-microscopy data thus also confirmed our immunostaining data that NRP2 can be present at the nuclear membrane. Immunoblot analysis from NRP2A and 2B-expressing PCa cells also detected both variants in the nuclear extracts (Fig. S2F, G) further confirming the ITEM results. The antibodies used in ITEM detect the N-terminal region of NRP2 and thus stained both variants in the intranuclear membrane space. However, we observed a distinct spatial distribution of NRP2A and NRP2B in the nuclear membrane through structural illumination microscopy (SIM), when we co-immunostained with nuclear pore protein Nup98 (Figs. 2A, B, S3A–C). NRP2A at the nuclear membrane was mainly detected at the outer side of Nup98 (close to the cytoplasm) (Figs. 2A, S3A). This observation was further validated by analyzing the intensities using of fluorophore pixels of NRP2A (green line) and Nup98 (red lines), which indicated that NRP2A is further from the nucleus than Nup98 and close to outer nuclear membrane (ONM). As Nup98 is a centrally located Nup (central FG Nups), it implies that the membrane-bound NRP2A is localized within the ONM (with the N-terminal facing towards the perinuclear space). However, NRP2B was detected at a side of Nup98, which is closer to the nucleus (Figs. 2B, S3A) suggesting its localization at the INM. A similar pattern of nuclear localization of NRP2A and 2B were observed in HEK293T cells (Fig. S3B, C). Finally, when we expressed both GFP-tagged NRP2A (C-terminal) and HA-tagged NRP2B (N-terminal) in HEK293T cells or in C4-2B cells, we observed that they did not co-localize at the nuclear membrane. NRP2B was close to the nuclear membrane suggesting its location at the INM, whereas NRP2A was close to the cytoplasmic side indicating its presence at the ONM (Figs. 2C, D, S3D). Because the ONM is continuous with the endoplasmic reticulum (ER) and proteins from the ER can diffuse to the ONM; the ONM proteins often co-localize with ER markers. This is not the case for proteins located at the INM that need an active transport system to cross the nuclear pore regions for their entry into the INM. This is indeed the case for NRP2A and NRP2B. NRP2A showed significant co-localization with ER marker, protein disulfide-isomerase (PDI), near the perinuclear region; however, insignificant overlapping was observed between NRP2B and PDI staining (Fig. 2E–G). To rule out the possibility that the C-terminal GFP-tag hinders the INM localization of NRP2A, we ectopically expressed N-terminal HA-tagged NRP2A. Once again, NRP2A-HA was detected at the side of Nup98 close to cytoplasm (as indicated

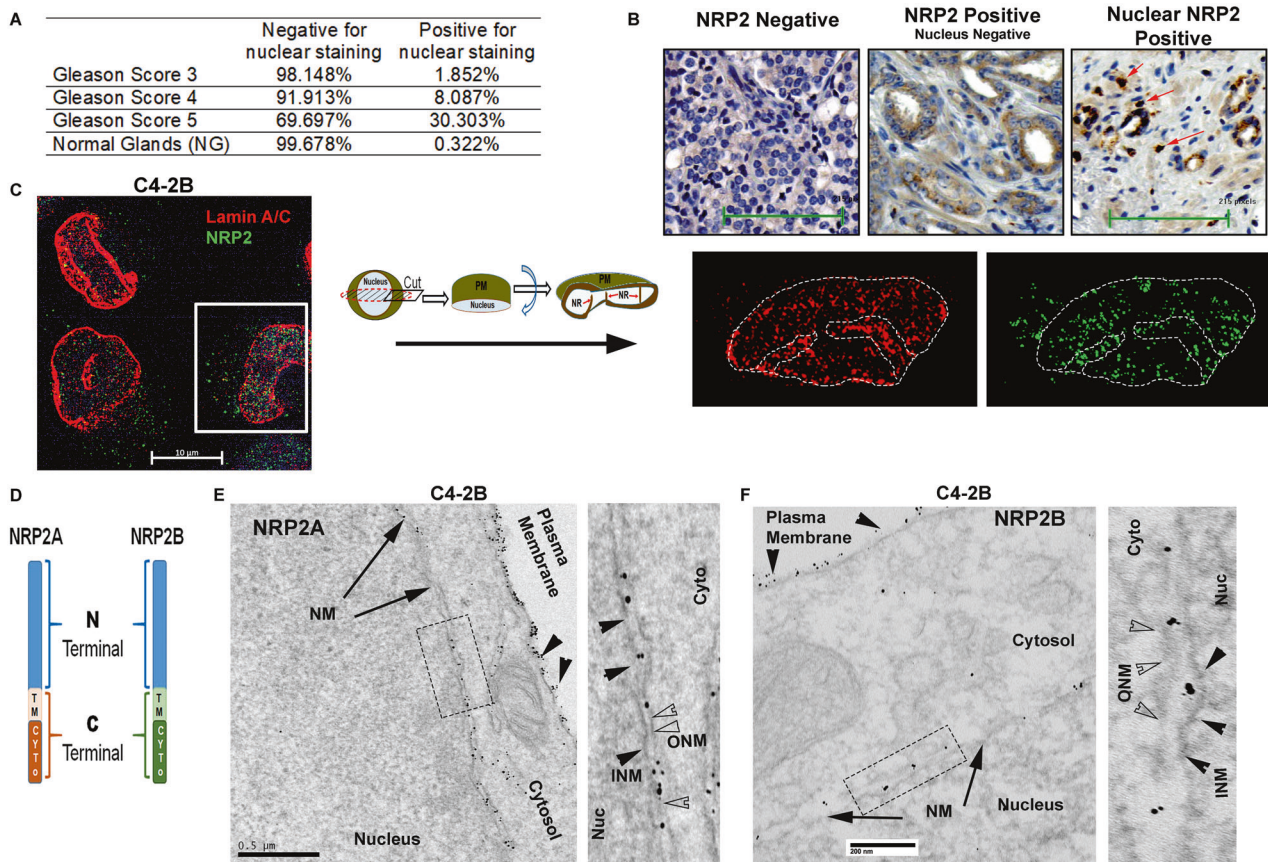


Fig. 1 NRP2 localization detected within the nucleus. **A** Percentage of nuclear NRP2-positive cells across the Gleason score. **B** Representative images of immunohistochemical staining for nuclear NRP2 in human prostate cancer tissues. Arrows indicate the nuclear positive NRP2. **C** Endogenous NRP2 staining (Alexa 488) in prostate cancer cell line C4-2B. INM was stained with lamin A/C (Alexa 594). DAPI indicates nuclear staining. Using Zen Blue lite software, cells were cut through the middle plane and then rotated across the x-axis. Inset is the magnified image of the nucleus of the cells. **D** Schematic diagram of NRP2 isomers. **E** TEM images of immunogold staining of untagged NRP2A in C4-2B cells ectopically expressing NRP2A. Cells were stained with NRP2 antibody and counterstained with gold-labeled secondary antibody. NRP2 staining appears as black punctate structures inside the cells. The nuclear and plasma membranes are indicated by the arrow and arrowhead, respectively. Inset is magnified. In the magnified image, ONM and INM are represented by opaque and black arrowheads, respectively. Scale Bar 500 nm. **F** Representative TEM images of immunogold staining of HA-tagged NRP2B ectopically expressed in C4-2B. Cells were stained with HA-antibody and counterstained with gold-labeled secondary antibody. The nuclear membrane and plasma membrane are indicated by arrows and arrowheads, respectively. Inset is magnified. ONM and INM are represented by opaque and black arrowheads. Scale Bar 200 nm.

by the line graph) (Fig. S3E) confirming its location at ONM. Since protein moves to INM from ONM by an active transport through nuclear pore, often its size exposed to the cytoplasm is the determinant factor for its passage. It has been experimentally shown that adding a bulky group to the cytoplasmic-exposed part of INM proteins hinders their movement. We observed similar phenomenon for NRP2B when we switched HA to GFP (a bulkier protein) at the C-terminus of NRP2B, as we detected no localization of GFP-tagged NRP2B in the INM. Our result thus suggested that NRP2B localizes to INM through an active transport and is regulated by its cytoplasmic tail (Fig. S3F).

Inner nuclear membrane localization of NRP2B depends on ligand dependent retrograde transport

VEGF-C promotes nuclear translocation of NRP2B. We studied whether the ligands of NRP2, such as VEGF-C and semaphorin-3F (SEMA3F), are needed for its nuclear translocation. We initially tested this with NRP2-Fc, which is a chimeric protein of the extracellular domain of NRP2 and the human IgG1 Fc fragment. Purified recombinant NRP2-Fc neutralizes the ligands of NRP2 and thus prevents their binding to cellular NRP2. NRP2-Fc treatment significantly inhibited the translocation of NRP2B into the nuclear

membrane implicating the requirement of NRP2 ligands in this process (Figs. S4A, 3A, B). Interestingly, while VEGF-C promotes the translocation of NRP2B into the nucleus, SEMA3F has no effect (Figs. 3A, B, S4A). The requirement of VEGF-C in this process was further proved by genetically knocking down VEGF-C (with shRNA, tagged with RFP), which inhibited nuclear translocation of NRP2 (cells expressing RFP) shown either through immunofluorescence or by WB (Fig. S4B, C). Our results suggested that specific ligand binding to NRP2 has the ability in promoting nuclear translocation. We further observed that we could block the VEGF-C induced nuclear translocation of NRP2B, when we inhibited the retrograde transport of the PCa cells using a retrograde transport inhibitor, Retro-2 (Fig. 3A, B). Moreover, when ER to Golgi transport was inhibited using Brefeldin-A (BFA), nuclear transport of NRP2B was also arrested (Figs. S4A, 3B). Our results therefore suggested that the translocation of NRP2 occurs from plasma membrane to the nuclear membrane via retrograde transport through the Golgi-ER. This ligand-induced retrograde mode of nuclear translocation is specific for NRP2B, as we did not observe this mode of transport for NRP2A (Fig. S4D). There was no additional increase in nuclear translocation of NRP2A upon VEGF-C addition, and retro-2 or BFA was unable to block the translocation of NRP2A.

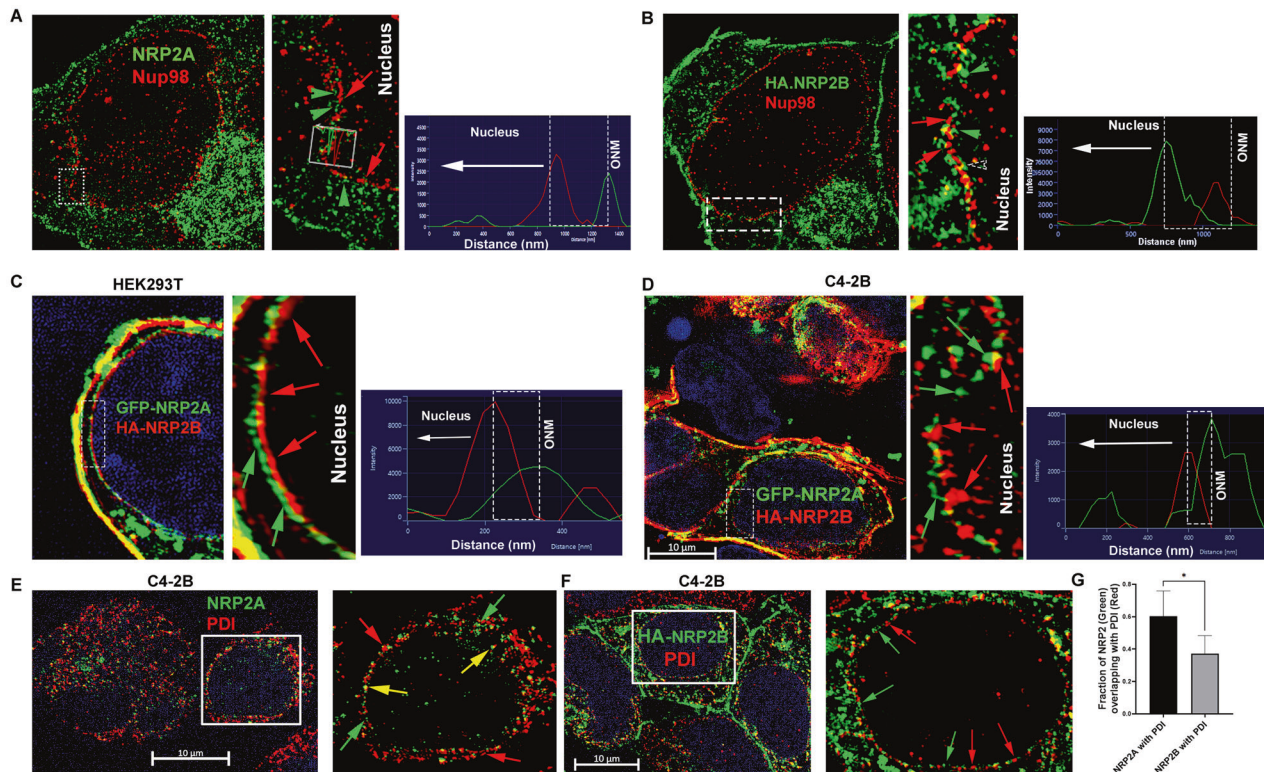


Fig. 2 NRP2 present in the nuclear membrane of the cell. **A** Immunofluorescence image of ectopically expressed untagged NRP2A (Alexa 488) in C4-2B cells. NRP2A staining was carried out with NRP2 antibody. The nuclear pore was stained with pore protein Nup98 (Alexa 594). Inset is magnified. Green arrowhead indicates NRP2A, whereas red arrows indicate Nup98. Green and red peaks in the line graph represent the relative position of NRP2A and Nup98 around the nucleus. **B** Immunofluorescence image of ectopically expressed HA-tagged NRP2B (Alexa 488) in C4-2B cells. NRP2B staining was carried out with HA-antibody. The nuclear pore was stained with central pore protein Nup98 (Alexa 594). Inset is magnified. NRP2B and Nup98 are indicated by green arrowheads and red arrows, respectively. Red and green peaks in the line graph represent the relative positions of NRP2B and Nup98 around the nucleus. GFP-tagged NRP2A was ectopically co-expressed with HA-tagged NRP2B in **(C)**. HEK293T and **(D)**. C4-2B cells. Inset is magnified. NRP2B was stained with HA (Alexa 594). The INM and ONM are indicated by the red and green arrows. Scale Bar 10 μ m. The nucleus was stained with DAPI. **E, F** NRP2A and HA-tagged NRP2B were ectopically over-expressed in C4-2B cells and were counterstained with PDI (Alexa 594). Insets are magnified views. Red and green arrows indicate the relative localization of NRP2 and PDI around the nucleus. Yellow arrows indicate co-localization. Scale Bar 10 μ m. **G** Bar graph indicates NRP2 and PDI co-localization quantitation.

SUMOylation is important for nuclear translocation of NRP2B. Next, we wanted to study the molecular mechanism by which VEGF-C promotes translocation to the INM. In silico analysis of NRP2 isoforms revealed that the C-terminal part of NRP2B contains a potential SUMOylation site at lysine-892 (Fig. S4E). SUMOylation of proteins is known to regulate their nuclear translocation. Hence, we tested whether NRP2 is SUMOylated and is required for nuclear translocation. Pull-down with SUMO1 followed by western blot with NRP2 suggested that NRP2B is post-translationally modified by SUMOylation. Moreover, mutation at lysine-892 to alanine (K892A) decreased the SUMOylated form of NRP2B confirming lys-892 as the site for SUMOylation (Figs. 3C, S4F). K892A-NRP2B also failed to translocate to the nuclear membrane and predominantly accumulated at the cell surface (Figs. 3D, S4G). All these results suggested that the C-terminal tail of NRP2B is SUMOylated and this is required for nuclear translocation. Finally, NRP2 SUMOylation was inhibited when VEGF-C was depleted (Fig. S4H) suggesting SUMOylation of NRP2 is dependent on VEGF-C. In addition, treatment with recombinant VEGF-C under starved condition enhanced the SUMOylated form of NRP2 in PCa cells (Fig. S4I). All these results therefore indicated that VEGF-C mediated SUMOylation at the C-terminal of NRP2B regulates its nuclear translocation from the cell membrane.

Identification of the binding partners of nuclear NRP2B. To better understand the function of nuclear NRP2, specifically NRP2B, it is

necessary to identify its interacting partners. Mass spectrometry (MS) analysis of immuno-precipitated samples with anti-NRP2 antibody from enriched nuclear extract of NRP2B expressing LNCaP C4-2B was conducted. The protein identification threshold value was 99% (peptide threshold 95%, at-least two independent peptide identifiers for each protein in two biological replicates) (Fig. 4A). We detected 176 proteins, which are common in two independent experiments and therefore have a significant probability to interact with nuclear NRP2 (Fig. 4B, Table S1). Using the gProfile, we have classified the proteins according to their functional involvement (Fig. S5A). Our analysis revealed that these proteins are involved in RNA metabolism, splicing, replications and translations processes.

We detected NRP2B in the nuclear pore regions through electron-microscopy (Fig. S5E) and our mass spectrometry (MS)-based proteomics data also identified a specific group of Nups associated with NRP2B (Fig. 4C). For example, we detected 16-peptides of Nup93 through MS (Fig. S5B), indicating, NRP2B and Nup93 are in same immune-complex. We were further able to validate this complex through co-IP-IB experiment (Fig. 4D, E). Similar validation was performed for Nup205 (Fig. S5C). Recent studies have shown that nuclear pores in addition to its role as gatekeepers for selective import or export of proteins/RNAs across the nucleus, also serve as active sites of gene transcription. A group of Nups such as basket or linker Nups serves as scaffolds for the organization of transcriptional hubs that regulate the

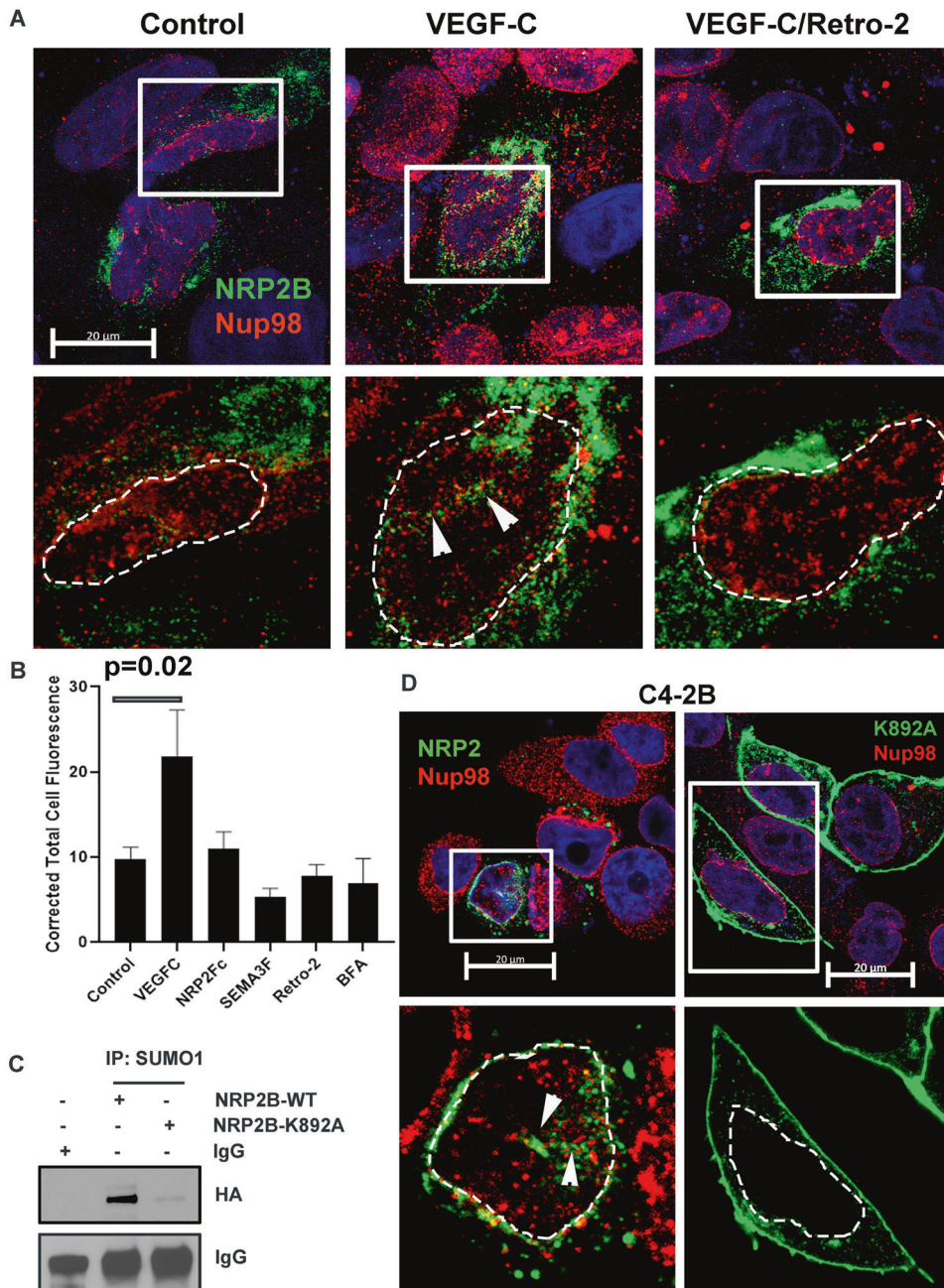


Fig. 3 VEGF-C-mediated retrograde transport and post-translational SUMOylation of NRP2B. **A** HA-tagged NRP2B was ectopically expressed in C4-2B cells. Immunofluorescence images representing the nuclear translocation of NRP2B under various conditions. NRP2B was detected using HA primary antibody and counterstained with Alexa 488-tagged secondary antibody. Arrowheads indicate invagination of the nuclear envelope. Nup98 was co-stained with NRP2B. Inset is magnified. DAPI was used for nuclear staining. Nuclei are marked with dotted lines. Scale Bar 10 μ m. **B** Bar graph shows quantification of nuclear NRP2B. **C** Immunoprecipitation with SUMO1 was carried out in C4-2B cells. HA-tagged wild type NRP2B and HA-tagged NRP2B K892A mutant were ectopically expressed in C4-2B cells. Immunoblots were carried out with HA-antibody. IgG bands show equal pull-down. **D** Immunostaining of HA-tagged wild type and mutant K892A NRP2B in the C4-2B cell line. NRP2B was stained with HA-antibody and counterstained with secondary antibody labeled with Alexa 488. Nup98 was stained with Alexa 594. Arrowhead represents nuclear invagination in C4-2B cells expressing wild type NRP2B. Insets are magnified views. Nuclei are demarcated with dotted lines. DAPI indicates nucleus. Scale Bar 20 μ m.

expression of specific genes [20, 21]. These Nups (Nup 210, Nup 93, Nup 98 and Nup160) are present in the inner core of the nuclear pore and form a dynamic multi-protein complex with TFs, chromatin modulators like SAGA proteins and RNA polymerases for gene transcription [22–26]. Because of our previous observation that NRP2 functions as a transcriptional regulator in advanced PCa [27], we hypothesized that NRP2, by associating with NUPs, interacts with the transcriptional machinery in PCa cells and thus

regulates gene expression. Interestingly, our MS analysis revealed interaction of NRP2 with AR, a transcription factor important for PCa progression (Fig. S5D). We have validated NRP2-AR interaction through colP-IB (Fig. 4F, G). Using 22RV1 cell line, we found that NRP2 also interacts with AR-splice variant v7 (AR-V7) (Fig. 4G). Moreover, pulling down endogenous NRP2 and immunoblot with AR-V7 specific antibody further validating NRP2-AR-V7 interaction (Fig. S5E). We further studied the association between AR and

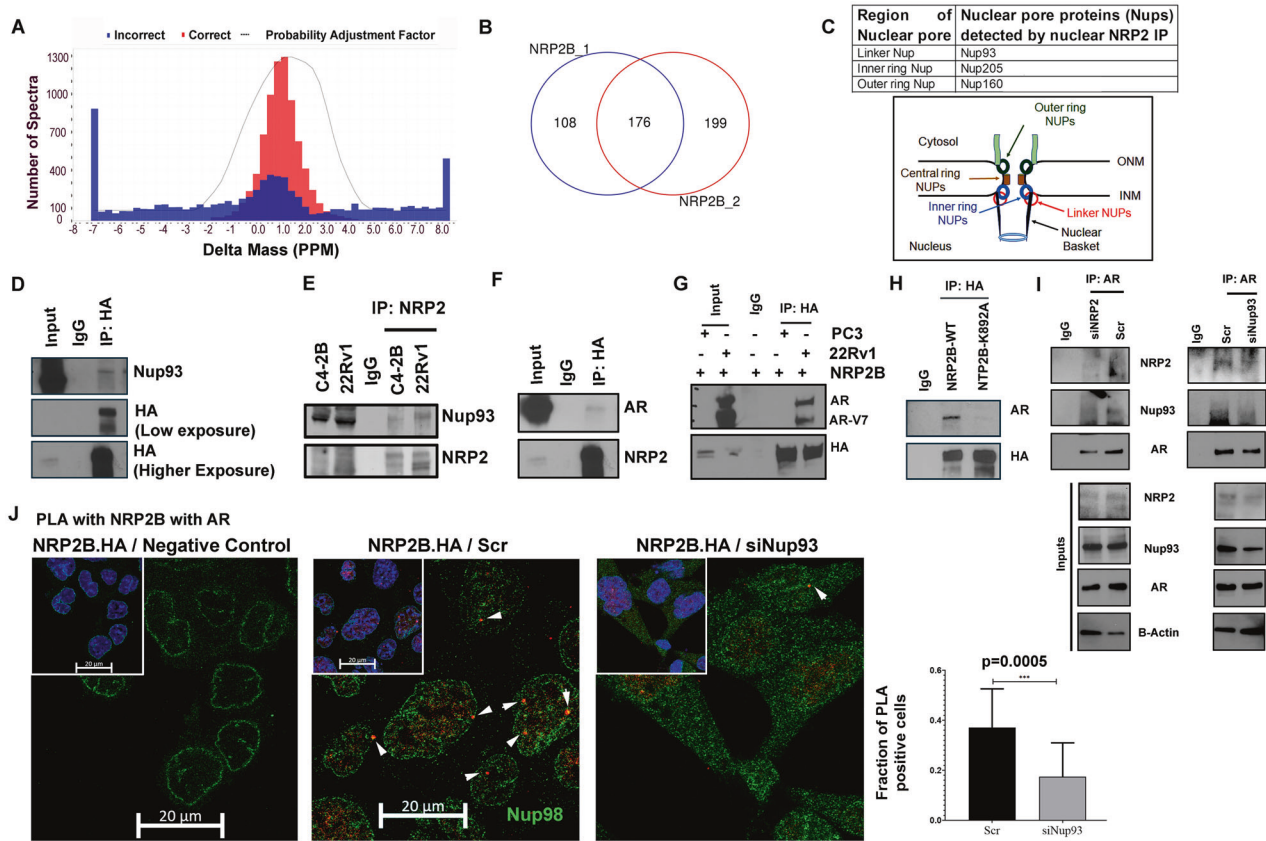


Fig. 4 NRP2 Mass-Spectrometry predicted its interactions with various nuclear-associated proteins. Following ectopic expression of untagged NRP2B in C4-2B cells, nuclear and post-nuclear fractions were separated, and a pull-down assay was performed on the nuclear fraction with NRP2 antibody. Mass-Spectrometry was carried out with the pull-down samples. Using the genes detected in NRP2 Mass-Spectrometry. **A** Sum of all the spectra associated with NRP2B pull-down sample is determined by the spectral graph. **B** Venn-diagram represent the overlapping genes identified in two independent NRP2B mass-spectrometry assay. **C** Group of nuclear pore proteins (Nups) identified through NRP2B Mass-Spectrometry. Schematic diagram indicating the relative positions of Nups around the nuclear pore. **D** Validation of NRP2-Nup93 interactions in C4-2B. C4-2B cells were transfected with HA-tagged NRP2B. IP was carried out with HA-antibody and immunoblots were carried out with anti-Nup93. **E** Endogenously, NRP2 and Nup93 interaction was validated in C4-2B and 22Rv1 cell lines. NRP2 was pull down with NRP2-specific antibody and IB with Nup93 antibody. **F** NRP2B and AR interaction was carried out in C4-2B following ectopic interaction of HA-tagged NRP2B. Pull-down was carried out with HA-antibody and IP was carried out against NRP2 and AR. **G** NRP2 and AR interaction was also monitored in PC3 and 22Rv1 following ectopic expression of HA-tagged NRP2B. IB was carried out against HA and AR. **H** Co-IP for AR with NRP2 was carried out with pull-down of NRP2 by HA-antibody in C4-2B cells expressing wild type and mutant K892A-NRP2B isoforms. NRP2B immunoblot was carried out with HA-antibody. **I** IP with AR antibody was carried out to test the interaction among AR, Nup93 and NRP2 under the presence or absence of NRP2 and Nup 93 from the nuclear fraction of LNCaP C4-2B cells. An immunoblot was performed with anti-AR, anti-Nup93 and anti-NRP2 antibody. The Co-IP was carried out in the presence of 50 ng/ml VEGF-C. **J** PLA was carried out to validating the NRP2-AR interaction within the nucleus. Following ectopic expression of HA-tagged NRP2B, PLA was carried out with HA and endogenous AR antibodies under the presence or absence of NUP93. As a negative control, only HA-antibody was used for PLA reaction. Arrowhead indicates the immune-reactive PLA puncta. Nucleus was counterstained with NUP98 to demarcate the nuclear periphery. DAPI used for nuclear staining. PLA quantification was shown in Bar diagram.

splice variant NRP2B in cancer cells. Our result indicated that wild type NRP2B can efficiently interact with AR. As expected, K892A NRP2B, which failed to translocate to INM because of its mutation at SUMOylation site, interacted less efficiently with AR (Fig. 4H).

NRP2 is required for the stabilization of the complex between Nups and transcription factors in aggressive PCa cells. We analyzed the nature of the complex formed with NRP2, NUPs and AR. Our results indicated that NRP2, AR or its splice variant AR-V7 interacted with the Nup93 (Figs. 4I, S5E, F). However, depletion of either NRP2 or Nup93 decreased the association between full-length AR, Nup93 and NRP2 (Fig. 4I). Further, treating PCa cells either with siNRP2 (recognizes both the isoforms) or siNRP2B could decrease the nuclear AR localization suggesting the importance of NRP2-containing complex in the retention of AR in the nucleus of PCa cells (Fig. S5G). The complex between NRP2B and AR was further validated by the proximity ligation assay (PLA).

The PLA puncta were formed close to nuclear periphery (shown through Nup98-positive staining) (Fig. 4J). However, depletion of Nup93 significantly decreased the association between AR and NRP2B. Our results therefore indicated that NRP2 (specifically NRP2B) recruits AR by forming a complex with Nups.

NRP2 facilitates recruitment of transcription factors to chromatin. Since, we observed NRP2 in the INM and formed a complex with Nups and AR, we wanted to investigate whether NRP2 directly interacts with nuclear chromatin or indirectly through other proteins to regulate transcription. We therefore performed a chromatin immunoprecipitation (ChIP) experiment using cell extracts of LNCaP C4-2B. NRP2-ChIP with formaldehyde as a cross-linker failed to pull down any DNA fragments. As formaldehyde forms a methylene-bridge between two macromolecules, that are ~ 2 Å apart, it can only crosslink molecules that are in proximity. Our result thus indicated that NRP2 is not in

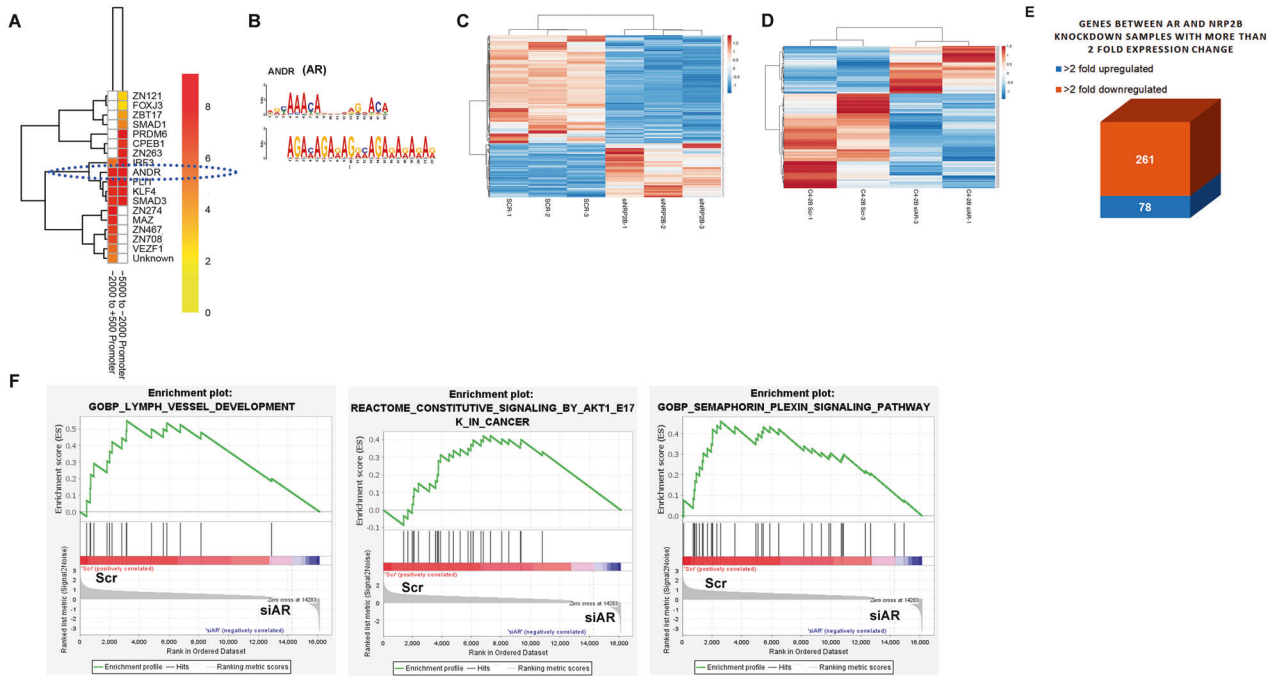


Fig. 5 Analysis of AR-NRP2 regulated gene expression. **A** TFs' binding probability within the consensus sequence derived from the NRP2-ChIP-seq was predicted through the heat map analysis. Consensus sequence map was generated using the indicated regions of promoter sequence from the NRP2 ChIP-Seq. **B** AR motifs was analyzed using the TOMTOM-MEME-motif analyzer. **C** Heat map for RNA-seq analysis of 200 differentially downregulated and 100 upregulated genes following depletion of NRP2B. **D** Heat map of gene expression profile following the depletion of AR by siRNA. **E** Box diagram representing the common up and downregulated gene expression following AR and NRP2B depletion. **F** GSEA analysis using AR-regulated genes.

close enough proximity to DNA for a direct interaction. However, NRP2-ChIP following two-step crosslinking with both disuccinimidyl glutarate (DSG, with a spacer length of ~ 8 Å) and formaldehyde was able to reproducibly pull-down chromatin in two independent biological replicates, thus implying an indirect interaction of NRP2 with the chromatin structure (Fig. S6A, B). Our result therefore suggested that NRP2 indirectly interacts with DNA while being a part of the large chromatin-interacting protein complex. Further analysis revealed that NRP2 interacts with the promoter regions (2000bp upstream to 500 bp downstream of transcriptional start site) of nearly 1 percent of genes—(Fig. S6C, D). In silico analysis using the promoter sequences following ChIP-Seq, revealed consensus transcriptional regulator binding motifs (Supplementary Fig. 6E). Using the HOCOMOCO database as an input in the TOMTOM-MEME-motif analyzer, we identified possible TFs that bind to these motifs (Fig. 5A, B). Interestingly, promoter consensus analysis indicated that NRP2 binding regions with chromatin overlapped with AR further validating our hypothesis that NRP2, Nup and AR forming a complex to activate AR-dependent gene expression in PCa cells (Fig. 5B). We also confirmed the interactions between NRP2 and another transcription factor, KLF4, in PCa cells by pull-down assays suggesting that NRP2 facilitates recruitment of some transcription factors to chromatin for gene transcription (Fig. S6F).

NRP2 regulates AR functions. Since, AR forms complex with NRP2 and Nup93, we hypothesized that NRP2 being a part of the complex, regulates the expression of some AR-driven genes in PCa cells. Using C4-2B as a model system, we thus compared the gene expression in PCa cells by RNA sequencing following depletion of either NRP2B or AR (Fig. 5C, D) and identified the common genes that are regulated by both AR and NRP2 (Fig. 5E). Out of the 339 common genes that were jointly regulated by AR-NRP2 axis, 78 genes were upregulated, and 261 genes were downregulated following NRP2 depletion (Fig. 5E). Analysis of

Gene enrichment sequence analysis (GSEA) revealed that these common gene-sets involved in lymph vessel development, AKT pathway, plexin-semaphorin signaling and others (Figs. 5F, S7A); implicating NRP2-AR complex regulates the expression of genes required for cancer progression. Interestingly, the regulation of NRP2 on the expression of AR-regulated genes seemed to be more pronounced when the PCa cells were treated with androgen (dihydroxy testosterone; DHT) (Fig. 6A). We also performed ChIP-qPCR to understand whether depletion of NRP2 can affect the binding of AR to the regulatory regions of these genes especially when the cells were treated with DHT. Our results confirmed that NRP2 depletion affected AR binding to the regulatory regions of the AR-regulated genes such as KLK3 (PSA) and KLK2 in both C4-2 and its syngeneic bone-metastatic version, C4-2B cells following androgen stimulation (Fig. 6B–D). Efficiency of NRP2 depletion was confirmed by western blot (Fig. S7B, C). In presence of DHT, we also observed a significant reduction of KLK3 (PSA)-promoter activity in both C4-2 and C4-2B cells upon NRP2 depletion (Fig. 6E, F). Since, Nup93 is a part of the NRP2-AR complex, we tested whether depletion of Nup93 can affect the AR-transcriptional activity. Using the KLK3 promoter luciferase assay we were able to show that depletion of Nup93 affected the AR-transcriptional activity similar to the depletion of NRP2 (Fig. 6F, G). Our results therefore suggested the presence of NRP2-Nup93-AR complex for AR-driven gene expression in PCa cells. Interestingly, the regulation of NRP2 on AR transcription was observed in PCa cells that express high level of NRP2. LNCaP, which is an androgen dependent PCa cells, expresses low level of NRP2 (Fig. S7D). LNCaP behaves like less aggressive primary PCa cells. Deletion of NRP2 in LNCaP did not change the efficiency of AR binding to the promoters of KLK3 and KLK2 (Fig. S7E). In conclusion, these results thus suggested that NRP2 expression is increased in cancer cells during the progression of PCa, which then facilitates a specific NRP2-AR complex for the transcription of some AR-driven genes.

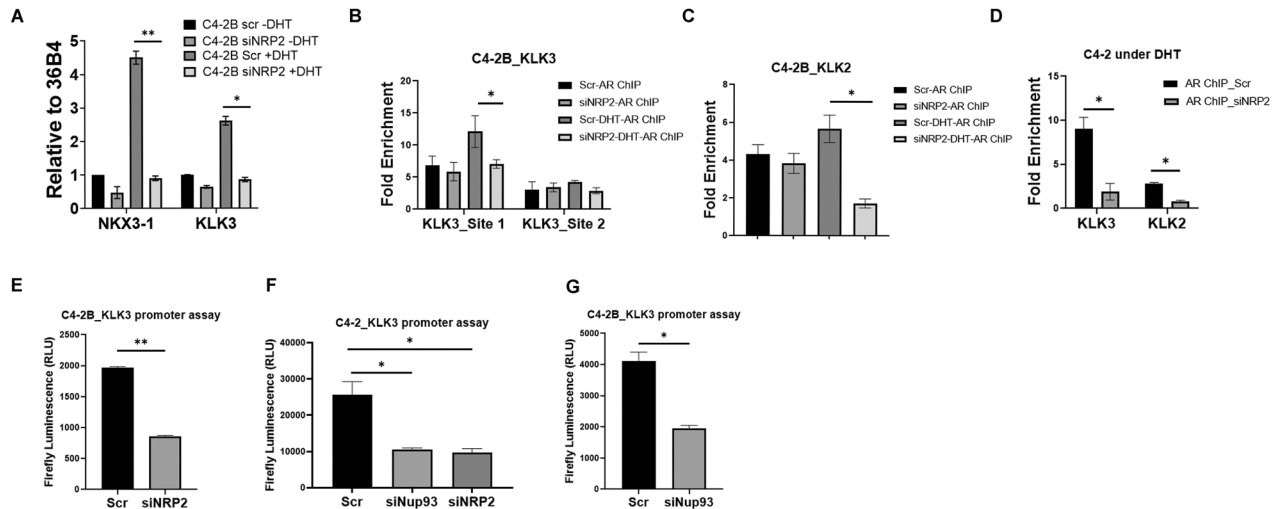


Fig. 6 AR-DNA interaction decreases following NRP2 depletion. **A** RT-PCR of NKX3-1 and KLK3 was carried out under steady state and DHT induced condition following the depletion of NRP2. **B–D** AR ChIP was carried out following the pull-down of crosslinking DNA with AR specific antibodies under steady state and DHT induced condition under the presence and absence of NRP2. Using pull-down DNA, RT-PCR was carried out with the primer of promoter sequences of these genes. Initially, NRP2 dependence on two AR-binding sites was assayed. In **(B)** proximal AR-binding site (Site 1) has more effect on NRP2 depletion. KLK2 binding was also analyzed using the qPCR in C4-2B as well as C4-2 as **(C, D)**. **E–G** KLK3 promoter luciferase assay was carried out following the depletion of NRP2 or Nup93 (in **F, G**). Firefly luciferase activity is represented as relative luciferase unit (RLU).

Blocking NRP2 enhances the sensitivity of enzalutamide in castration-resistant metastatic prostate cancer cells. Our results suggested that NRP2 promotes AR function in CRPC by recruiting it in a specific transcription complex that has the ability to promote several cancer promoting genes. We therefore hypothesized that blocking NRP2-mediated AR recruitment would enhance the therapeutic efficacy of enzalutamide, a second-generation anti-androgen frequently used in clinics to treat CRPC. As previously described, we blocked NRP2 function by treating LNCaP C4-2B cells with NRP2-Fc (soluble NRP2). The experiment was carried out in the presence of VEGF-C (50 ng/ml) to activate nuclear translocation of NRP2 (Fig. 7A). As expected, addition of NRP2Fc significantly affected colony sizes compared to control. Interestingly, addition of enzalutamide and simultaneously addition of NRP2Fc significantly affected ($p=0.008$) the colony number as well as colony sizes compared to control VEGF-C treated condition. Thus, the colony formation assay revealed that NRP2Fc in combination with enzalutamide can enhance the anti-tumor effect of enzalutamide. Similar to the result of colony formation assay mentioned before, we observed that inactivation of NRP2 axis can affect the tumor growth in mice. We performed the experiment in subcutaneous xenograft tumor model developed by implanting inducible shNRP2 expressing C4-2B cells in the athymic nude mice (Fig. S7F–I). For that we have implanted one million C4-2B cells carrying doxycycline inducible shNRP2 with low growth factor containing Matrigel in a 1:1 ratio. Our results indicated that depletion of NRP2 (by adding doxycycline) itself affect the tumor growth and proliferation (Fig. S7F–H). Moreover, depletion of NRP2 along with the addition of enzalutamide further decreased the tumor growth compared to NRP2 depletion itself (Fig. S7F, G). Overall, our results in both colony formation assay and xenograft tumor model indicate that depletion of NRP2/inactivation of the NRP2 signaling axis can increase therapeutic efficacy of enzalutamide therapy.

NRP2 inhibition increases the therapeutic efficacy of enzalutamide in vivo model. Using intratibial mice model with LNCaP C4-2B cells, we compared the tumor growth within the bone following NRP2 depletion alone or in combination with enzalutamide

(Fig. 7B). Here we used the luciferase expressing stable C4-2B cell line with doxycycline inducible shNRP2 (Fig. S8A). NRP2 was depleted in tumor by adding doxycycline (2 mg/ml) in the drinking water containing 2% sucrose solution. In addition, enzalutamide was injected intraperitoneally. After confirming the tumor growth by the IVIS, we randomized the mice into four groups. The control group received no enzalutamide and doxycycline. The second and the third groups were treated with only enzalutamide and doxycycline (to deplete, NRP2) respectively. The fourth group was treated with both enzalutamide and doxycycline. We performed the bone morphometric analysis using micro-CT for all the groups (Fig. 7C). Micro-CT analysis indicated that there is a significant loss of bone mineral density in control indicating tumor-induced bone degradation (a measure of tumor growth inside the bone cavity). NRP2 depletion alone and especially in combination of enzalutamide (Fig. 7C) showed less tumor-induced bone degradation compared to control or enzalutamide treated mice. Using micro-CT images, bone morphometric analysis also revealed that depletion of NRP2 in tumor cells decreased the bone loss as compared to control and enzalutamide treatment alone (Fig. 7D–G). However, NRP2 depletion in combination with enzalutamide treatment showed an improvement of the overall bone morphology both in terms of retention of bone volume and maintenance of trabecular bone (Fig. 7D–G) over the rest of the groups. Further, our analysis of the cancer cell cellularity by H&E staining in decalcified bone section suggested a significant increase in necrotic zones for combination treatment compared to control (Figs. 7H, S8B). Our results also indicated that the combination therapy elicited enhanced cleaved caspase-3 expression within the cancer cells in bone (Figs. 7I, S8C). This might be due to the fact that NRP2 depletion on the tumor cells decrease vascularity, increase stress which may result in increased necrosis and apoptosis as we seen in this experiment. Depletion of NRP2 was validated by IHC (Fig. 7J).

In summary, our results suggested that targeting NRP2 in combination with enzalutamide would be a better approach than using enzalutamide alone for the treatment of PCa with bone metastasis.

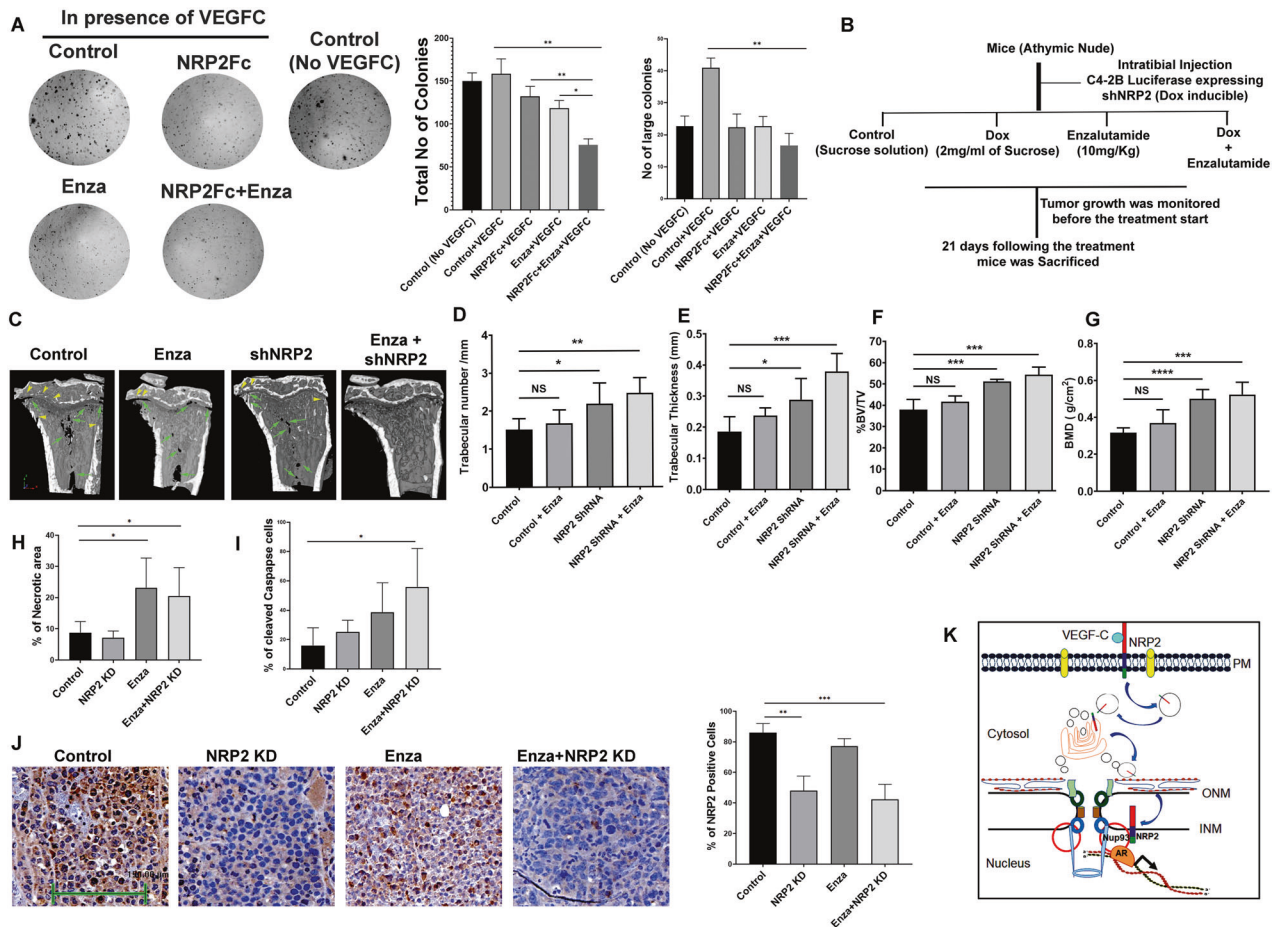


Fig. 7 Inhibition of nuclear transport of NRP2 increased AR-targeted therapeutic efficacy. **A** A colony formation assay was performed under VEGF-C treated condition to test for sensitivity to enzalutamide following the addition of NRP2Fc. The colony formation was also analyzed with VEGF-C untreated cells. Right, bar diagrams represent the number of colonies and the relative size of the colonies under the experimental conditions. **B** Schematic diagram of intratibial injection. **C** Micro-CT images of tumor containing bone under various condition. **D–G** Bone morphometric analysis in terms of trabecular number, Trabecular thickness, Bone volume (BV)/total volume (TV) and bone mass density (BMD) of bone under different condition. **H** Analysis of tumor necrosis under various condition. **I** IHC analysis for Cleaved caspase staining under different experimental condition. **J** IHC for NRP2 staining under different experimental condition to show the knockdown efficiency in tumor cell. **K** Schematic diagram representing how NRP2 is translocated from the plasma membrane to the nucleus of the cells to regulate TF-DNA interactions.

DISCUSSION

Amplification of AR signaling is one of the key features of CRPC due to increased expression of AR and generation of its constitutively active forms by alternate splicing and mutations at its ligand-binding domain [28]. In addition, AR forms distinct collaborative networks with other transcriptional regulators in PCa cells to promote expression of genes necessary for cancer progression [29]. Studies have reported changes in AR-binding profile correlates with disease progression and is mainly caused by specific AR-transcription complex and thus divergence of AR-binding profiles were detected in CRPC with respect to untreated PCa. For example, in CRPC tissue, specific sets of metabolic genes are enriched only near AR-binding sites [30, 31]. Targeting AR collaborating network in CRPC can therefore inhibit the cancer-specific gene expression and enhance the efficacy of second-generation AR therapy. Our current study reports that NRP2 is upregulated significantly in CRPC and aids AR-driven gene expression. We show that NRP2-AR mediated transcriptional complex is predominantly observed in CRPC and important for cancer progression and therapy resistance.

Elevated NRP2 expression correlates with poor cancer-specific survival in a PCa patient cohort [32]. Our study provides a mechanistic insight into how NRP2 regulates AR-driven gene

transcription in PCa cells. We observed that NRP2B, a specific splice variant of NRP2, localizes in the INM of aggressive PCa cells and forms a complex with nucleoporins (Nups) and AR. Nups at the nuclear pore regulate nucleocytoplasmic transport as well as are reportedly involved in DNA damage repair, chromatin silencing and transcriptional activation of genes [20, 33–35]. Studies with yeast, flies, metazoan and mammalian cells indicated that transcription factors are associated with the nuclear pore complex (NPC) through Nups and are required for the enhancement of transcriptional memory as well as positioning of euchromatic regions around the pore [34, 36–40]. Nups such as Nup93, Nup98, Nup153 and Nup210, regulate transcription in mammalian cells [23, 25, 41–44]. For example, the interaction between Nup210 and the transcription factor, Mef2C necessitates the transcription of genes required for muscle differentiation. Importantly, downregulation of Nup210 hinders the expression of genes for myogenic differentiation without any effect on nucleocytoplasmic transport through NPCs [45]. These result underscores the direct role of Nups in gene transcription. This evidence therefore indicate that certain Nups function as a scaffold to facilitate the organization of the transcription complex for gene expression. One advantage of active transcription near the nuclear pore is that the transcribed mRNA is efficiently

exported to the cytoplasm for translation. This Nup-dependent transcriptional complex is highly dynamic, and its formation is dependent on various physiological or pathological contexts. In cancer, Nup-regulated gene expression is evident in acute myeloid leukemia (AML), liver cancer, and PCa [24, 46, 47]. In PCa, Myc is a key driver of tumorigenesis and development of CRPC. Interestingly, the involvement of NPC in Myc-mediated transcription of specific genes was reported. Nup153 (a basket protein present in NPC) associates with Myc and facilitates its interaction with the SAGA complex for transcription of genes necessary for migration and proliferation, highlighting the importance of NPC-dependent gene transcription in PCa [41, 48]. Currently, the molecular players involved in cancer cells for such a dynamic formation of transcriptional complexes and their roles in cancer progression are not well understood. In this context, our finding that NRP2B translocates to INM to stabilize the Nup-AR-transcriptional complex has provided an in-depth understanding of how the dynamic transcriptional complexes with Nups can form in PCa. Since the expression of NRP2 increases with the progression of PCa, the possibility of the formation of these AR-NRP2-Nup complexes is high, which could be important for differential transcription of genes observed in aggressive PCa.

We observed a ligand dependent (VEGF-C) retrograde transport of NRP2B in the INM, whereas NRP2A moves to ONM (outer nuclear membrane) by passive diffusion. The two isoforms differ in their 93-amino acid long carboxyl-terminal region. Therefore, we concluded that the carboxyl-terminal domains of the isoforms are responsible for their specific localization and function in the nucleus. Our *in silico* analysis and biochemical assays indicated that the lysine at 892 of NRP2B undergoes VEGF-C dependent SUMOylation. Mutation caused by conversion of lysine to alanine abrogated the nuclear transport of NRP2B as well as its interactions with AR. This result provided a mechanistic understanding of how NRP2B translocates differently than NRP2A and thus function distinctly. Although, VEGF-C is the most potent NRP2 ligand, we speculate other ligands such as VEGF-A or HGF which are also present in the cancer microenvironment, might activate its nuclear translocation. Further experiments are needed to validate the effects of other ligands. Recently, the non-redundant functions of individual isoforms of NRP2 were recognized. Interestingly, the expression of NRP2B in human tissue was correlated with an advanced stage of the cancer and poor progression-free survival of patients [49].

To understand the contribution of NRP2 in genome-wide AR-mediated gene transcription, RNA sequencing following NRP2, or AR depletion was performed with PCa cells. Our results indicated that a group of genes were equally affected by both NRP2 and AR depletion. This implies that AR and NRP2 jointly regulate these genes. To validate that AR-binding in these genes is affected by the presence of NRP2, we have performed the AR-ChIP following NRP2 depletion. We observed that specific AR-binding sites in chromosomes decreased when the PCa cells were induced with DHT, indicating a role of NRP2 in the binding of activated AR at specific regions of chromatin. We observed a decrease in the promoter activity (by luciferase reporter assay) and total mRNA expression (by RT-PCR) of AR-stimulated genes following NRP2B depletion and stimulation with DHT in CRPC cells. All these results thus corroborate that targeting NRP2 axis in CRPC cells affects the AR-regulated gene expression and thus improves the efficacy of AR-targeted therapy. We tested our hypothesis using *in vivo* intratibial model of PCa bone metastasis and show that depletion of NRP2 with enhances the sensitivity of enzalutamide and recovered the overall bone health as evidenced by increased trabecular number and volume over untreated animals. Currently, hormone sensitive PCa patients with metastatic dissemination are treated with upfront second-line AR inhibitors such as enzalutamide or abiraterone acetate. However, these patients often become resistant to these therapies. AR-splice variants are one

of the causative factors for such resistance. Since NRP2 inhibition blocks both full-length AR and its splice variants, simultaneous inhibition of NRP2 and AR-axis can be an effective therapeutic approach in these patients.

Overall, our results unravel a novel role of NRP2 as a transcriptional regulator of AR and indicate a stabilizing function of NRP2 in the transcriptional complexes comprised of AR and Nups in CRPC cells. NRP2 therefore either initiates or maintains sustained expression of genes important for cancer progression and therapy resistance. Targeting NRP2, especially its function at the nuclear membrane could therefore be an effective therapeutic strategy in advanced cancer. One way to achieve this goal would be by preventing its translocation to the INM. Small molecule inhibitors against NRP2 can be developed in the future to inhibit its nuclear translocation and function in enhancing AR activity.

METHODS

Cell culture, plasmid constructs, and transfection

Human prostate cancer cell lines PC3 (ATCC, Manassas, VA, CRL1435), LNCaP (ATCC, Manassas, VA, CRL-1740), 22Rv1 (ATCC, Manassas, VA, CRL-2505), HEK293T (ATCC, Manassas, VA, CRL-11268), LNCaP C4-2, and LNCaP C4-2B (Kind gift from Prof. Allen Gao) were cultured in RPMI 1640 (Thermo Fisher Scientific, Gibco, NY, 11875093) with 10% FBS in the presence of antibiotics penicillin-streptomycin. Wild type NRP2A (Origene, RG220706 and RC220706) and NRP2B (Origene, RG210928 and RC210928) plasmids were purchased from Origene (Rockville, MD). An HA-tag was added after 21 amino acid residues from N-terminal end of NRP2 and a stop codon was also introduced at C-terminus end just after the NRP2-coding regions. Point mutation at 892 and at 856 of the plasmids were generated through site-directed mutagenesis (Agilent, CA, QuikChange II Site-Directed Mutagenesis Kit, Catalog #200523) as per the manufacturer instructions. KLK3 promoter luciferase construct was kind gift of Dr. Paramita Ghosh (UC Davis) [50]. siRNA for VEGF-C (Dharmacon RNA Technologies, Chicago, IL & Qiagen, Valencia, CA, L-012071-00-0020, LQ-012071-00-0005), NRP2 (Dharmacon RNA Technologies, L-017721-00-0010, LU-017721-00-005; Qiagen, SI04995011, SI04995039, SI04995018, SI04995025), and Nup93 (Dharmacon RNA Technologies, L-020767-01-0005), AR (Dharmacon RNA Technologies, L-003400-00-0010) as well as mCherry-tagged shVEGF-C (Rockville, MD, Genecopoeia, HSH111156-mU6) were used for depletion of respective proteins. Cells were transfected using TransIT-X2 Transfection Reagent (Madison, WI, Mirus, MIR6000) (Dharmacon RNA Technologies, T-2005-02). Tissue procurements as well as tissue classification are described in Borkowetz et. al 2019.

Western blot, ELISA, Membrane protein isolation, and co-immunoprecipitation (Co-IP)

Western blot and Co-IP was carried out as per our previously published materials (Dutta et. al., 2016). Nuclear and post nuclear/cytosolic fractions were separated using the NE-PER Nuclear and Cytoplasmic Extraction Reagents (Thermo Fisher Scientific, 78833) following the manufacturer protocol. For pulling down the SUMOylated proteins, N-ethyl maleimide was used at 10 mM working conditions. Surface Biotinylation assay was performed with EZ-Link NHS-Biotin (Thermo Fisher Scientific, 20217) as per the manufacturer instruction. Proteins were analyzed by western blot. Antibodies used for this study were as follows; NRP2 (Santa Cruz, sc-13117; R&D System AF2215; Protein Atlas, HPA054974), AR (Cell Signaling, 5153), ARv7 (Cell Signaling, 19672), HDAC1 (Cell Signaling, 34589), KLF4 (R&D System, HPA054974; Cell Signaling, 12173), PDI (Cell signaling 3501), Rho-GDI (Santa Cruz, sc-360; Cell Signaling, 2564), GAPDH (Cell Signaling, 5174), Nup98 (Cell Signaling, 2598), HA-antibody (Cell Signaling, 3724 and 2367), Lamin A/C (Cell Signaling, 4777), SMC1 (Cell Signaling, 4802), SUMO1 (Cell Signaling, 4930), Histone H3 (Cell Signaling, 5192), Cleaved Caspase-3 (Cell Signaling, 9579), NRP2 IHC specific antibody (Sigma-Aldrich HPA039980), Nup93 (Bethyl Laboratories Inc, A303-979A), HRP-conjugated secondary antibody, conformation specific (Cell Signaling, 3678), Nup205 (Bethyl Laboratories Inc, 303-935A), Nup188 (Bethyl Laboratories Inc, A302-323A).

Plasmid modification and site-directed modification

A hemagglutinin (HA) epitope tag was introduced downstream of the predicted signal sequence cleavage site by a three-step modification

involving site-directed mutagenesis. An EcoRI fragment of 181 bp covering the translation start of an expression vector containing the NRP2-coding sequence (NRP2 Human Tagged ORF Clone, OriGene Technologies, Herford, Germany) was cloned in pBluescript KSII(-). Site-directed mutagenesis following the manufacturer's protocol (Agilent, CA, Quik-Change II Site-Directed Mutagenesis Kit, 200523) and using complementary primers (forward: 5'-TGAGAGGCCAAGCGGTCCACCGTGGGA-3'; reverse: 5'-TCCGCACGGTGGGACCGGTTGGCTCTCA-3') generated an AgeI restriction site, which was used to insert a 5'-phosphorylated complementary DNA oligo hybrid (forward: 5'-CCGGAATATCCATATGATGTTCCAGATATGCT-3'; reverse: 5'-CCGGAGCATAATCTGGAACATCATATGGATATT-3'). HA-tagged NRP2 expression vectors were generated by replacement with the modified EcoRI fragment. Coding sequence determination by the Sanger method verified the predicted amino acid modification of NRP2 of the mature protein (R₂₁G₂₂Q₂₃P₂₄EYPYDVPDYAPVP₂₆P₂₇C₂₈G₂₉...). Recovery of the NRP2 carboxyterminal sequences in myc/DDK-tagged NRP2 expression vectors (NRP2A, NRP2B, OriGene) modified with HA-tag was performed by PCR-based insertion of stop codons at the native sites. 3'-terminal fragments of NRP2 expression vectors were PCR-modified (common forward: 5'-CACCATGGAGTCCAGTACCAGGC-3'; NRP2A reverse: 5'-CGAGCGGCCGCTACGCTATGCCTC-3'; NRP2B reverse: 5'-CGAGCGGCCGCTACGCTAGCAGTG-3'). Antisense primers were designed to introduce a TAG stop codon at the native site, followed by a NotI restriction site. After cloning into pCR4-TOPO (TOPO TA cloning kit, Life Technologies, Darmstadt, Germany), NotI restriction was used to generate NRP2A and NRP2B expression vectors by replacing parental expression vectors with the modified fragments. The Sanger method was used to verify NRP2 isoform coding sequences.

Using the site-directed mutagenesis kit, NRP2B-Del-Cyto construct was produced by the primers specified in the primer table. HA-tagged NRP2B (NM_201267.2) mentioned above was used as template. At the 856aa position of NRP2B (NM_201267.2), a STOP codon (TAA instead of TAC) has been inserted to get the cytosolic-fragment deleted membrane-bound NRP2 fragment (NRP2ΔC). Similarly, using the same HA-tagged NRP2B as template, a point mutation (Lysine to Alanine) at aa892 was introduced using the primer specified in the primer table.

Confocal and electron microscopy

Confocal microscopy was carried out as per our published protocol (Dutta et al., 2016). Cells were grown on poly-D/L lysine (BD Biosciences, Sparks, MD) coated cover slips before fixation for confocal analysis. All the confocal images were captured either with a Zeiss LSM 800 with Airyscan or with a Zeiss ELYRA PS.1 Super Resolution Microscope and data were analyzed and processed with Zeiss Zen Blue software.

For nuclear localization of NRP2B analysis under various experimental condition, C4-2B (or HEK) cells were transfected with either NRP2A-HA or NRP2B-HA plasmid. After 24 h of transfection, the cells were serum starved for overnight. Following starvation most of the NRP2 were in the membrane. NRP2B or NRP2A localization were chased with various experimental treatment condition for 1 h under the following reagents VEGF-C (50 ng/ml, R&D System, 752-VC-025), NRP2Fc (100 ng/ml, R&D System, 2215-N2-025), SEMA3F (100 ng/ml, R&D System, 9878-S3-025), Brefeldin A (0.5 μM, Sigma, B6542). After 1 h of chase, cells were fixed with 4% paraformaldehyde for 20 mins at room temperature. Following fixation, cells were washed and block with blocking solution (1% BSA + 0.2% Saponin in PBS). Cells were stained with respective primary antibodies (NRP2 and Nup98) for overnight at 4 °C. Next, cells were washed with 1% Tween-20 containing PBS and incubated with secondary antibodies in blocking buffer for 1 h at room temperature. After thorough washing (10 min x3 times), cells were counterstained with DAPI and mounted for images.

For electron microscopy, cells were cultured in 35 mm dishes (MatTek, Ashland, MA, P35G-2-14-CGRD). Before staining, cells were rinsed with 0.1 M phosphate buffer pre-warmed to 37 °C. Then cells were fixed with 4% paraformaldehyde in 0.1 M phosphate buffer pH7.4 containing 7.5% sucrose for 30 min at room temperature. Dishes were washed with 0.1 M phosphate buffer (3 × 5 min each) followed by blocking with aldehydes with 50 mM glycine in 0.1 M phosphate buffer for 15 min. Then cells were permeabilized with 0.25% saponin in 0.1 M phosphate for 30 min at room temperature. Cells were rinsed with 0.02% saponin in 0.1 M phosphate buffer (2 × 5 min each). Blocking was carried out with 0.1 M phosphate buffer containing 0.02% saponin, 1% BSA, 0.2% fish gelatin and 5% goat serum in 0.1 M phosphate buffer (blocking buffer) for 30 min. Then cells

were incubated with no primary antibody (control) or with primary antibodies overnight at 4 °C. Primary antibodies were made up in blocking buffer (about 100–200 μl /MatTek dish). Cells were kept in the refrigerator overnight. The next day, dishes were rinsed with 0.1 M phosphate buffer containing 0.02% saponin and 1% BSA (4 × 5 min each) and incubated with appropriate fluoronanogold secondary antibodies (Nanoprobes, Inc. Yaphank, NY, Cat. No: 7504 and 7502) in blocking buffer for 2 h at room temperature. After secondary antibody incubation, cells were further rinsed with buffer containing 0.02% saponin and 1% BSA (3 × 5 min each), then 0.02% saponin (3 × 5 min each) and finally just 0.1 M phosphate buffer (3 × 5 min each). Finally, cells were again incubated with fixative (4% paraformaldehyde with 0.05–0.1% glutaraldehyde in 0.1 M phosphate buffer pH 7.4) for 15 min and then washed with 50 mM Glycine in 0.1 M phosphate buffer 3 times for a total of 5 min. Next gold enhancement was carried out and TEM images was taken in FEI Tecnai G2 Spirit Biotwin microscope.

ChIP-Seq

ChIP was performed as per the manufacturer protocol using the ChIP-kit from MAGnify Chromatin Immunoprecipitation System (Thermo Fisher Scientific) described elsewhere (Dutta et al., 2016). Crosslinking was carried out with both disuccinimidyl glutarate (DSG) as well as formaldehyde. DSG was added to 10⁷ cells to a final concentration of 2 mM and incubated for 45 min at RT on a rotating condition. At the end of fixation, samples were centrifuge at 1500 rpm for 10 min. Cell pellet was washed with 20 ml PBS1X/1 mM PMSF and further centrifuged at 1500 rpm for 5 min. After washing twice, cells were re-suspended in 10 ml PBS1X/1 mM PMSF. Next, 270 μl of second cross-linker in terms of 37% formaldehyde was added in that mixture and incubated for 15 min at RT. Next, we followed the kit protocol as described. Using anti-NRP2 and anti-AR antibodies, Libraries were prepared using the New England Biolabs NEB Next Ultra II DNA Library Prep Kit for Illumina and sequenced by the UNMC Sequencing Core Facility using an Illumina NextSeq 500 Genome Analyzer. Initial raw sequence files were processed as follows. Adaptor sequences and low quality (Phred score <20) ends were trimmed from sequences using Trim Galore software package. Resulting fastq files were aligned to the human genome (GRCh38/hg38) using the sequence aligner software Bowtie2. The software package Picard routine Mark Duplicates was used to remove sequence duplications. Peak calling (FDR adjusted *p* value ≤ 0.05) was determined using MACS2 software. The UCSC genome browser was used for visualization.

mRNA isolation and qRT-PCR

RNA was extracted from cells using RNeasy mini kit (Qiagen, 74104) and quality was analyzed using Bio-analyzer. cDNA was prepared from 1 μg of mRNA following Transcriptor First Strand Synthesis Kit protocol (Roche, Indianapolis, IN, 04379012001). Quantitative real-time PCR (RT-PCR) was carried out with Power SYBR[®] Green master mix (Life Technologies, Grand island, NY, 4368706) as per our previously published protocol [51] using the primer sets shown in the table below.

RNA-Seq

RNA-seq was carried out from the control vs. siNRP2 and control vs. siAR in triplicate samples. RNA was extracted using the RNeasy Mini Kit (Qiagen, Germantown, MD) and RNA integrity quality was analyzed using the Agilent Bio-analyzer. A paired end read (2 × 50 bp) sequencing run of RNA libraries were carried out with Illumina NextSeq 500. Sequences were aligned to human reference genome hg38. Data analysis was performed with the help of the Bioinformatics Core at UNMC. RNA abundance was estimated with feature Counts from the Sub-read package version 1.6.3. Downstream analyses were performed with the DESEQ2 R package version 1.18.1. A Principal component analysis (PCA) was performed using <https://biit.cs.ut.ee/clustvis/>. Differentially expressed genes (DEGs) were identified by pairwise comparisons with the DESEQ2 package (v.1.12.3). Genes were retained as differentially expressed when the fold-change (FC) was >2 or <-2.

Mass-spectrometry analysis

Mass-Spectrometry was carried out on LNCaP C4-2B cells over-expressing NRP2B. After nuclear and post-nuclear fraction separation, IP with the NRP2 antibody was carried out while rotating at 4 °C. Pull-down was carried out with magnetic beads. Following the extractions of the samples, SDS page was run for 3 min. Bands were excised from the SDS gel followed by in gel digestion with trypsin. Mass-Spectrometry analysis was carried out through

LC-MS/MS using Thermo Q-Exactive-HF mass spectrometer and a nano RSLC Ultimate 3000 from Dionex. Spectra was processed using Mascot (Matrix Science, London, UK; version 2.6.1) and were subjected to a cutoff of 1% false discovery rate. Spectra was processed by MODIRO ver.1.1 (Protagen, Germany) software (from Proteomics & Metabolomics Facility of the Nebraska Center for Biotechnology at University of Nebraska, Lincoln).

Colony formation assay

LNCAp C4-2B cells were mixed in 0.3% Noble agar (in RPMI medium supplemented with 10% FBS) at 37 °C and immediately plated at 5000 cells/well on the top of a solidified agar layer of the 6-well plates (0.6% Noble agar in the same growth medium). Media was supplemented every fourth day along with the respective drug and inhibitors (50 ng/ml VEGF-C, 100 nM NRP2Fc, 10 nM Enzalutamide). After 21 days, colonies were stained with crystal violet solution (0.04% crystal violet-2% ethanol in PBS) for 1 h followed by washing with PBS and then was photographed.

Proximity ligation assay and immunofluorescence

At first, HA-tagged NRP2B was ectopically expressed in NRP2 depleted cells. Following 24 h ectopic expression, Nup93 was depleted from the cells for the next 48 h. At the end of the 72 h, cells were fixed with 4% paraformaldehyde for 20 min followed by treatment with 10% NP40 for 2–3 min. Proximity ligation assay was performed using the Duolink kit (Sigma-Aldrich, DUO92101-1KT), according to manufacturer's protocol, using red reagent (excitation 554 nm, emission 594 nm). After completion of the protocol, immunofluorescence was carried out with Nup98 antibodies for 1 h and additional secondary antibody for 30 min (Alexa 488). DAPI was used for counter staining. Images were captured using a Zeiss confocal microscope, with a 63× objective.

Luciferase assay

Promoter luciferase assay for AR-binding/activity was carried out in C4-2, C4-2B, and LNCAp cells transfected with 2 µg of pGL3-hPSA-luc. Using firefly luciferase assay kit (Promega), luminescence was determined. After 48 h of transfection, cells were lysed and the using the equal amount of protein from various condition, luciferase activity was analyzed according to the manufacturer protocol.

Intratumoral mouse model

In vivo mouse model of prostate cancer bone metastasis Animal study was carried in accordance with the UNMC IACUC guidelines. To assess the importance of NRP2 inhibition in combination of AR-inhibition by Enzalutamide; GFP-Luciferase and stable shNRP2 expressing C4-2B cells (50000 cells/mice in per 20 µL HBSS) was intratumorally injected into male athymic nude mice (8 weeks old Cri:NU(NCr)-Foxn1nu mice from Charles River, cancer cells injected in left tibia, 5 mice per group). PBS was injected as sham control into the right tibia. Appearance of tumor was monitored by IVIS imaging after 5 days of injection and once the tumor appeared, mice were randomized into four groups containing 5 mice each (achieve 80% power to detect a mean difference in dead cells of 20% using a two sided t-test). The control and enzalutamide treated group received 2% sucrose in water. The NRP2 knockdown (NRP2 KD) was carried out by adding doxycycline in drinking water containing 2% sucrose solution (doxycycline dose 2 mg/ml) [52]. Enzalutamide added intraperitoneally at 10 mg/kg body weight. Enzalutamide was added for 5 days a week for 3 weeks and doxycycline in drinking water was also added 5 consecutive days followed by 2 days normal water for 3 weeks. At the end of 3 weeks treatment, mice were sacrificed and the tumor containing bones were fixed in 10% formalin. For IHC, bones were further decalcified using 0.5 M EDTA for 2 weeks with intermittent replacement of fresh solution. Paraffin-embedded decalcified bone section was stained with H&E, Cleaved caspase 3 and NRP2. Tumor necrotic area was analyzed through Ventana Image Viewer and using Graphpad Prism a bar diagrams were plotted. For micro-CT, only formalin-fixed bones were used to take images.

In vivo prostate cancer subcutaneous mouse model

Subcutaneous tumor analysis was conducted in accordance with the UNMC IACUC guidelines. To analyze whether depletion of NRP2 can inhibit the tumor growth, we have developed stable doxycycline inducible shNRP2 expressing clones of C4-2B, where NRP2 can be depleted inducibly by addition of doxycycline (Dox). C4-2B shNRP2 cells (1×10^6 cells) were implanted into the right flank of 8 weeks athymic nude mice. Once the tumors become palpable (~30 mm³), animals were randomized into four

groups ($n = 5$). One group acts as a control (no treatment, except sucrose water). The second group received doxycycline whereas third group receive enzalutamide as mentioned above by i.p. The last group received both doxycycline as well as enzalutamide. Tumors were regularly monitored and tumor size was measured over the period of time until sacrifice (29 days from day of C4-2B injection). Tumor volume was calculated by using the formula: $1/2 ab^2$ [53].

Micro-CT analysis

Formalin-fixed bones were scanned through the X-ray micro-tomography system (Skyscan 1172, Bruker, Kontich, Belgium, at 55 kV and 181 µA, resolution 8.89 µm, exposure time 815 ms, and aluminum filter 0.5 mm-thick). To generate composite 3D images, raw data were reconstructed using NRecon software. Bone quality-control was analyzed by using the region of interest (ROI) around the growth plate. The bone morphometric analysis was carried out by using mean bone volume (BV), bone volume/tissue volume (BV/TV), trabecular thickness and bone mineral density (BMD).

Primer sequence used for either RT-PCR or for site-directed mutagenesis.

Gene	Primer 5' to 3'
36B4_F	ATGCAGCAGATCCGCATGT
36B4_R	TCATGGTGTCTTGCCCATCA
ChIP KLK3_1F: (Proximal)	TTGTGCCACTGGTGAGAAAC
ChIP KLK3_1R	TCAGAGACAAAGGCTGAGCA
ChIP KLK3_2F	GCAGTCTAGGTGGATGCTGT
ChIP KLK3_2R	GGTTTGCAAGTTGCCAGTA
ChIP KLK2_F	TCTCTGTGAGCAAAGGGATG
ChIP KLK2_R	TCTTAGGCCCTTCAAGCTG
Hum PSA_F	TTGTCTTCTCACCTGTCC
Hum PSA_R	GGGAATGCTTCTCGCACTC
Hum NKX3.1_F	GCCAAAGACCTCAAGCTCAC
Hum NKX3.1_R	AGGAGAGCTGCTTTCGCTTA
Hum NRP2_F	GTGAAGAGCGAAGAGACAACCA
Hum NRP2_R	GCAGTCTCCCCACTCTG
Hum NRP2A_F	ATCTCGGCTTTTGCAGGTGAGA
Hum NRP2A_R	ATTGCTCCAGTCCACTCGTAT
Hum NRP2B_F	TCGGCTTTTGCAGGTGAGAA
Hum NRP2B_R	CACCGTGTCCACTGTGGCT
NRP2B_DeI Cyto_F	CTGGTGTCCACTAACCCGGTCCGCTATCGGCCAA
NRP2B_DeI Cyto_R	TTGGCCGATAGCGGAACCGGTGTAGTGGAGCACCAG
NRP2B_K892A_F	CACCCTAACCATTCGCTAGAGCAAGACCGTGGCT
NRP2B_K892A_R	AGCCACGGTCTGCTTAGCCGCAATGGTTAGGGTG

REFERENCES

- Powers E, Karachaliou GS, Kao C, Harrison MR, Hoimes CJ, George DJ, et al. Novel therapies are changing treatment paradigms in metastatic prostate cancer. *J Hematol Oncol.* 2020;13:144.
- Schmidt KT, Huitema ADR, Chau CH, Figg WD. Resistance to second-generation androgen receptor antagonists in prostate cancer. *Nat Rev Urol.* 2021;18:209–26.
- Imamura Y, Sadar MD. Androgen receptor targeted therapies in castration-resistant prostate cancer: Bench to clinic. *Int J Urol.* 2016;23:654–65.
- Tucci M, Zichi C, Buttigliero C, Vignani F, Scagliotti GV, Di Maio M. Enzalutamide-resistant castration-resistant prostate cancer: challenges and solutions. *Oncol Targets Ther.* 2018;11:7353–68.
- Giacinti S, Poti G, Roberto M, Macrini S, Bassanelli M, DIP F, et al. Molecular Basis of Drug Resistance and Insights for New Treatment Approaches in mCRPC. *Anticancer Res.* 2018;38:6029–39.
- Roumiguie M, Paoletti X, Neuzillet Y, Mathieu R, Vincendeau S, Kleinclauss F, et al. Apalutamide, darolutamide and enzalutamide in nonmetastatic castration-resistant prostate cancer: a meta-analysis. *Future Oncol.* 2021;17:1811–23.

7. Tucci M, Leone G, Buttiglieri C, Zichi C, Di Stefano RF, Pignataro D, et al. Hormonal treatment and quality of life of prostate cancer patients: new evidence. *Minerva Urol Nefrol.* 2018;70:144–51.
8. Vander Ark A, Cao J, Li X. Mechanisms and approaches for overcoming enzalutamide resistance in prostate cancer. *Front Oncol.* 2018;8:180.
9. He Y, Wei T, Ye Z, Orme JJ, Lin D, Sheng H, et al. A noncanonical AR addiction drives enzalutamide resistance in prostate cancer. *Nat Commun.* 2021;12:1521.
10. Schweizer MT, Haugk K, McKiernan JS, Gulati R, Cheng HH, Maes JL, et al. A phase I study of niclosamide in combination with enzalutamide in men with castration-resistant prostate cancer. *PLoS ONE.* 2018;13:e0198389.
11. Shafran JS, Andrieu GP, Gyroffly B, Denis GV. BRD4 regulates metastatic potential of castration-resistant prostate cancer through AHNK. *Mol Cancer Res.* 2019;17:1627–38.
12. Asangani IA, Dommetti VL, Wang X, Malik R, Cieslik M, Yang R, et al. Therapeutic targeting of BET bromodomain proteins in castration-resistant prostate cancer. *Nature.* 2014;510:278–82.
13. Coleman DJ, Gao L, Schwartzman J, Korkola JE, Sampson D, Derrick DS, et al. Maintenance of MYC expression promotes de novo resistance to BET bromodomain inhibition in castration-resistant prostate cancer. *Sci Rep.* 2019;9:3823.
14. Wang L, Xu M, Kao CY, Tsai SY, Tsai MJ. Small molecule JQ1 promotes prostate cancer invasion via BET-independent inactivation of FOXA1. *J Clin Invest.* 2020;130:1782–92.
15. Sulpice E, Plouet J, Berge M, Allanic D, Tobelem G, Merkulova-Rainon T. Neuropilin-1 and neuropilin-2 act as coreceptors, potentiating proangiogenic activity. *Blood.* 2008;111:2036–45.
16. Parker MW, Linkugel AD, Goel HL, Wu T, Mercurio AM, Vander, et al. Structural basis for VEGF-C binding to neuropilin-2 and sequestration by a soluble splice form. *Structure.* 2015;23:677–87.
17. Rossignol M, Gagnon ML, Klagsbrun M. Genomic organization of human neuropilin-1 and neuropilin-2 genes: identification and distribution of splice variants and soluble isoforms. *Genomics.* 2000;70:211–22.
18. Fricker M, Hollinshead M, White N, Vaux D. Interphase nuclei of many mammalian cell types contain deep, dynamic, tubular membrane-bound invaginations of the nuclear envelope. *J Cell Biol.* 1997;136:531–44.
19. Drozd MM, Vaux DJ. Shared mechanisms in physiological and pathological nucleoplasmic reticulum formation. *Nucleus.* 2017;8:34–45.
20. Ibarra A, Hetzer MW. Nuclear pore proteins and the control of genome functions. *Genes Dev.* 2015;29:337–49.
21. Rodriguez-Navarro S, Fischer T, Luo MJ, Antunez O, Bretschneider S, Lechner J, et al. Sus1, a functional component of the SAGA histone acetylase complex and the nuclear pore-associated mRNA export machinery. *Cell.* 2004;116:75–86.
22. Garcia-Oliver E, Garcia-Moliner V, Rodriguez-Navarro S. mRNA export and gene expression: the SAGA-TREX-2 connection. *Biochim Biophys Acta.* 2012;1819:555–65.
23. Labade AS, Karmodiya K, Sengupta K. HOXA repression is mediated by nucleoporin Nup93 assisted by its interactors Nup188 and Nup205. *Epigenetics Chromatin.* 2016;9:54.
24. Sump B, Brickner JH. Nup98 regulation of histone methylation promotes normal gene expression and may drive leukemogenesis. *Genes Dev.* 2017;31:2201–3.
25. Franks TM, Hetzer MW. The role of Nup98 in transcription regulation in healthy and diseased cells. *Trends Cell Biol.* 2013;23:112–7.
26. Liang Y, Franks TM, Marchetto MC, Gage FH, Hetzer MW. Dynamic association of NUP98 with the human genome. *PLoS Genet.* 2013;9:e1003308.
27. Dutta S, Roy S, Polavaram NS, Baretton GB, Muders MH, Batra S, et al. NRP2 transcriptionally regulates its downstream effector WDFY1. *Sci Rep.* 2016;6:23588.
28. Coutinho I, Day TK, Tilley WD, Selth LA. Androgen receptor signaling in castration-resistant prostate cancer: a lesson in persistence. *Endocr Relat Cancer.* 2016;23:T179–97.
29. Sharma NL, Massie CE, Ramos-Montoya A, Zecchini V, Scott HE, Lamb AD, et al. The androgen receptor induces a distinct transcriptional program in castration-resistant prostate cancer in man. *Cancer Cell.* 2013;23:35–47.
30. Massie CE, Lynch A, Ramos-Montoya A, Boren J, Stark R, Fazli L, et al. The androgen receptor fuels prostate cancer by regulating central metabolism and biosynthesis. *EMBO J.* 2011;30:2719–33.
31. Tan KN, Avery VM, Carrasco-Pozo C. Metabolic roles of androgen receptor and Tip60 in androgen-dependent prostate cancer. *Int J Mol Sci.* 2020;21:6622.
32. Borkowetz A, Froehner M, Rauner M, Conrad S, Erdmann K, Mayr T, et al. Neuropilin-2 is an independent prognostic factor for shorter cancer-specific survival in patients with Acinar adenocarcinoma of the prostate. *Int J Cancer.* 2020;146:2619–27.
33. Palancade B, Liu X, Garcia-Rubio M, Aguilera A, Zhao X, Doye V. Nucleoporins prevent DNA damage accumulation by modulating Ulp1-dependent sumoylation processes. *Mol Biol Cell.* 2007;18:2912–23.
34. Ruben GJ, Kirkland JG, MacDonough T, Chen M, Dubey RN, Gartenberg MR, et al. Nucleoporin mediated nuclear positioning and silencing of HMR. *PLoS ONE.* 2011;6:e21923.
35. Radman-Livaja M, Ruben G, Weiner A, Friedman N, Kamakaka R, Rando OJ. Dynamics of Sir3 spreading in budding yeast: secondary recruitment sites and euchromatic localization. *EMBO J.* 2011;30:1012–26.
36. Kuhn TM, Capelson M. Nuclear pore proteins in regulation of chromatin state. *Cells.* 2019;8:1414.
37. Kuhn TM, Pascual-Garcia P, Gozalo A, Little SC, Capelson M. Chromatin targeting of nuclear pore proteins induces chromatin decondensation. *J Cell Biol.* 2019;218:2945–61.
38. Raices M, D'Angelo MA. Nuclear pore complexes and regulation of gene expression. *Curr Opin Cell Biol.* 2017;46:26–32.
39. Ptak C, Aitchison JD, Wozniak RW. The multifunctional nuclear pore complex: a platform for controlling gene expression. *Curr Opin Cell Biol.* 2014;28:46–53.
40. Dieppois G, Stutz F. Connecting the transcription site to the nuclear pore: a multi-tether process that regulates gene expression. *J Cell Sci.* 2010;123:1989–99.
41. Ibarra A, Benner C, Tyagi S, Cool J, Hetzer MW. Nucleoporin-mediated regulation of cell identity genes. *Genes Dev.* 2016;30:2253–8.
42. Kitazawa T, Rijli FM. Nuclear pore protein meets transcription factor in neural fate. *Neuron.* 2017;96:259–61.
43. Gomez-Cavazos JS, Hetzer MW. The nucleoporin gp210/Nup210 controls muscle differentiation by regulating nuclear envelope/ER homeostasis. *J Cell Biol.* 2015;208:671–81.
44. D'Angelo MA. Nuclear pore complexes as hubs for gene regulation. *Nucleus.* 2018;9:142–8.
45. Raices M, Bukata L, Sakuma S, Borlido J, Hernandez LS, Hart DO, et al. Nuclear pores regulate muscle development and maintenance by assembling a localized Mef2C complex. *Dev Cell.* 2017;41:540–54.e7.
46. Holzer K, Ori A, Cooke A, Dauch D, Drucker E, Riemenschneider P, et al. Nucleoporin Nup155 is part of the p53 network in liver cancer. *Nat Commun.* 2019;10:2147.
47. Rodriguez-Bravo V, Pippa R, Song WM, Carceles-Cordon M, Dominguez-Andres A, Fujiwara N, et al. Nuclear pores promote lethal prostate cancer by increasing POM121-driven E2F1, MYC, and AR nuclear import. *Cell.* 2018;174:1200–15.e20.
48. Su Y, Pelz C, Huang T, Torkenczy K, Wang X, Cherry A, et al. Post-translational modification localizes MYC to the nuclear pore basket to regulate a subset of target genes involved in cellular responses to environmental signals. *Genes Dev.* 2018;32:1398–419.
49. Gemmill RM, Nasarre P, Nair-Menon J, Cappuzzo F, Landi L, D'Incecco A, et al. The neuropilin 2 isoform NRP2b uniquely supports TGFbeta-mediated progression in lung cancer. *Sci Signal.* 2017;10:eaag0528.
50. Savoy RM, Chen L, Siddiqui S, Melgoza FU, Durbin-Johnson B, Drake C, et al. Transcription of Nrdp1 by the androgen receptor is regulated by nuclear filamin A in prostate cancer. *Endocr Relat Cancer.* 2015;22:369–86.
51. Stanton MJ, Dutta S, Zhang H, Polavaram NS, Leontovich AA, Honscheid P, et al. Autophagy control by the VEGF-C/NRP2 axis in cancer and its implication for treatment resistance. *Cancer research.* 2013;73:160–71.
52. Polavaram NS, Dutta S, Islam R, Bag AK, Roy S, Poitz D, et al. Tumor- and osteoclast-derived NRP2 in prostate cancer bone metastases. *Bone Res.* 2021;9:24.
53. Kersemans V, Cornelissen B, Allen PD, Beech JS, Smart SC. Subcutaneous tumor volume measurement in the awake, manually restrained mouse using MRI. *J Magn Reson Imaging.* 2013;37:1499–504.

ACKNOWLEDGEMENTS

The authors thank all staff members of the Advanced Microscopy Core and Genomics Core Facility of UNMC. We also extend our sincere thanks to the UNMC Bioinformatics and Bio-statistician Core for their support to analyze the data. The raw data has been deposited in Gene Expression Omnibus with the accession number GSE205150.

AUTHOR CONTRIBUTIONS

SD and KD has designed the project and SD performed most of the work. NSP, RI, SB, SR have assisted some of the work. TM has developed the NRP2-HA-tagged plasmid. SAA did the mass spec. AD took the electron microscopic images. MI, AB, SC, SF, MW, GBB, LCH, MHM were involved in TMA development and staining of NRP2. PG help us in promoter assay. PG, KJP, SKB and MHM critically evaluated the work and time to time provide their suggestion. DLK performed and analyzed the ChIP-seq.

FUNDING

This work was supported by grants for SD (1R21CA241234-01, NE-LB506, Lageschulte Fund), KD (R01CA182435, R01CA239343, DoD W81XWH2110628), MHM and LHH (DFG project number 273676790), and MHM (DFG project number 416001651). MM is funded by the Rudolf-Becker-Foundation for his professorship. The construction of the prostate cancer tissue microarray was funded by the DFG Forschergruppe-1586 SKELMET to LCH and SF.

COMPETING INTERESTS

The authors declare no competing interests.

ADDITIONAL INFORMATION

Supplementary information The online version contains supplementary material available at <https://doi.org/10.1038/s41388-022-02382-y>.

Correspondence and requests for materials should be addressed to Samikshan Dutta or Kaustubh Datta.

Reprints and permission information is available at <http://www.nature.com/reprints>

Publisher's note Springer Nature remains neutral with regard to jurisdictional claims in published maps and institutional affiliations.